LBL-37733
UC-401

Center for Advanced Materials

CAM

The Structure and Reactivity of Adsorbates on Stepped Rh and Pt Surfaces Investigated by LEED, HREELS, TPD, XPS and STM

J.D. Batteas
(Ph.D. Thesis)

June 1995

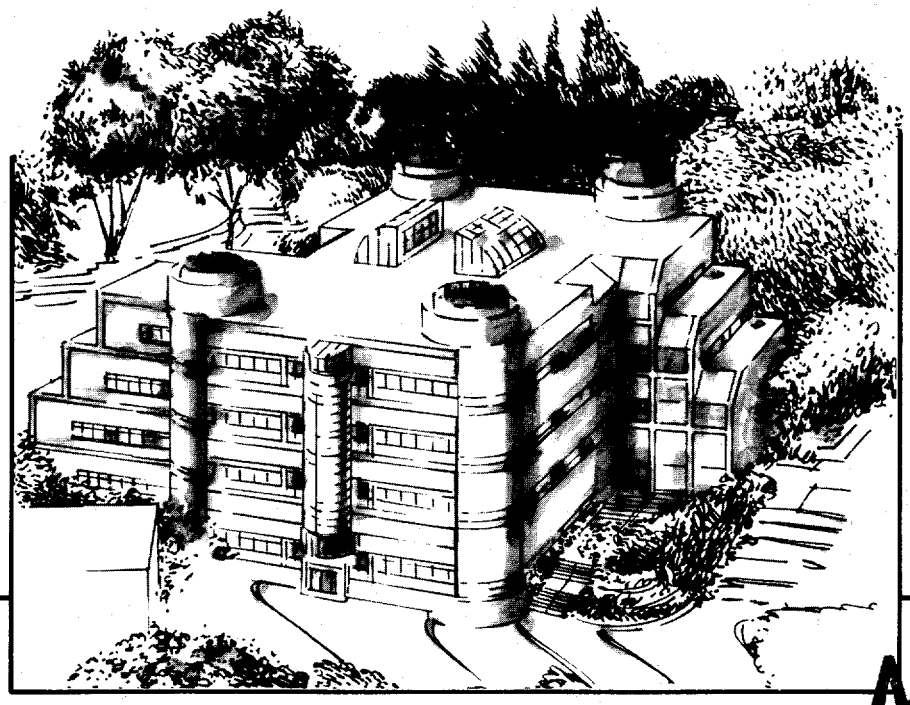

Materials and Chemical Sciences Division
Lawrence Berkeley Laboratory • University of California
ONE CYCLOTRON ROAD, BERKELEY, CA 94720 • (415) 486-4755

Prepared for the U.S. Department of Energy under Contract DE-AC03-76SF00098

DISCLAIMER

LBL-37733
UC-401

The Structure and Reactivity of Adsorbates on Stepped Rh and Pt Surfaces Investigated by LEED, HREELS, TPD, XPS and STM

James Daryl Batteas
Ph.D. Thesis

Department of Chemistry
University of California, Berkeley

and

Materials Sciences Division
Lawrence Berkeley Laboratory
University of California
Berkeley, CA 94720

June 1995

This work was supported by the Director, Office of Energy Research, Office of Basic Energy Sciences, Materials Sciences Division, of the U.S. Department of Energy under Contract No. DE-AC03-76SF00098.

The Structure and Reactivity of Adsorbates on Stepped Rh and Pt Surfaces Investigated by LEED, HREELS, TPD, XPS and STM

by

James Daryl Batteas

B.S. (University of Texas at Austin) 1990

A dissertation submitted in partial satisfaction of the

requirements for the degree of

Doctor of Philosophy

in

Chemistry

in the

GRADUATE DIVISION

of the

UNIVERSITY of CALIFORNIA at BERKELEY

Committee in charge:

Professor Gabor A. Somorjai, Chair
Professor Angelica M. Stacy
Professor Roya Maboudian

1995

The Structure and Reactivity of Adsorbates on Stepped Rh and Pt Surfaces Investigated by LEED, HREELS, TPD, XPS and STM

by

James Daryl Batteas

Abstract

The Structure and Reactivity of Adsorbates on Stepped Rh and Pt Surfaces Investigated by LEED, HREELS, TPD, XPS and STM

by

James Daryl Batteas

Doctor of Philosophy in Chemistry

University of California at Berkeley

Professor Gabor A. Somorjai, Chair

Defects on surfaces such as steps play an important role in surface chemistry. In order to obtain an understanding of the influence of steps in surface chemical reactions, the structure and reactivity of small molecules (O_2, CO, H_2S, and C_2H_4) on atomically stepped surfaces of Rh and Pt have been investigated by low-energy electron diffraction (LEED), high-resolution electron energy loss spectroscopy (HREELS), temperature programmed desorption (TPD), X-ray photoelectron spectroscopy (XPS) and *in situ* scanning tunneling microscopy (STM) experiments.

The detailed structures of CO and oxygen bonded to the Rh(110) surface were determined by fully dynamical tensor LEED intensity analyses. The CO molecules bond near the short bridge sites with the CO molecular axis tilted approximately 24° from the surface normal. Oxygen atoms are bound asymmetrically in the 3-fold fcc hollow-sites to the (111) facets of the steps. The interactions of CO and oxygen on the Rh(311) surface

were examined by LEED, HREELS and TPD experiments. The reaction of CO with the ordered phases of O shows two distinct reaction channels, a low temperature reaction limited channel (200 K) and a high temperature diffusion limited channel (350 K). Models of the reaction geometry and dynamics are proposed.

The thermal decomposition of ethylene was examined on the Rh(311) surface by LEED, TPD, HREELS and XPS. The stable decomposition species (C_2H, CH and C_2) are formed near 300 K, approximately 100 K lower on the stepped Rh(311) than on the flatter Rh(111) surface. The formation of these species at lower temperatures is attributed to the stepped nature of the surface.

Finally, *in situ* STM has been used to examine surface structural changes of a stepped Pt(111) crystal under coadsorption of sulfur and CO. This is the first direct evidence for a new mechanism by which a surface covered with an unreactive, strongly chemisorbed overlayer can form new sites, for bonding and reactions to occur, by massive surface restructuring at the step edges. This new surface phenomenon answers some of the puzzles of metal surface catalysis and its implications are described.

Dedicated

to J.D. and Dorothy Batteas

Contents

Acknowledgments

This is the key part of any dissertation: the part where the author tries to find the words to thank all of the people who helped to make their doctoral work possible. I have learned so much from so many, and I greatly appreciate the time and effort of everyone. I want to begin by thanking Gabor Somorjai. I greatly appreciate his willingness to give me advice on anything. I am grateful for his support in all of my endeavors both in his lab and outside of it. I was also privileged to work with Michel Van Hove and Miquel Salmeron who are experts in their fields of surface crystallography and scanning probe microscopy. I want to thank them for their guidance and support of my work.

Many individuals have made my time in Berkeley a rewarding experience and unselfishly offered assistance whenever I needed it. I must begin by extending great appreciation to Scott Perry. I am very thankful for his friendship and mentorship over that past few years. I want to thank Michael Quinlan, Uli Starke and everyone that let me bug them with questions that helped push me through my first few years. I also wish to acknowledge Alex Boffa, Angelo Barbieri, Denis Gardin, Nick Materer, Brian McIntyre and Jim Dunphy. They let me ask dumb questions with extreme patience. I have greatly enjoyed working with Peter Jacobs, Erin Starkey, Simone Rizzi, Craig Gerken and Renée Minick, each of whom had to put up with my sometimes less than clear explanations. I also must acknowledge Heather Galloway, Rob Carpick, Anna Lio, Peter Frantz, Jun Hu, Gang-Yu Liu, Frank Ogletree, and Enrico Magni, who helped me through my final months of proposal writing and interviewing. They were willing to listen to terrible talks prepared in exhaustion and to help me sort out my thoughts. I am indebted to them for their kindness. It is also important to acknowledge the contributions of Bob Kehr, Mae Lum and Gloria Osterloh. They always seemed to know how to find or get everything I needed. I must of course acknowledge Jana Steiger who was always willing to listen to my woes over coffee. Finally I must express my thanks to my wife Holly Gaede, who has endured

my many mood swings, my hopes and my anxieties. Without her this would not have been possible.

This work was supported by the Director, Office of Energy Research, Office of Basic Energy Sciences, Materials Sciences Division of the U.S. Department of Energy under Contract No. DE-AC03-76SF00098.

List of Figures

List of Tables

Chapter 1

Introduction

1.1 Surface chemistry of defects

In many catalytic surface chemical reactions the structure of the metal substrate has been shown to exhibit an influence on reaction rates and the types of surface chemical species present during reactions. These differences in surface chemistry have been attributed to defects on the surface, such as atomic steps and kinks, where low-coordination number metal atoms exist. These metal atoms on the surface bind atoms and molecules more strongly than those in the close-packed planes of the surface.[1,2]

The approach used in this research has been to obtain a molecular level understanding of the chemistry of these surface defects through the study of model metal catalyst surfaces, such as single crystal metal surfaces, investigated in controlled environments. The use of single crystal surfaces allows for a wide range of surface analytical techniques to be employed where the scattering of electrons and ions from the surface can be used to obtain information about the structure, bonding, and interactions of atoms and molecules on the surface. Most surface chemical reactions have been

investigated on the close-packed face-centered cubic (111) and (100) surfaces which ideally have no atomic steps, but have been shown by scanning tunneling microscopy (STM) to typically exhibit atomic steps spaced by 100-400 Å flat terraces. So even these "flat" surfaces have large concentrations of step defects on the surface which can do chemistry. A clear example of the enhancement of chemical activity by step defects is found in H-D exchange studies on Pt surfaces made by molecular beam scattering experiments. In these experiments it was found that for densely stepped surfaces the H-D reaction probability approached unity. Experiments made on well prepared defect free Pt(111) surfaces however, found that the reaction probability dropped below the detection limit of the experiment of 10^{-3}. [3] Another clear example of the role of surface steps as enhancers in surface catalytic reactions is acetylene heterocyclization to thiophene on sulfided Pd(111). In this work the step density on the sulfided surface increases with annealing temperature. The increase in the step density was found to scale 1:1 with the yield of thiophene formed on the surface. [4]

In the research presented here the surface chemistry of stepped surfaces such as the face-centered cubic (110), (311) and vicinal (111) surfaces (figure 1.2) has been investigated. In particular two surface chemical reactions have been studied since these are the most well known of all surface reactions. First, the oxidation of CO to CO_2 over Rh and Pt surfaces, and second the dehydrogenation of ethylene over Rh. CO oxidation is an important reaction that occurs readily on Rh surfaces and is found in the catalytic converter of every automobile. The basic processes in ethylene dehydrogentaion are found in many reforming reactions. These reactions have been investigated using a full range of surface analytical techniques to elucidate the structure and reactivity of atomic and molecular adsorbates on densely stepped surfaces.

The work presented here is organized into a general introduction of all of the experimental and theoretical methods applied, followed by the detailed results of the work, concluding with an overview of surface chemical bonding. The separate chapters contain

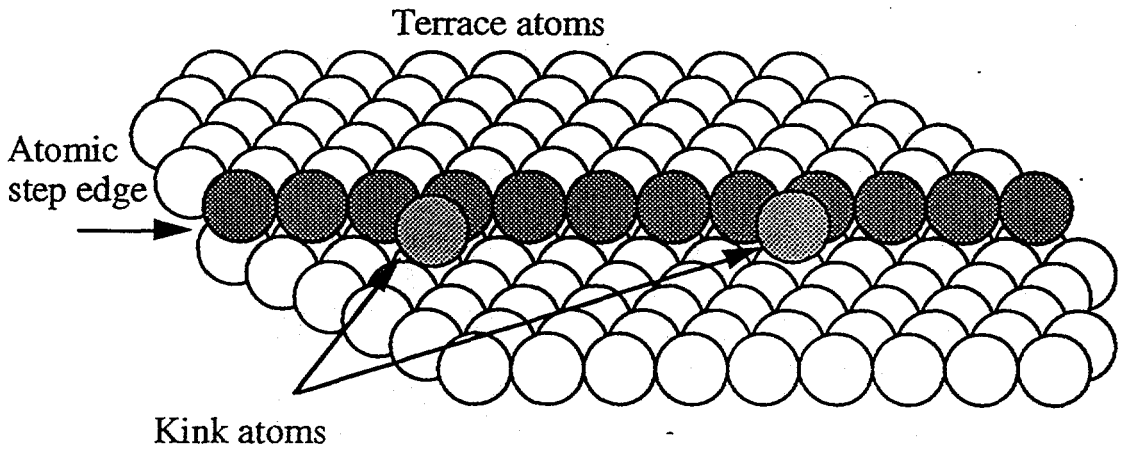

Figure 1.1: Perspective view of an fcc(111) surface indicating the terrace, atomic step, and kink atoms on the surface.

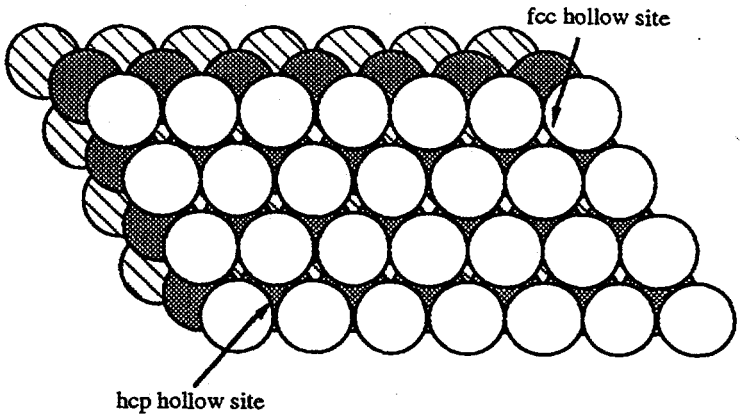

fcc (111) surface

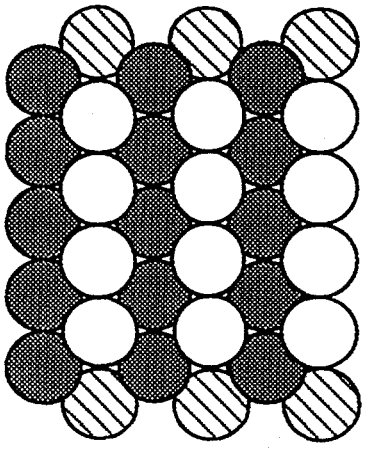

fcc (110) surface

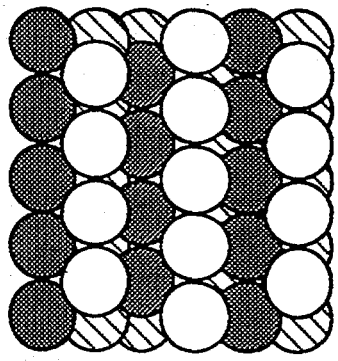

fcc (311) Surface

Figure 1.2: Hard sphere models of the face-centered cubic (111), (110) and (311) surfaces.

the details for each experiment, such that each chapter can be read independently. Chapter 2 contains a summary of the experimental methods used, including a brief overview of surface structure determinations using automated tensor LEED structure analysis. Chapters 3 and 4 detail the bonding of CO and oxygen on the Rh(110) surface, at saturation coverages, as determined by automated tensor LEED. The chemisorption of oxygen and CO on the Rh(311) surface are next discussed in Chapters 5 and 6. Their interactions are described in Chapter 7, incorporating the structural details for oxygen and CO bonding on Rh from Chapters 3 - 6, to develop a picture of the reaction dynamics on these open surfaces. Chapter 8 moves to examine ethylene decomposition on the open Rh(311) surface as compared to the less densely stepped Rh(331) and (111) surfaces. Chapter 9 provides the details of *in situ* surface structure changes that occur on a vicinal Pt(111) surface under coadsorption of S and CO, describing the first observed coadsorbate induced restructuring of a metal surface. The interaction of the restructured surface with oxygen is also described. Finally in Chapter 10 an overview of the current understanding of surface chemical bonding is reviewed.

1.2 Summary of results

The overall conclusions of this work are summarized as follows. Stepped surfaces are found to provide unique adsorption geometries on the surface where the metal sites can modify the local bonding of adsorbates. These modifications allow for enhancement of decomposition processes as well as accommodation of relative geometries between adsorbed species which make intimate interactions possible that cannot occur on flat surface terraces. The step edges are also found to be very "flexible" in that they appear to readily restructure with the adsorption of atoms and molecules. This makes the steps sites "active" in the bonding and reactions occurring on surfaces.

The work on CO oxidation over Rh(311) and ethylene dehydrogenation on Rh(311) point to the highly reactive nature of the such densely stepped surfaces. The formation of CO_2 and the decomposition of ethylene have been found at temperatures much lower than those observed on relatively flat surfaces (lower defects densities). While in this work these chemical changes have been explained primarily from the standpoint of the geometric influence of the surface steps, much work remains to be done on the electronic influences of surface defects in their chemistry. The concluding work which moves towards examining model catalyst surfaces under "real" catalytic conditions shows that extreme changes can occur at step edges. The massive transport of material observed at the Pt step edges under CO and sulfur coasdorption was not expected based on any of the previous knowledge of these systems from typical ultra-high vacuum studies of stepped Pt surfaces. This work points to the necessity of *in situ* measurements of surface structure before, during and after any surface modifications. It is this *in situ* work that will lead to the next breakthrough in our understanding of surface chemistry.

1.3 References

[1] *Introduction to Surface Chemistry and Catalysis,* G.A. Somorjai, Wiley, 1994.

[2] *Chemsitry in Two Dimensions, Surfaces,* G.A. Somorjai, Cornell University Press, 1979.

[3] T.H. Lin and G.A. Somorjai, J. Chem. Phys. 81 (1984) 704.

[4] A.J. Gellman, J.C. Dunphy and M. Salmeron, Langmuir 8 (1992) 534.

Chapter 2

Experimental Methods

The study of surface chemistry requires detailed knowledge of the structure and composition of surfaces at the atomic level. A wide variety of surface sensitive techniques have been developed over the last 25 years to allow these properties to be probed. Since often no one technique can be used to answer all of the questions about a surface chemical reaction, surface chemists employ a combination of methods to develop a complete picture of the processes occurring on surfaces. The methods used in the work to be presented will be briefly described here. Various ultra-high vacuum systems were used, but only the uses of ultra-high vacuum will be described. This will be followed by sample preparation methods and an overview of the surface analytical techniques used in this work. These techniques include Auger electron spectroscopy (AES), low-energy electron diffraction (LEED), temperature programmed desorption (TPD), high-resolution electron energy loss spectroscopy (HREELS), X-ray photoelectron spectroscopy (XPS), and scanning tunneling microscopy (STM). Detailed surface structures have been determined using fully-dynamical low-energy electron diffraction structure calculations, automated tensor LEED (ATLEED).

2.1 Ultra-high vacuum

In this work a variety of ultrahigh-vacuum systems were employed to examine the properties of the surface under investigation. The majority of surface science studies are done under ultra-high vacuum conditions (pressures of $< 10^{-9}$ Torr) for two main reasons. First, since electrons interact strongly with matter they are inherently surface sensitive. Electrons in the energy range of 1-1000 eV interact with only the top 100 Å of the surface as shown in figure 2.1. Thus much surface information can be obtained from electron spectroscopic techniques which scatter or diffract electrons from surfaces. However, in order to utilize these methods, the mean-free path of the electrons used must be large enough to leave the electron source, interact with the surface, and return to the detector to be analyzed. This is achieved under ultra-high vacuum conditions where the mean free path of electrons in vacuum approaches 10^7 cm. The second reason is that operating under ultra-high vacuum conditions allows for the surface composition to be accurately controlled. Under ambient conditions of 760 Torr of gas at 300 K, surfaces are covered by a variety of contaminants. Only under ultra-high vacuum conditions can the surface composition be controlled to within 1%, as it will require on the order of 1 hour for a single monolayer ($\sim 10^{15}$ atoms or molecules/cm^2) of a species to cover the surface from the gas phase (assuming a constant sticking probability of unity).

In order to obtain ultra-high vacuum conditions in the experiments described a variety of pumps have been used. These include mechanical pumps, adsorption pumps, turbo molecular pumps, oil diffusion pumps, and ion pumps. A review of these pumps can be found in a variety of surface science texts, however the laboratory book Experimental Physical Chemistry [1] proves a nice concise review of these vacuum techniques. Each of the vacuum systems were initially evacuated with either mechanical pumps or adsorption pumps to bring the chamber pressure down to the 10 mTorr range.

The systems could then be further evacuated with either a turbo molecular pump or an oil diffusion pump. These pumps would typically bring the chamber pressure down to the 10^{-7} Torr range. Final evacuation to ultra-high vacuum was accomplished by ion pumps, which are very clean since they have no oil, and quiet since they contain no moving parts. The ion pump would bring the chamber pressure to $< 5 \times 10^{-10}$ Torr after baking the chambers at 150°C for approximately 40 hours. Baking of the ultrahigh vacuum systems was always required so as to remove residual water and hydrocarbons from the walls of the stainless steel chambers.

2.2 Sample preparation

2.2.1 Single crystal surfaces

In order to have control over surface structure and composition, single crystal metal samples of 99.999% purity are used. All of the crystal samples used were on the order of ~ 1 cm in diameter and 2-3 mm in thickness. The samples were prepared by spark erosion from oriented single crystal boules. The surfaces were cut to within 1° of the desired crystallographic orientation as determined from Laue X-ray back-reflection. The samples were polished to a mirror finish, first with SiC polishing papers, followed by polishing in Al_2O_3 slurry or diamond pastes ranging from 6 μm to a finish of 0.03 μm. These sample were then introduced into an ultrahigh vacuum system for sample cleaning to prepare atomically clean surfaces (contamination < 5% of a monolayer).

2.2.2 Sample Cleaning

Although all of the metal single crystal samples used were of high purity, the residual contamination, in the crystal bulk, and from polishing, can sometimes segregate

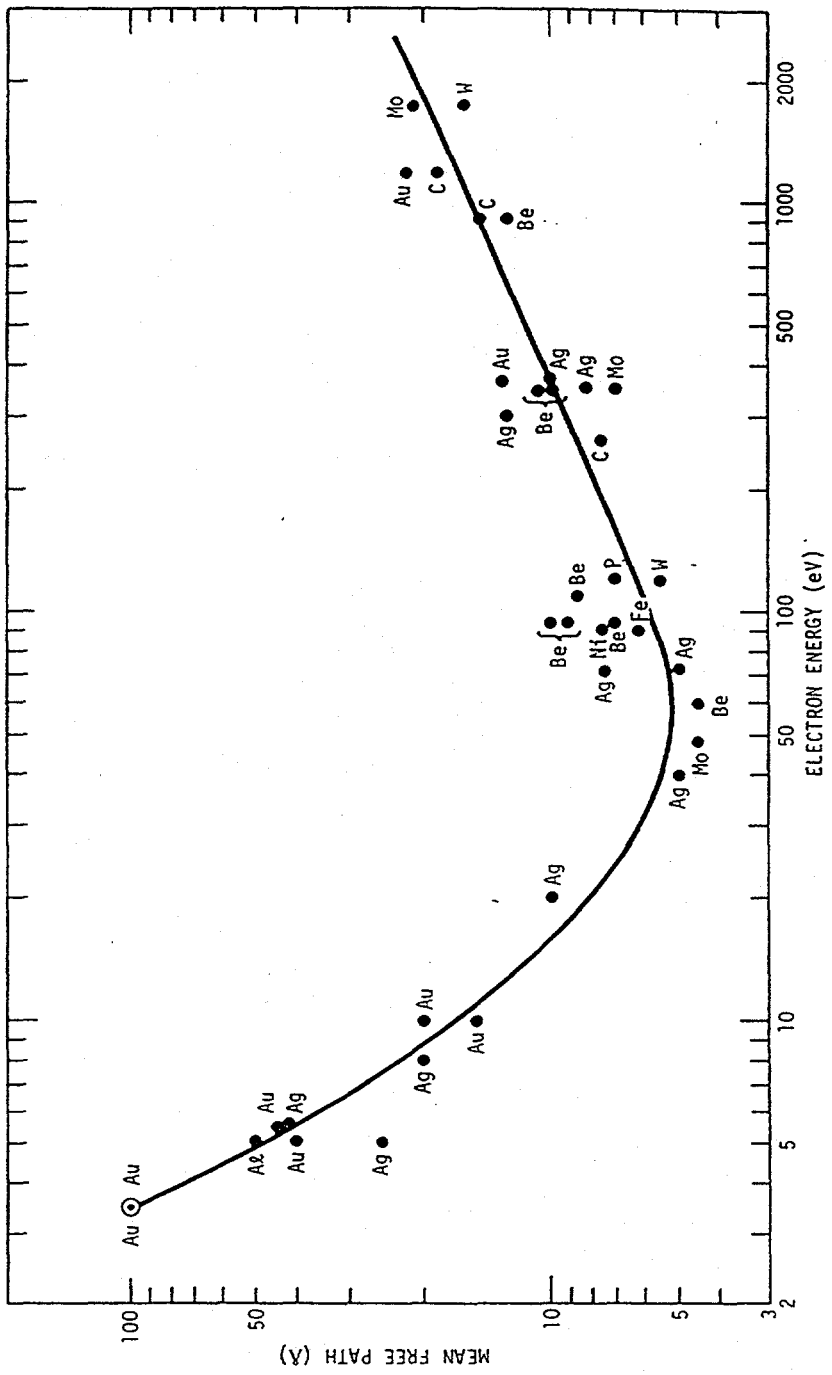

Figure 2.1: The mean free path of electrons in a material as a function of electron energy.

tto the surface during heating. In order to remove this residual contamination, the oriented and polished surfaces are cleaned by a combination of Ar ion sputtering and thermochemical treatments to remove bulk contaminants near the surface region.

The samples are mounted by spot welding the crystal onto a sample manipulator or sample car, where the crystals could be heated by passing current through the samples (~ 20 A) or by electron bombardment. Temperature measurements were made with type K (chromel-alumel) thermocouples formed by spot welding 0.005" chromel and alumel wires together and placing the junction at the sample. This allowed the sample temperatures to be monitored between 77 K and 1500 K.

In the Rh samples, the major contaminants were found to be B, C, and S. The most promising cleaning method appeared to be heating the samples first in 10^{-4} Torr of H_2 for several hours at 1000 K. This seemed to remove most the bulk contamination. This was followed by Ar sputtering at 10^{-4} Torr for 30 minutes to 1 hour at 300 K followed by oxygen cleaning at 5×10^{-7} Torr and 600 K. After a few days, the surfaces were found to be free of contaminants, and required only daily cleaning in O_2 and annealing in vacuum to maintain good surface conditions.

In the Pt samples the major contaminants were found to be C, S, Si, and Ca. These surfaces were harder to clean than the Rh surfaces. Ca and Si could only be removed by Ar sputtering at 10^{-4} Torr for 30 minutes to 1 hour at 300 K. C and S could easily be removed by annealing the crystal in O_2 at 5×10^{-7} Torr and 900 K. Once cleaned the samples would remain free of Ca and Si for typically 1 to 2 weeks, after which further sputtering and annealing of the sample was required.

2.3 Auger Electron Spectroscopy

Auger electron spectroscopy is utilized as a tool for the determination of elemental surface composition and concentrations of species at the surface. The technique employs a

monoenergetic beam of electrons on the order to 1500 eV which is used to excite core level electrons in a material. The ejection of the core level electrons leads to relaxations of higher level electrons resulting in both X-ray fluorescence and secondary electron emission via the Auger process. In the Auger process, shown schematically in figure 2.2, incident electrons excite the loss of a core level electron. A higher energy electron then decays to the to the energy level of the excited electron, and either releases energy via a photon (X-ray fluorescence) or transfers energy to a higher level, secondary electron, which is also ejected. These transitions are specific for each element and thus an energy analysis of the ejected secondary electrons may be used to obtained the elemental composition of the surface. The spectroscopy is surface sensitive due to the low mean free path of electrons in materials, as described previously. This technique can be used to determine concentrations of a given species on a surface to within 5 % of a monolayer. A typical Auger spectrum for a dirty Rh sample is shown in figure 2.3. The Rh transitions, a S transition, and an O transition are indicated. The spectra are plotted as the derivative of the number density per unit energy (dN(E)/dE) so as to be able to distinguish the Auger electrons from the normal secondary electron background present.

The saturation coverages of species on surfaces may be determined by the use of an Auger uptake curve. In this experiment, the relative peak ratios of a given species, such as C, with respect to the metal is measured as a function of exposure. This can also allow for a determination of the saturation coverage of the species on the surface. [2]

2.4 Low-energy electron diffraction (LEED)

Almost half of the detailed surface structures known have been obtained from the dynamical analysis of low-energy electron diffraction (LEED) data from single crystal surfaces. When electrons are scattered from a surface they interact only with the top few atomic layers of the material due to the strong interactions between electrons and matter.

Auger Electron Spectroscopy

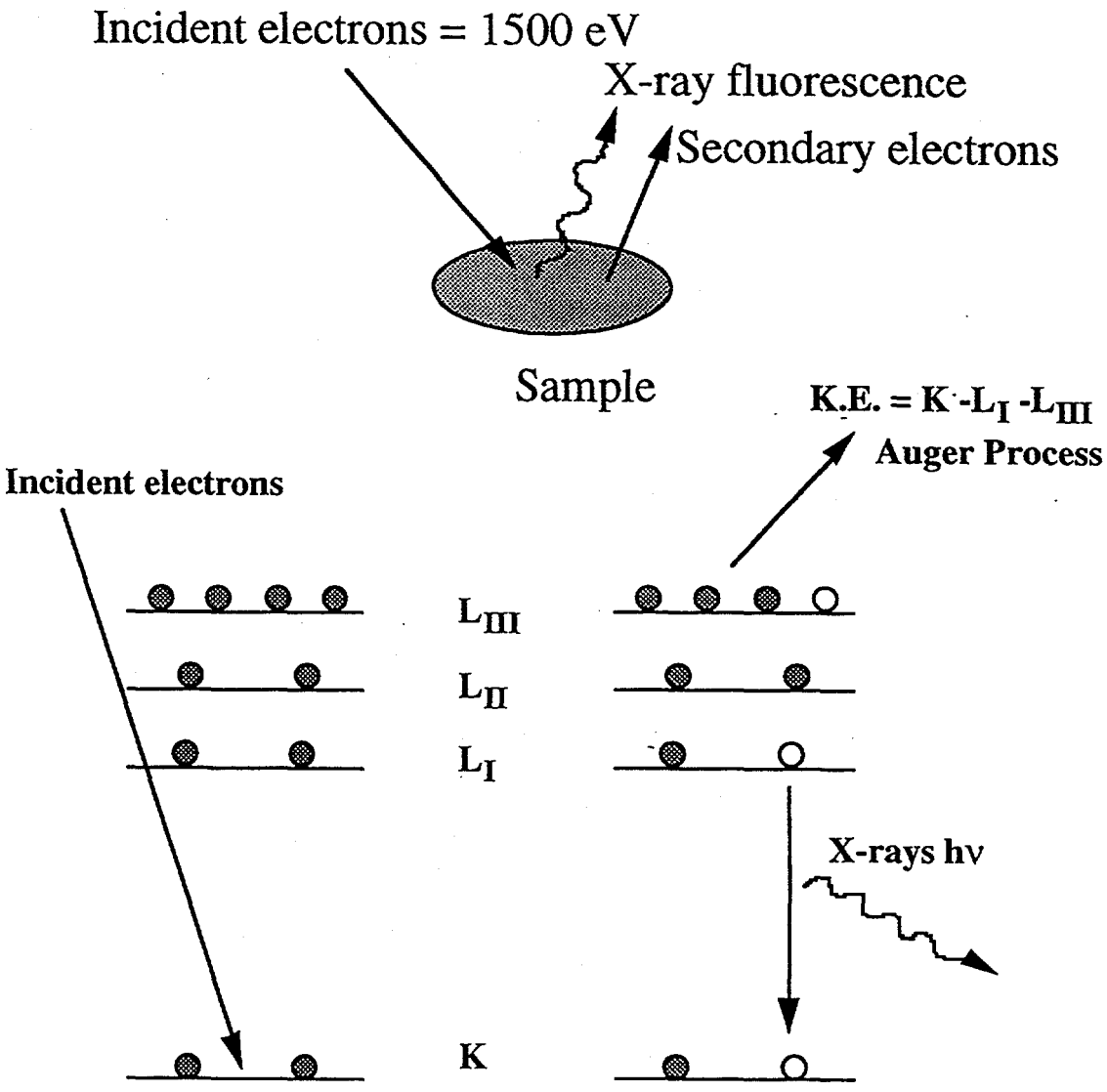

Figure 2.2: Schematic of the Auger process.

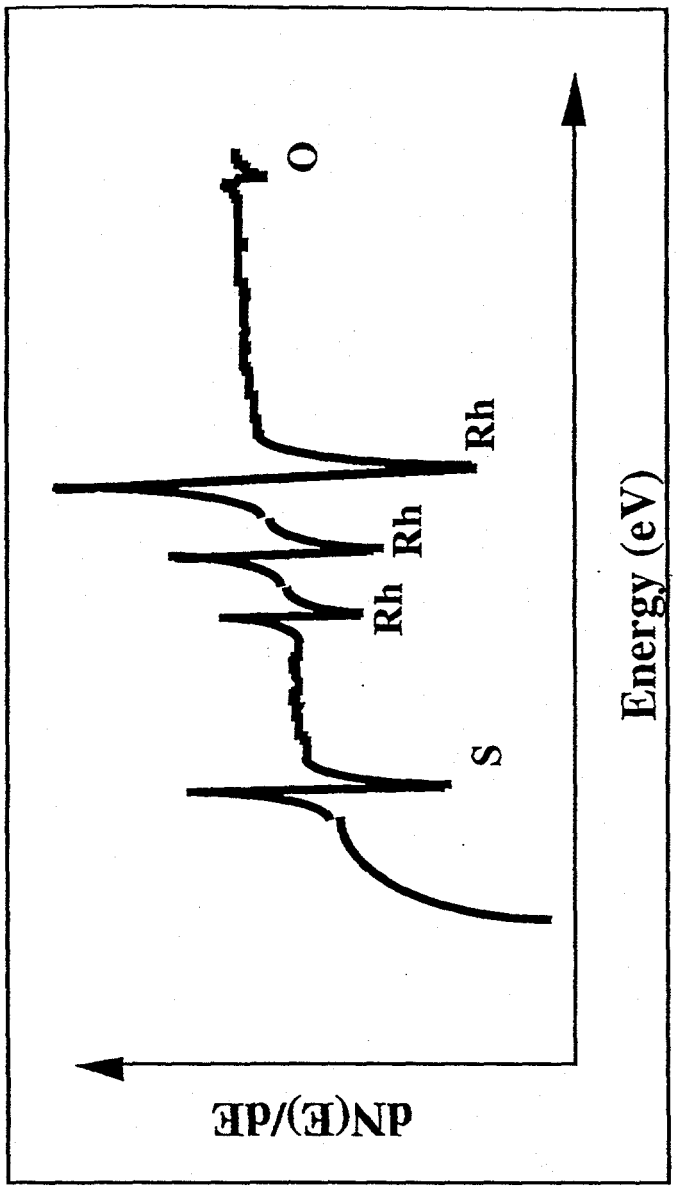

Figure 2.3: An example Auger spectrum of a contaminated Rh sample showing the S, Rh and O transitions.

This interaction makes electrons useful probes of the structure of surfaces. Electrons in the range of 30 to 200 eV have de Broglie wavelengths comparable to the lattice spacings in crystals. By scattering low-energy electrons from well ordered single crystals, diffraction patterns may be obtained. The diffracted beam intensities as a function of energy contain information on the surface structure. The surface structure may be determined by fitting a theoretical model to these experimental intensity vs. energy (I-V) curves.

The current state-of-the-art experimental approach involves two different experimental methods for the detection of diffracted electrons, the "video-LEED" technique and the "digital-LEED" technique. The "video-LEED" technique used in the work presented here, is shown in figure 2.4. Electrons are backscattered from the single crystal sample and passed through energy selecting grids which allow only the elastically scattered electrons to pass through. The electron impacts are monitored on a fluorescent screen where the diffraction pattern is observed. This pattern is then recorded by a high sensitivity video camera and digitized by a computer. The electron beam energy is varied over a given energy range with images collected every 2-3 eV. From these images the integrated intensities as a function of energy for various diffracted beams may be measured to produce experimental I-V curves as a database for structure calculations.

I-V spectra may also be used as a "fingerprinting" technique to obtain qualitative structural information without a detailed calculation. [3-5]. This is due to the local site dependence of the diffraction process, the adsorption site may be inferred for surface structures that have the same local environment but different chemical nature or different long range ordering. For example the I-V curves for O adsorbed in a 3-fold hollow site on a metal surface will look similar to C adsorbed on the same surface in the same site.

Low-Energy Electron Diffraction: (Surface Structure)

Electron Energy = 30 - 200 eV

1. **de Broglie $\lambda \sim$ lattice spacing**
2. **Surface sensitive**

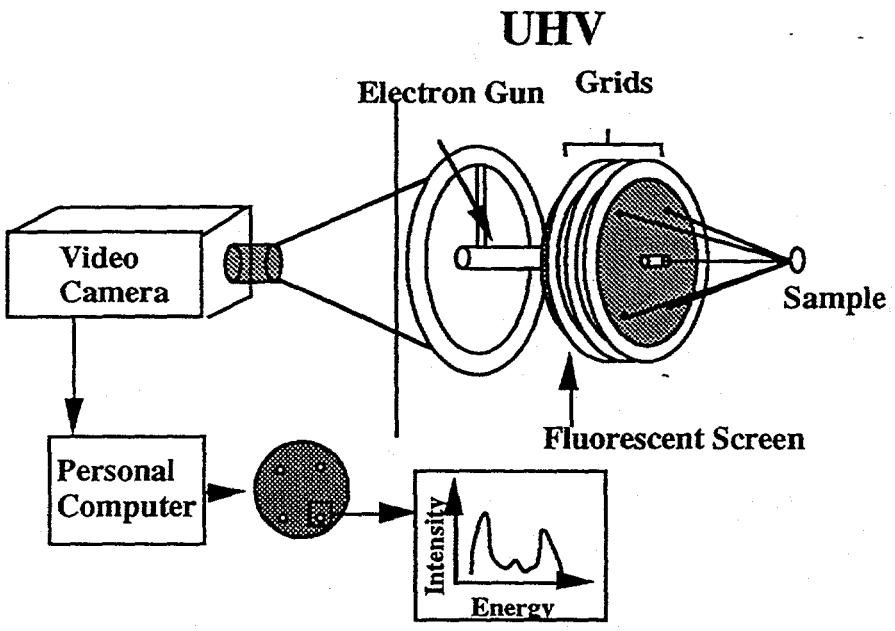

Figure 2.4: Schematic of the video-LEED data acquisition system.

2.4.1 Automated tensor low-energy electron diffraction (ATLEED)

The modeling of the surface structure to obtain bond lengths and bond angles requires a fully dynamical LEED intensity analysis of experimental LEED I-V curves. The details of the surface structure are contained in these I-V curves; however no direct method of obtaining this information is available as in X-ray crystallography, due to the strong electron-atom interactions which cause complex multiple scattering events within the surface. To obtain structural information from electron diffraction data the exact scattering paths of the electrons must be calculated for a series of model structures producing theoretical I-V curves. These models are based upon the symmetry of the LEED pattern, and any information available from other techniques. The I-V curves for these structures are calculated and compared to experiment, with the best agreement identifying the best fit structure.

Different methods of calculating theoretical I-V curves have been described in several books on LEED. [6-8] The fit between experiment and theory is quantified by a reliability factor (R-factor). Various R-factors may be employed to measure the goodness of fit between peak position, intensity, or average deviation. A recent advance to this analysis is automated tensor LEED (ATLEED). This is a perturbative process which couples the R-factor to an automated search routine. With this method a "structural space" within 0.3-0.4 Å of a calculated reference structure may be rapidly searched to find the best fit structure for the given experimental data. The process for the structure determination is outlined in figure 2.5. Several recent papers describe this approach in detail.[9-11]

2.5 Temperature programmed desorption (TPD)

The technique of temperature programmed desorption (TPD) allows for the desorption kinetics of adsorbed overlayers on surfaces to be examined. Using this

Solving a Surface Structure: The Tensor LEED Approach

$I = [A]^2$

$I = [A + \delta A_o]^2$

$\delta A_o \sim \delta r_{ij}$

1. Collection of experimental I-V data.
2. Calculation of a reference geometry.
3. Search over structural space (0.30-0.40Å).
4. Re-calculate the search result to check stability.

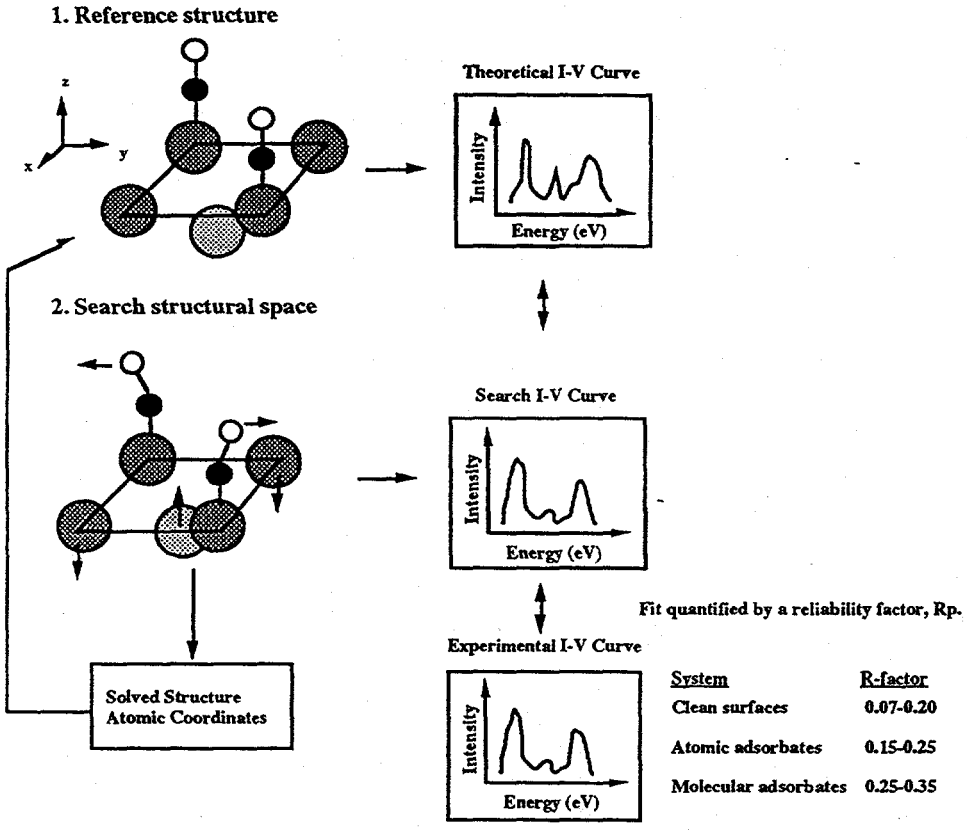

Figure 2.5: In the automated tensor LEED approach to surface structure determinations, changes in the diffracted beam amplitudes are to a first approximation linearly related to changes in the atomic positions of the model calculation. The theoretical I-V curves are fit to the experimental I-V curves, with the fit quantified by a reliability factor (R-factor). Typical Pendry R-factors (Rp) for various systems are shown. The resulting search structure is re-entered as a reference calculation to check the stability of the solved structure.

technique the concentrations of adsorbed overlayers, interactions between adsorbed species, the binding energies of adsorbed atoms and molecules, as well as surface chemical reactions may be examined. In this work, TPD experiments were carried out by monitoring gases desorbed from the surface with a UTI 100 C quadrupole mass spectrometer, as the surface temperature is linearly increased at a rate between 10-25 K/s. The single crystal surface was positioned with the surface normal perpendicular to the mass spectrometer, approximately 2 -3 cm from the ionizer of the mass spectrometer. For TPD experiments carried out in the limit of rapid pumping, the desorption rate is proportional to the mass spectrometer signal detected. The rate of desorption of a given species is then plotted as a function of temperature giving a thermal desorption spectrum. It has been shown [12] that from the desorption spectrum , the binding energies of the adsorbed atoms and molecules on the surface may be related to the temperature at the peak rate of desorption. For a first order process, the peak desorption temperature is independent of surface coverage.

$$E_d/RT_p^2 = (A_1/\beta)\exp(-E_d/RT),$$

where E_d is the desorption energy, R the molar gas constant, T_p is the peak temperature of desorption, A_1 is the pre-exponential for desorption, and β is the heating rate. For a second order process, the desorption is dependent on the surface coverage, as shown by

$$E_d/RT_p^2 = (A_2/\beta)\Theta\exp(-E_d/RT),$$

where is the A_2 is the second order pre-exponential, and Θ is the surface coverage.
In this work, the upper limits for the energies of surface chemical reactions could also be determined using this technique. [12]

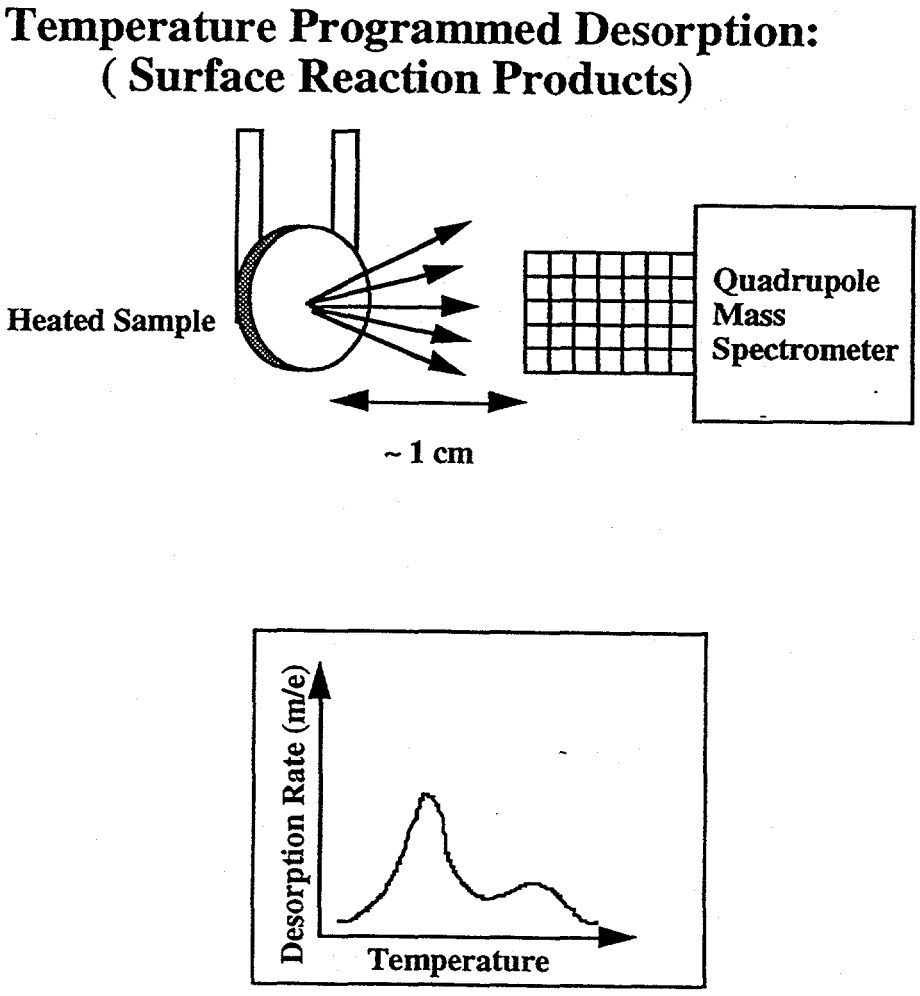

Figure 2.6: Schematic of the temperature programmed desorption experiment.

2.6 High-resolution electron energy loss spectroscopy (HREELS)

By analyzing the energy losses from low-energy electrons (1-5 eV) scattered from surfaces the vibrational modes of adsorbates can be examined to aid in the determination of atomic and molecular species present on the surface and their structure at the surface. This technique is described in detail by H. Ibach and D. Mills in their classic book on HREELS. [13] A schematic of the HREELS method is shown in figure 2.7. The incident electrons are scattered from the surface and detected in the specular direction. In the experiments to be described, these electron were scattered at an angle of 55° from the surface plane. The advantage of the HREELS technique over other surface vibrational techniques is the ability to observe all of the vibrational modes for a given species on a surface. The interpretation of HREELS spectra comes through the understanding of the electron scattering mechanisms probed by the HREELS technique. These can be broken down into long range (10-100 Å, dipole scattering) and short range (direct scattering) interactions with the surface.

The long range interaction is dominated by the interaction of the electrostatic potential of the incoming electron with the dynamic dipoles of each vibrational mode. This dipole scattering leads directly to the "surface dipole" selection rule for surface vibrational spectroscopy. This selection rule requires than some component of the modes dipole moment be perpendicular to the surface. If the dipole moment is parallel to the surface then this dipole is screened by its image dipole in the metal surface. Thus only vibrational modes with a component of their dipole perpendicular to the surface may be detected by this method. Also, only vibrations which belong to totally symmetric representations (A_1, A and A') are usually found in the specular directions.

The short range interaction is referred to as impact scattering. In this mechanism the electron interact with the charge densities of the atoms on the surface, much as in

Electron Energy Loss Spectroscopy: (Surface Vibrational Spectra)

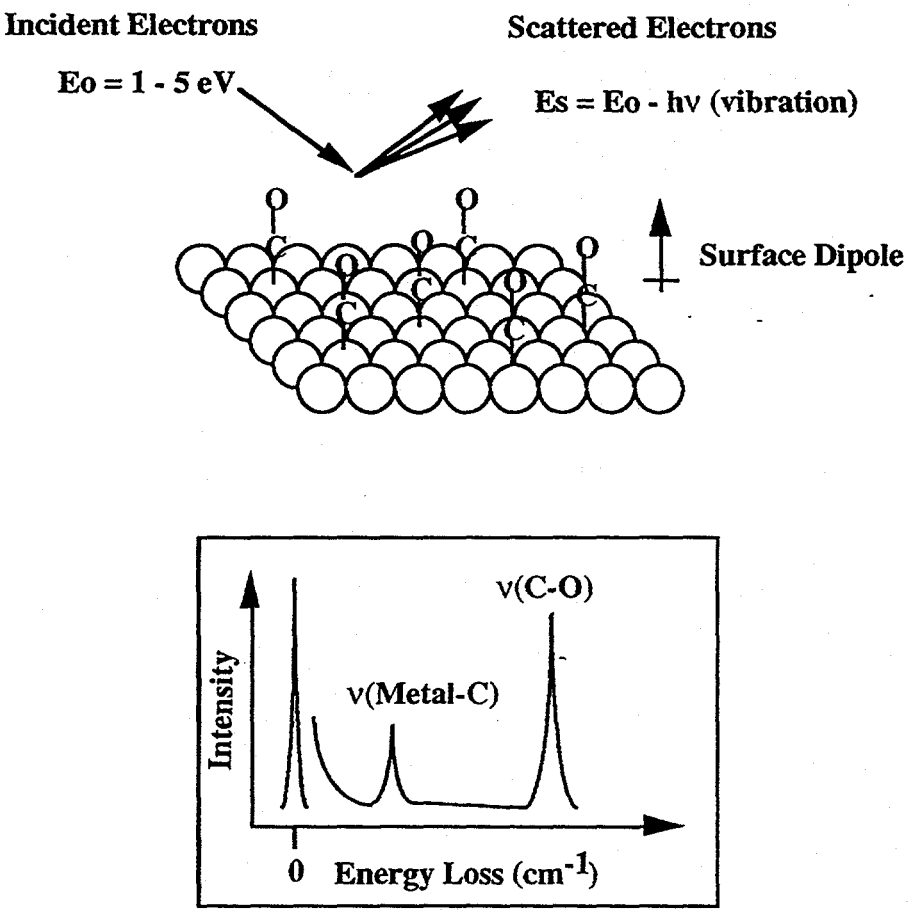

Figure 2.7: Schematic of the high resolution electron energy loss experiment.

LEED. This scattering mechanism may be distinguished from the dipole scattering mechanism by examining the angular dependence of the intensities of the vibrational modes. Modes that appear via the dipole scattering mechanism exhibit a strong angular dependence (typically decay to the noise level by angle >15° off-specular) and their intensity as a function of scattering angle scales with the change in elastically scattered intensity as a function of angle. The modes that are due to impact scattering are highly isotropic and their intensities thus vary little as a function of angle.

2.7 X-ray photoelectron spectroscopy (XPS)

X-ray photoelectron spectroscopy (often referred to as electron spectroscopy for chemical analysis, ESCA) allows for the identification of different chemical species (surface composition) and their local electronic environments (such as oxidation state) on surfaces. In this technique X-rays are generated via the excitation of electronic transitions in a Mg anode. The X-rays emitted by these specific transitions have a narrow lineshape and are of a specific energy. The emitted X-rays are then used excite core level electronic transitions in a sample and electrons emitted from the sample are collected by a concentric hemispherical analyzer. The electrons are emitted based on the follow relationship:

$$B = h\nu - K - \phi_S,$$

where B is the binding energy of the electron, hν is the energy of the incident X-rays, K is the kinetic energy of the emitted electron and ϕ_S is the work function of the spectrometer. The number density of electrons per energy, N(E)/E, are measured as a function of kinetic energy or binding energy to produce the photoelectron spectrum. [21]

In this work XPS studies were made a PHI 5400 ESCA. The ESCA chamber is attached to a sample preparation chamber equipped with electron beam heating and variable

leak valves for gas introduction. A transfer arm is then used to move the sample under vacuum (7 X 10^{-10} torr) into the XPS chamber for analysis. In the studies to be presented, the MgKα line (1253.6eV) was used as the excitation source, run at 15 kV and 400 W power. The pass energy of the CHA was varied between 127.5 eV during survey scans (binding energies 0-1200 eV) to 8.95 eV for high resolution scans of < 30 eV width, which allowed for a resolution of 0.22 eV.

2.8 Scanning tunneling microscopy (STM)

The scanning tunneling microscope (STM) allows for the direct imaging of surface structure at the atomic level. The technique utilizes the principles of electron quantum mechanical tunneling between a sharpened metal tip, with a radius of curvature of approximately 1000 Å, and a conducting substrate to produce a measurable tunneling current (~ 1 nA) which is supplied to a feedback loop to maintain a constant tip-sample separation. Under these conditions, the tip may then be rastered over the surface to produce a map of the charge density topography of the surface from which surface structure may be deduced. [14-17]

The motion of the tip with respect to the surface is controlled with Ångstrom resolution through the use of piezoelectric materials (Pb-Zirconate-Titanate). A schematic of the basic parts of a scanning tunneling microscope is shown in figure 2.8. A tip typically made from either cut Pt(70%)/Rh (30%) wire, or oriented W wire is mounted on a sectored piezoelectric transducer. This sectored piezo allows for the precise motions of the tip to be made by applying voltages to the different piezo sectors. In this way the tip may be scanned over the surface while maintaining the tip within tunnel range of the surface (< 10 Å).

In this work the microscope was operated in two different scanning modes (figure 2.9) the topographic mode (constant current) and the current mode (constant height).

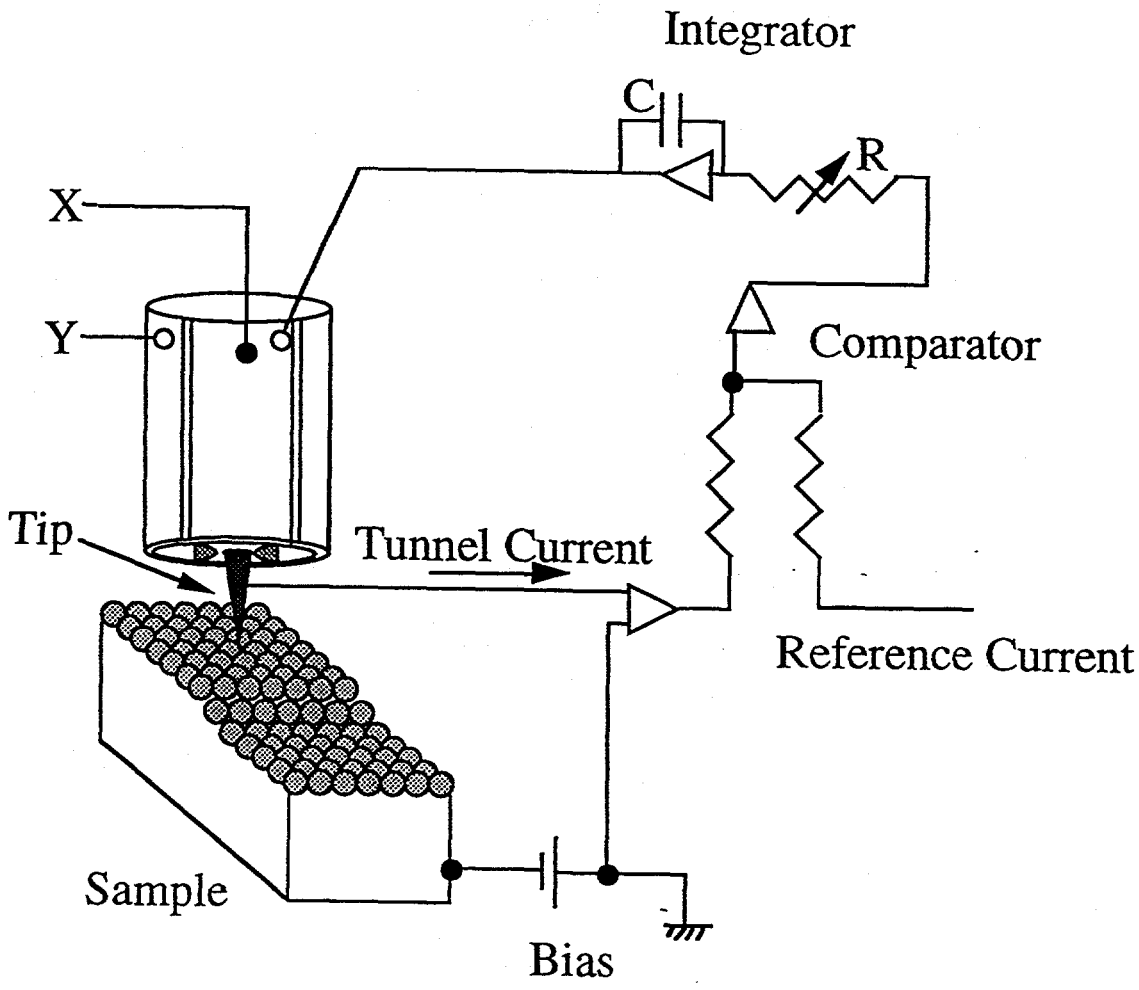

Figure 2.8: Schematic of the basic parts of the scanning tunneling microscope.

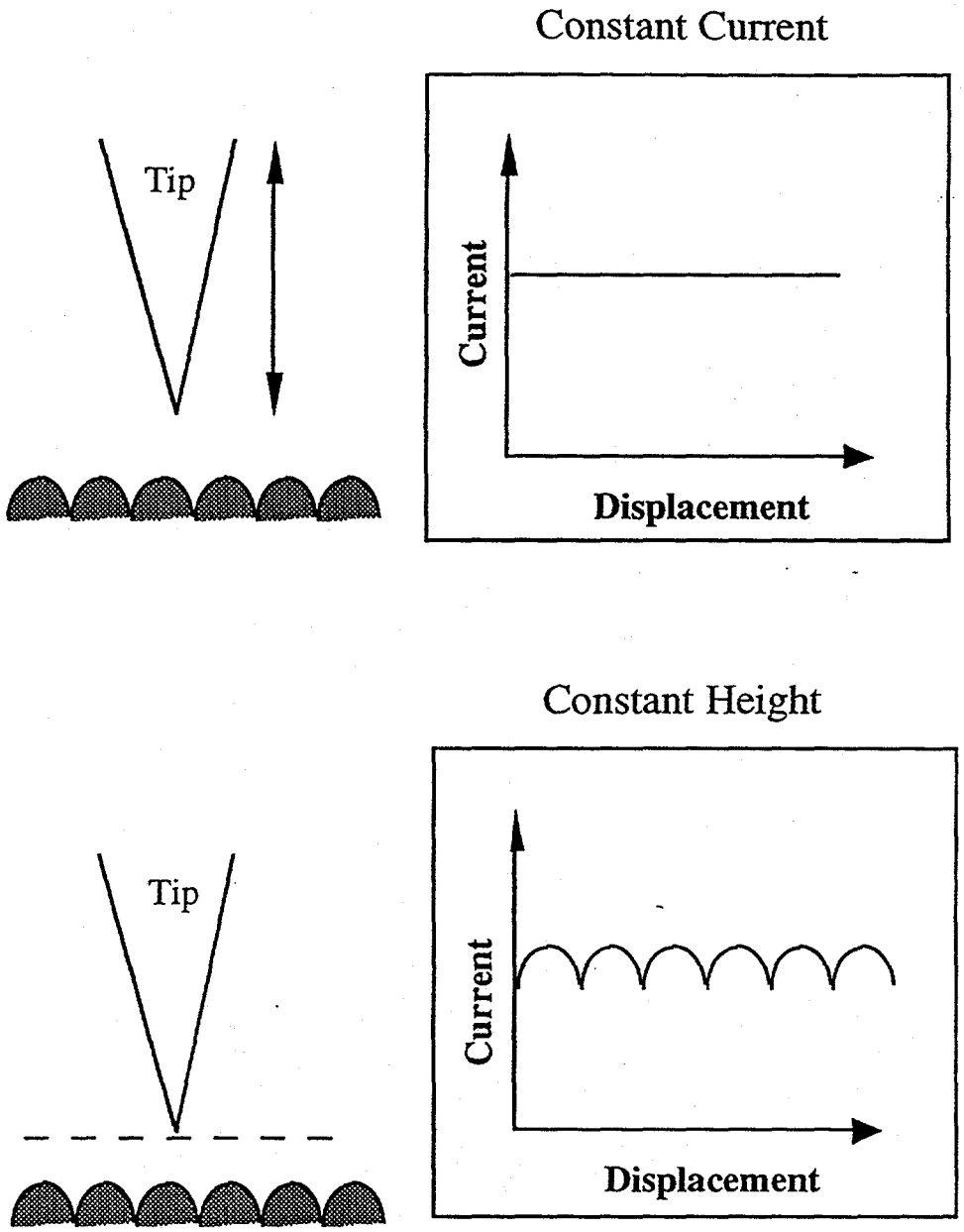

Figure 2.9: The two STM operation modes used in this work, the constant current mode (topographic images) and the constant height mode (current images).

In the topographic mode, the tip height over the surface is varied so as to maintain a constant tunneling current. In this mode the tip height is plotted as a function of the lateral tip position to produce an image of the surface. This method of scanning is slower that the current mode as the tip must be constantly moved towards and away from the surface. In the current mode the tip is positioned at a fixed distance from the surface and scanned at this distance. The current variations are then plotted as a function of the lateral tip position to produce an image of the surface.

The STM is a very versatile tool in that surface may be examined at the atomic level under a variety of conditions of pressure and temperature. This makes the STM useful for the study of surface reactions. The STM also allows for dynamic processes such as surface diffusion and reconstruction to be examined in real time.

The basic principle of operation for the STM involves the exponential decay of tunneling current in the sample-tip gap:

$$I \sim \exp(-2d\kappa),$$

where I is the tunnel current, d is the tip sample distance, and κ is decay length of the electron wavefunction. (figure 2.10) From this relationship, it is found that changes in the tunneling distance of 1 Å varies the tunneling current by approximately a factor of 10. It is this exponential sensitivity of the tunneling current to the tip-sample separation that provide the STM with its high spatial resolution. The microscope has a higher sensitivity to the tip-sample distance (on the order of 0.1 Å) compared to a lateral spatial resolution on the order of 1 Å. This resolution however depends strongly on the tip conditions. The tunneling between the tip and sample occurs at defects on the end of the tip and the images have been shown to depend strongly on the structure and chemical composition of the portion of the tip "active" in the tunneling process.

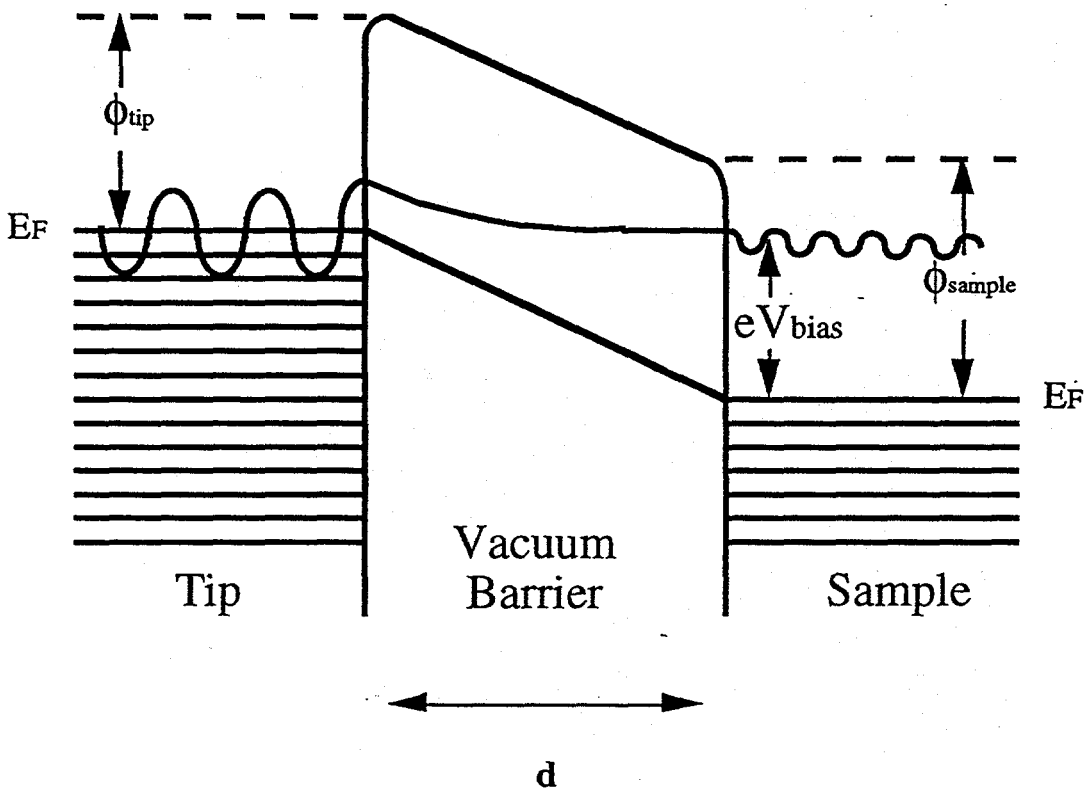

Figure 2.10: One dimensional tunneling barrier between the tip and sample for a positive sample bias. The wavefunction decays exponentially in the gap, d, between the tip and sample.

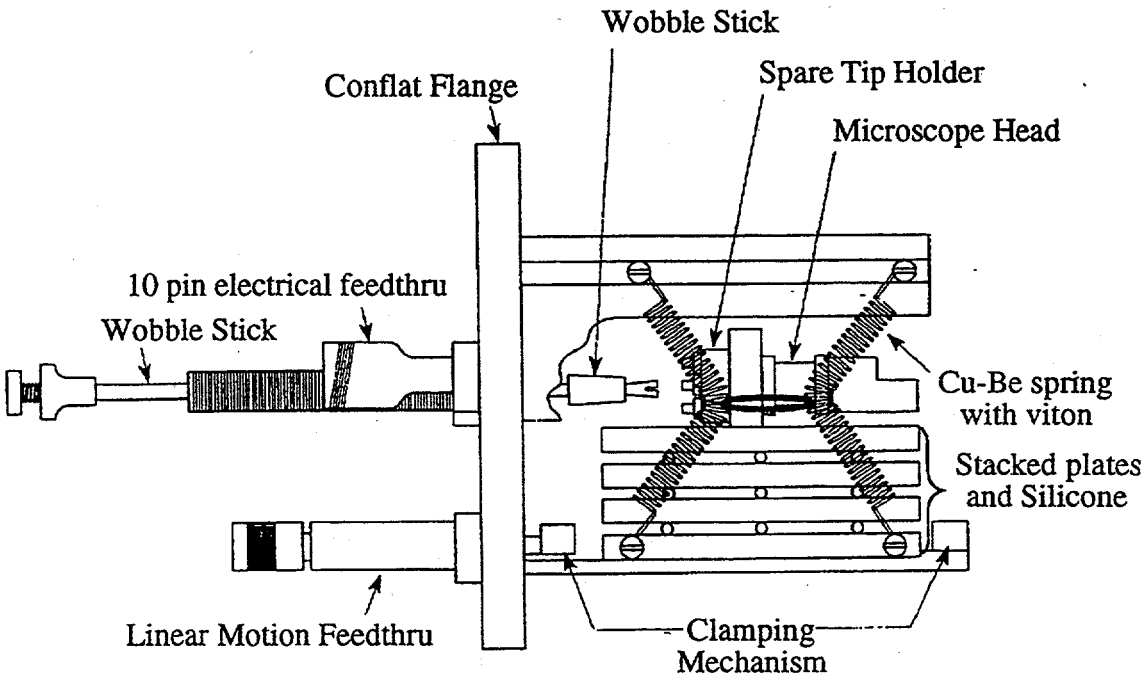

Figure 2.11: Schematic of the scanning tunneling microscope used in this work. The microscope is a double tube design with a large inner piezo which allowed for the tips to be changed in vacuum by using the wobble stick. *In situ* tip cleaning was also available.

Theoretical STM calculations have shown that these differences are a function of the local electronic structure at the end of the tip as well as the surface. [18]

2.9. Appendix I: Surface structure notation

Let us briefly introduce the surface structure notation used in the examples. This notation is covered in detail in several books on surfaces and surface structures. [7,19,20] Surface structures which exhibit the same two-dimensional unit cell periodicity as their bulk structures are referred to as (1x1) structures. The (1x1) refers to the unit vectors of the surface unit cell. These vectors may be written as:

$$\mathbf{a} = m_{11}\mathbf{a}' + m_{12}\mathbf{b}'$$
$$\mathbf{b} = m_{21}\mathbf{a}' + m_{22}\mathbf{b}',$$

where **a** and **b** are the vectors of the primitive reciprocal unit cell. The coefficients may be defined by a matrix:

$$M = \begin{bmatrix} m_{11} & m_{12} \\ m_{21} & m_{22} \end{bmatrix}$$

From this matrix, the surface structure may be expressed in terms of the (1x1) unit cell. Thus for a (1x1) structure, the matrix would be $\begin{bmatrix} 1 & 0 \\ 0 & 1 \end{bmatrix}$. When a new surface periodicity is present, the notation for that structure is given in a format that is referenced to the clean surface unit vectors of the (1x1) surface. For example, an adsorbate structure on the surface which doubles the periodicity of the surface unit vectors in both directions, is then referred to as a (2x2) surface structure, or a $\begin{bmatrix} 2 & 0 \\ 0 & 2 \end{bmatrix}$ structure. (figure 2.12) In some

structures where the surface vectors are related to the clean surface vectors by a translation and a rotation, the structure may be expressed in the form (n x m)R Θ°, where n and m are the vector lengths and Θ is the angle of rotation. For example a structure with a periodicity of $\sqrt{3}$ and a rotation of 30° is expressed as ($\sqrt{3}$x$\sqrt{3}$)R30°.

The nomenclature for atomic an molecular adsorption sites is based upon the coordination of the adsorbate (number of adsorbate-substrate nearest neighbor bonds formed) to the substrate. These bonding sites are referred to as top site, bridge site, 3-fold hollow site, and 4-fold hollow site, for 1,2,3, and 4 nearest neighbors respectively.

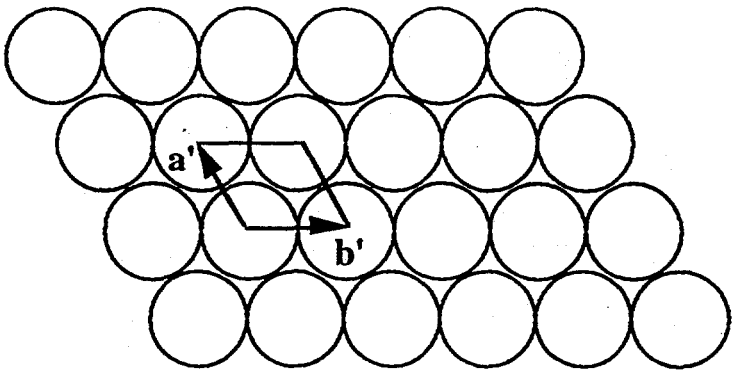

Clean surface (1x1) unit cell

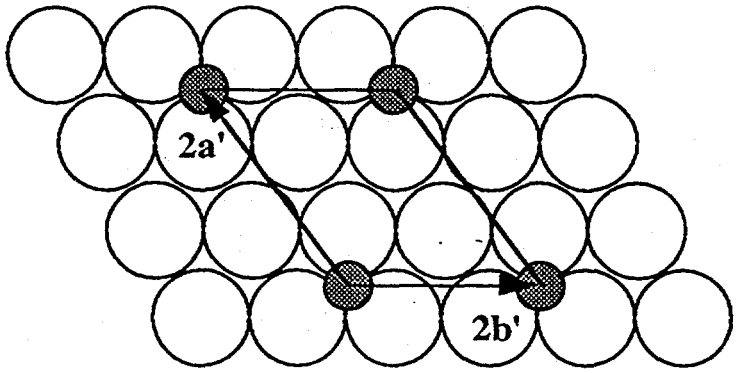

Adsorbate surface (2x2) unit cell

Figure 2.12: The primitive unit cells for a (1x1) and (2x2) surface structure.

2.10 References

[1] *Experiments in Physical Chemistry, 4th ed.*, D.P. Shoemaker, C.W. Garland, J.I. Steinfeld and J.W. Nibler, McGraw-Hill, Inc., 1981.

[2] D.P. Woodruff and T.A. Delchar, *Modern techniques of Surface Sciences*, Cambridge University Press, 1986.

[3] W.S. Yang, F. Jona, and P.M. Marcus, Phys. Rev. B, 27 (1983) 27.

[4] P. Hu, L. Morales de la Garza, R. Raval, and D.A. King, Surf. Sci. 249 (1991) 1.

[5] D.E. Gardin, J.D. Batteas, M.A. Van Hove, and G.A. Somorjai, Surf. Sci. 296 (1993) 25.

[6] J.B. Pendry, *Low-Energy Electron Diffraction*, Academic Press, New York, 1974.

[7] M.A. Van Hove, W.H. Weinberg, and C.-M.Chan, *Low-Energy Electron Diffraction: Experiment, Theory, and Surface Structure Determination*, Springer-Verlag, Berlin, Heidelberg, 1986.

[8] M.A. Van Hove and S.Y. Tong, *Surface Crystallography by LEED: Theory, Computation and Structural Results* , Springer-Verlag, New York 1979.

[9] M.A. Van Hove, W. Moritz, H. Over, P.J. Rous, A. Wander, A. Barbieri, N. Materer, U. Starke, and G.A. Somorjai, Surf. Sci. Rep. 19 (1993) 191.

[10] P.J. Rous, Prog. in Surf. Sci. 39 (1992) 3.

[11] P.J. Rous, M.A. Van Hove, and G.A. Somorjai, Surf. Sci. 226 (1990) 15.

[12] P.A. Redhead, Vacuum **12** (1962) 203.

[13] H. Ibach and D.L. Mills, *Electron Energy Loss Spectroscopy ans Surface Vibrations*, Academic Press, New York, 1982.

[14] G. Binning, H. Rohrer, C. Gerber and E. Weibel, Appl. Phys. Lett. **40** (1982) 178.

[15] G. Binning, H. Rohrer, C. Gerber and E. Weibel, Phys. Rev. Lett. **49** (1982) 57.

[16] G. Binning, H. Rohrer, C. Gerber and E. Weibel, Phys. Rev. Lett. **50** (1983) 120.

[17] G. Binning and H. Rohrer, Rev. Mod. Phys. **59** (1987) 615.

[18] P. Sautet, J. C. Dunphy, D. F. Ogletree, C. Joachim, and M. Salmeron, Surf. Sci. **315** (1994) 127.

[19] *Introduction to Surface Chemistry and Catalysis,* G.A. Somorjai, Wiley, 1994.

[20] *Chemsitry in Two Dimensions, Surfaces,* G.A. Somorjai, Cornell University Press, 1979.

[21] G. Ertl and J. Küppers, *Low Energy Electrons and Surface Chemistry*, Verlag-Chemie, Weinheim, 1974.

Chapter 3

The Bonding of CO on Rh(110)

The structural geometries of both the clean and CO covered Rh(110) surfaces have been determined by a LEED intensity analysis. The clean surface exhibits a top layer contraction of 0.09 ±0.02Å and a second layer expansion of 0.03±0.03Å relative to the bulk interlayer spacing. Upon the adsorption of 1 monolayer of CO the molecules are arranged in a zig-zag fashion along the [-110] direction to produce the observed glide plane symmetry in the LEED pattern. The clean surface relaxations are removed and each CO bonds near a short bridge site with the CO molecular axis oriented approximately 24° from the surface normal. This bonding geometry results in a Rh-C bond length of 1.97±0.09Å and a C-O bond length of 1.13±0.09Å.

3.1 Introduction

In order to obtain a fundamental understanding of surface chemical reactions, a detailed knowledge of the adsorption geometries for the atoms and/or molecules involved is required. The adsorption and reaction of CO on the Rh(110) surface have been the subject of many recent studies due to the catalytic importance of Rh in CO hydrogenation and oxidation reactions. [1-5] The oxidation of CO has been shown to be structure sensitive and to have a higher rate on Rh(110) when compared to the closed-packed (111) surface. [6]

The available structural information for CO adsorption on the (111) and (110) faces of Rh is summarized here. On the Rh(111) surface, from low-energy electron diffraction (LEED), CO forms two ordered structures, a $(\sqrt{3}x\sqrt{3})R30^o$ and a (2x2) structure at coverages of 1/3ML and 3/4ML respectively. Both structures have been examined by dynamical LEED intensity analyses. The $(\sqrt{3}x\sqrt{3})R30^o$ structure consists of CO molecules bonded to top sites with a C-O bond length of 1.07Å and a Rh-C bond length of 1.95Å. [7] In the (2x2) structure the molecules are arranged with one bridge bonded CO and two CO molecules near top sites. All were found to have a C-O bond length of 1.15Å and a Rh-C bond length of 2.03Å. [8] For both of these CO structures however, no metal relaxations were included and no tilting of the CO molecules in the high coverage (2x2) structure was reported. To our knowledge this is the only Rh surface for which a detailed structure for CO is known.

The clean Rh(110)-(1x1) surface is unreconstructed with a relaxation of the top interlayer spacing by -6.9% relative to the bulk interlayer spacing. [9] If CO is adsorbed on the clean (1x1) surface, at a saturation coverage of 1 monolayer, a p2mg(2x1) surface structure is formed as first reported by Marbrow and Lambert in 1977. [10] It was deduced from symmetry that in this structure the CO molecules are arranged in a zig-zag fashion along the [-110] direction on top of the atomic rows to produce the observed glide

plane symmetry in the LEED pattern; however no LEED intensity analysis was performed. A recent study of CO on Rh(110) by X-ray photoelectron spectroscopy (XPS) reports that the CO molecules in this structure are bonded in the short bridge sites. [11] The p2mg(2x1) structure for CO is also formed on the (110) faces of Ir, Ni, Pd, and Pt. [12-15] LEED intensity analyses for CO on Ni(110) [16] and Pd(110) [17] indicate both bridge and top sites respectively with a varying degree of tilt of the CO molecules. On Ni(110) the metal-C plane is tilted by 27° from the surface normal while on Pd(110) this tilt angle is only 11°. From photoelectron diffraction (PED), angle-resolved photoemission extended fine structure (ARPEFS), and surface-extended X-ray adsorption fine-structure (SEXAFS) experiments also for CO on Ni(110) the CO was found to tilt in this structure by 16° to 19°, with linear metal-C-O arrangements. [18-20] The tilting in each of these structures is attributed to intermolecular repulsions in the high density of CO molecules and may be larger on Ni than Pd due to a smaller lattice parameter for Ni.

In this paper we report a LEED intensity analysis for the clean Rh(110)-(1x1) structure and the Rh(110)-p2mg(2x1)-2CO structure. Upon adsorption of 1 monolayer of CO, the relaxations of the clean surface are removed, resulting in an essentially bulk terminated substrate structure. The CO molecules are found to be bonded in the short bridge site with the CO molecular axis tilted by approximately 24° from the surface normal. We will detail the structure analysis and compare these results to those of CO structures on other transition metal surfaces.

3.2. Experimental

All measurements were made under ultra-high vacuum conditions with a typical base pressure of 3 X 10^{-10} torr. The LEED measurements were made with a conventional Varian 4-grid LEED optics with an off-axis electron gun. The optics also functioned as a retarding field energy analyzer for Auger electron spectroscopy (AES). The Rh(110)

crystal was cut from a boule of 99.999% purity and polished to within 0.5° of the [110] direction. The primary contaminants were B, C, and S which were removed by cycles of annealing at 1000K in 10^{-4} torr H_2 (1 h), sputtering in 10^{-5} torr Ar at 300K (1 h), heating at 500K in 10^{-7} torr O_2 (15 min.), followed by a final anneal to 1100K (5 min.) in vacuum. Residual oxygen was removed by the addition of CO at elevated temperatures. This was repeated until the sample was clean by AES. CO was supplied by Matheson with a purity of 99.5% and was used without further purification.

LEED images and LEED I-V spectra were collected over the energy range of 34-220 eV for the clean surface, and 34-199 eV for the CO structure. In the data analysis for the clean surface 4 symmetry inequivalent beams for a total energy range of 639 eV were used. The data set for the CO structure used 9 symmetry inequivalent beams for a total energy range of 951 eV. This consisted of 5 integer and 4 fractional order beams. The (2x1) surface phase was prepared by the adsorption of CO at T = 300K with an exposure of 16-24L, based upon the uncorrected ionization gauge measurement. (1L = 1 x 10^{-6} torr•s) The LEED measurements were made at 190K. Data acquisition was carried out with a Dage-MTI SIT-68 high sensitivity video camera coupled with a PC for rapid data acquisition and subsequent analysis of the integrated diffracted beam intensities. This allowed a complete set of images to be generated in approximately 300 s. In order to minimize any possible electron beam induced damage, such as desorption and cracking of the CO overlayer, the incident electron beam current was limited to 10 - 50 nA in the applied energy range. To check that no damage was occurring, the I-V spectra were measured with the sample position changed 3 times during each measurement to limit any degradation as well as measuring the spectra in reversed energy order. All I-V spectra were collected at normal incidence conditions, where normal incidence was verified by comparing symmetry equivalent beams.

3.3. Theory

The surface structures of both the clean (1x1) and p2mg(2x1) surface phase of CO were determined with an automated search method [21] based on the tensor LEED (TLEED) approximation [22,23]. With this method only one fully dynamical calculation of the Van Hove-Tong [24] type for each initial structural model is required. This calculation provides a set of reference amplitudes and their dependence on displacements for use in the TLEED routine. From this the diffracted beam intensities for any model with a geometry within 0.3 - 0.4Å of the reference geometry may be rapidly calculated. The TLEED method has been combined with an automated search algorithm, employing R-factors that quantify the fit between the theoretical and experimental I-V spectra. In our calculations we have used the Pendry R-factor (Rp) which emphasizes peak positions in the spectra at the expense of intensities. [25]

In the reference structure calculations, the top three metal layers of the clean surface were treated as one composite layer. In the CO structure, the two CO molecules in the unit cell and the top two metal layers were treated as two separate composite layers. This was done using the Beeby matrix inversion scheme, which treats multiple scattering within a layer exactly [26]. The scattering between the layers and the bulk was computed using renormalized forward scattering (RFS) [26]. In all of the calculations, we employed a maximum angular momentum value of 7 for the phase shifts. Phase shifts were obtained from a surface cluster for CO on Rh(111) at 3/4ML coverage using muffin-tin radii of 0.92Å for Rh, 0.74Å for C and 0.69Å for O. The reasoning for the small radius used for Rh is explained elsewhere. [27] Damping of the electrons was modeled with the imaginary part of the optical potential set to V_{0i}=-5 eV. The inner potential was initially set to V_0=10 eV and then fit to experiment. Thermal vibrations were modeled by using temperature dependent phase shifts. The Debye temperature of Rh was taken to be 480K, which is a typical value for other surface structure studies on Rh, with an enhancement of

1.4. The O and C Debye temperatures are based upon equal amplitudes of vibration with the Rh surface. [24] Error bars in the calculation were obtained using Pendry's method [25,28].

3.4. Structure Analysis

Prior to any adsorption experiments, the structure of the clean (1x1) surface was verified. The top three metal interlayer spacings were allowed to vary during the calculation. This resulted in a top layer contraction of 0.09±0.02Å and a second layer expansion of 0.03±0.03Å relative to the bulk interlayer spacing of 1.345Å. The third layer remained bulk like. This resulted in an R-factor of Rp=0.17. This result is in good agreement with a previous analysis of the clean Rh(110) surface [9].

When a saturated overlayer of CO is adsorbed on the Rh(110) surface at T=300K, a p2mg(2x1) surface structure is formed. The coverage of CO for this structure has been shown by Bowker et. al. to be 1 monolayer (ML) (0.95±0.05ML). [1] Based upon the bonding geometries for CO on Ni(110) [16] and Pd(110) [17], for which tilted CO on bridge and top site are reported respectively, we examined both adsorption sites as trial structures for the Rh(110).

Suspecting that Rh and Pd would react similarly with CO, our initial test geometry was that for a top site bonded CO with a C-O bond of length 1.15Å and a Rh-C bond length of 2.00Å, with the molecular axis tilted by 10° from the surface normal. The structure search was initially restricted to maintain both the glide and mirror plane symmetries. Optimization of the atomic positions for the two CO molecules and the top two metal layers was done in a two step process: first the displacements perpendicular to the surface were optimized, followed by the lateral displacements. The final result for the top site model was an unacceptable Rp=0.62. After removal of all of the symmetry

requirements, to allow the atoms to move in any direction, the R-factor was still only reduced to Rp=0.43.

The initial reference structure for the bridge bonded model had a C-O bond length of 1.15Å and a Rh-C bond length of 1.90Å with the molecular axis tilted by 10° from the surface normal. Again the glide and mirror plane symmetries were imposed and the perpendicular and lateral displacements optimized. This resulted in an R-factor of Rp=0.31, which is in the range of best fits for many molecular structures on surfaces. [29-31] The theory-experiment fits are shown in figure 3.1. To check the stability of this minimum, searches were started from various displacements in parameter space and the structure was recalculated as a reference structure and again optimized. In each of these cases the same minimum was found within the error bars for the atomic coordinates. Finally all of the symmetry requirements were removed. This resulted in an Rp=0.15; however all of the displacements were within the error bars of the structure with full symmetry. Thus the improvement of the R-factor is due only to the increased number of parameters being fit, from 9 to 25. The final best fit geometry for the full symmetry case for the Rh(110)-p2mg(2x1)-2CO structure is shown in figure 2 and tabulated in table 1. The final geometry resulted in a bridge bonded molecule, with a C-O bond length of 1.13±0.09Å, and a Rh-C bond length of 1.97±0.09Å on an essentially bulk terminated (110) surface, with the molecular axis tilted by 24±4° from the surface normal. The angle of the tilt of the Rh-C plane with respect to the surface normal was found to be 13±4° and the angle between the Rh-C plane and C-O axis was 11±4°. The top two metal layers are expanded by 0.15Å with respect to the clean surface.

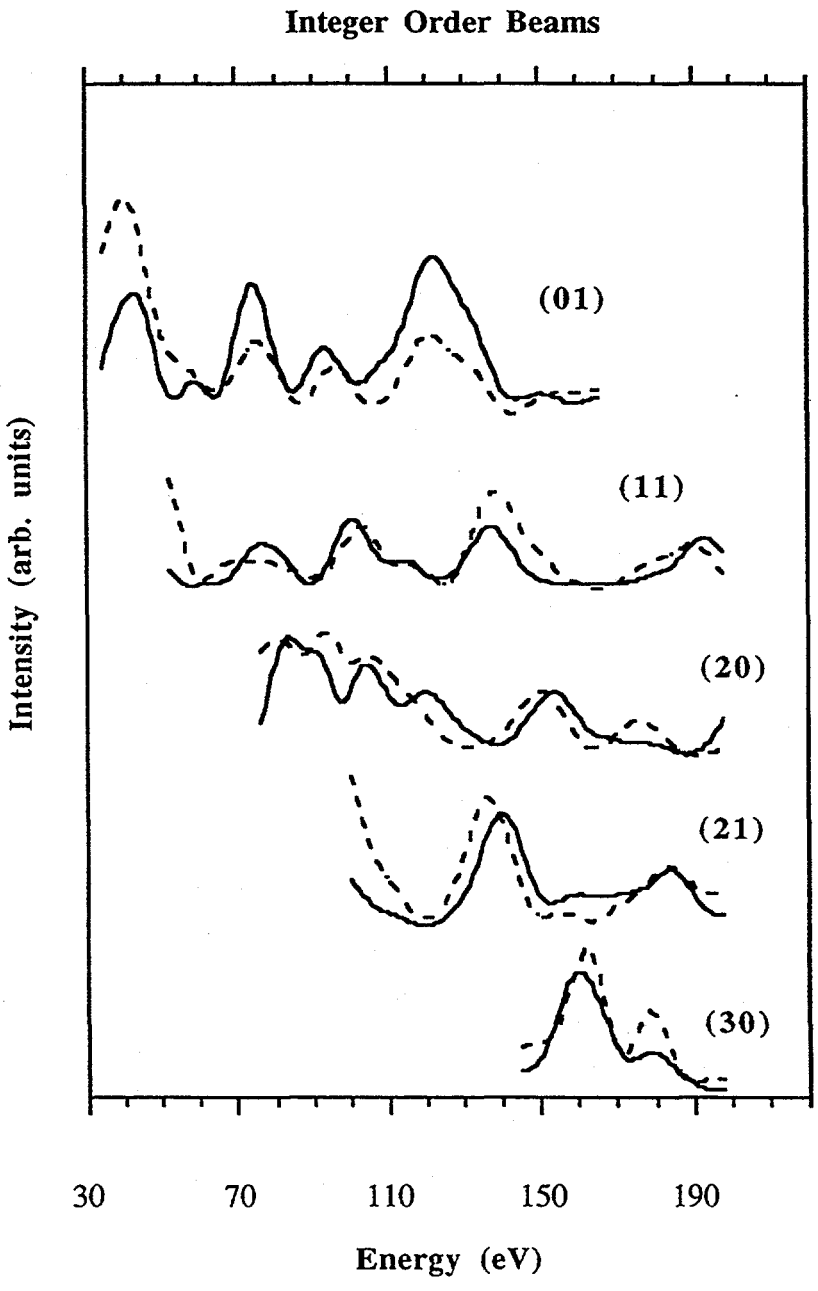

Figure 3.1a: Best fit I-V spectra for the Rh(110)-p2mg(2x1)-2CO structure, which illustrate the agreement between theory (-----) and experiment (——) for the integer order beams.

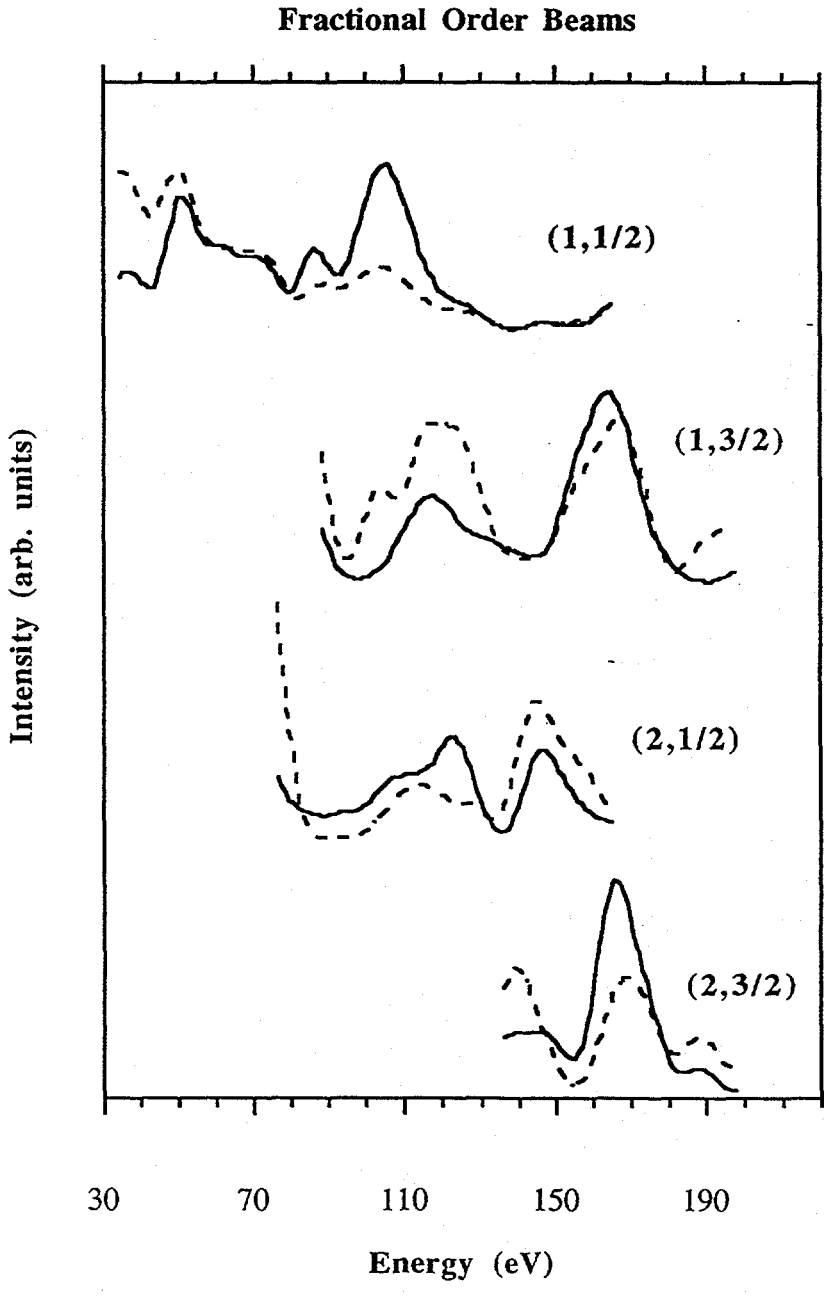

Figure 3.1b: Best fit I-V spectra for the fractional order beams.

3.5. Discussion

The results of CO structures on various transition metal surfaces are shown in table 2. It is clear from this table that predicting the site occupation of CO on a particular metal surface is not a trivial problem. The fine balance between the adsorbate-substrate and adsorbate-adsorbate interactions is demonstrated in the wide variety of structures formed. Even on metals which exhibit very similar chemistry and are very close in the Periodic Table the adsorption site is very coverage and metal dependent. Let us discuss the low and high coverage cases for CO adsorption on Ni, Rh, and Pd.

For relatively low coverage structures where short range (5Å) CO-CO interactions should be at a minimum, such as the $(\sqrt{3}x\sqrt{3})R30^{o}$ CO (Θ=1/3ML) structure on (111) surface of Ni, Rh, and Pd, the CO is bonded in the bridge site on Ni, on top on Rh, and in the fcc hollow on Pd, with the CO molecular axis perpendicular to the (111) plane and with similar C-O and metal-C bond lengths. It has been proposed that a larger contribution of 4d electrons from Pd relative to Rh results in the high coordination adsorption site on Pd(111). [32] If we now extend this reasoning to CO adsorption on the (110) surface, we would expect CO on Pd(110) to be bridge bonded and on Rh(110) to be top site bonded, which is the opposite to that found experimentally. This may be due to the fact that we are now in a regime where CO-CO interactions become an important factor that needs to be included with knowledge of the valence band structures of the metal relative to the CO.

Let us compare the three high coverage (1 monolayer) p2mg(2x1)-2CO structures on the fcc(110) surfaces of Ni, Rh, and Pd. On Ni and Rh, nearly identical structures are observed for CO. Both are bonded in bridge sites with essentially equal bond lengths: on Ni: d(C-O) = 1.12Å, d(Ni-C) = 1.95Å; on Rh: d(C-O) = 1.13Å, d(Rh-C) = 1.97Å. The

Figure 3.2: Side and top views of the Rh(110)-p2mg(2x1)-2CO structure, compared with a side view of the clean (1x1) surface structure. The angle δ refers to the Rh-C tilt and φ to the C-O tilt, while a represent the angle between the surface normal and the C-O molecular axis.

Table 3.1:

	Lateral coordinates		Perpendicular coordinate
	X	Y	Z
Atomic coordinates			
O1	-0.81	0.00	0.00
O2	0.81	2.69	0.00
C1	-0.34	0.00	1.03
C2	0.34	2.69	1.03
Rh1	0.00	1.34	2.44
Rh2	0.00	4.02	2.44
Rh3	1.90	0.00	3.81
Rh4	1.90	2.69	3.81
bulk repeat vector	1.90	1.34	1.34
2D repeat vectors	3.80	0.00	0.00
	0.00	5.38	0.00

Table 3.1: Table of Cartesian coordinates for the best fit structure of the Rh(110)-p2mg(2x1)-2CO.

Table 3.2:

Surface	Structure	Θ(ML)*	Site	d(C-O)Å	d(M-C)Å	Technique	Ref.
Cu(100)	c(2x2)	1/2	Top	1.13	1.92	NEXAFS	[35]
	c(2x2)	1/2	Top	1.13	1.90	LEED	[36]
Ni(111)	c(4x2)	1/2	Hollow (fcc/hcp)	1.19	1.78	SEXAFS	[37]
	$(\sqrt{3}x\sqrt{3})R30^o$	1/3	Bridge	1.13	1.78	PED	[38]
Ni(100)	c(2x2)	1/2	Top	1.13	1.80	PED	[38,39]
	c(2x2)	1/2	Top	1.13	1.70	LEED	[36,40-42]
Ni(110)	p2mg(2x1)	1	Bridge $\delta=27^o, \varphi=10^o$	1.12	1.95	LEED	[16]
	p2mg(2x1)	1	Top $\delta=19^o, \varphi=0^o$	1.15	1.95	PED	[18]
	p2mg(2x1)	1	Bridge $\delta=16^o, \varphi=0^o$	1.16	1.94	ARPEFS	[19]

* Θ(ML)= CO molecules/metal

δ = angle between the surface normal and the metal-C plane.

φ = angle between the metal-C plane and the C-O axis.

Table 3.2: The structures of CO on various transition metal surfaces.

Surface	Structure	Θ(ML)*	Site	d(C-O)Å	d(M-C)Å	Technique	Ref.
Pd(111)	$(\sqrt{3}x\sqrt{3})R30^o$	1/3	Hollow (fcc)	1.15	2.04	LEED	[43]
Pd(100)	$(2\sqrt{2}x\sqrt{2})R45^o$	1/2	Bridge	1.15	1.93	LEED	[44]
Pd(110)	p2mg(2x1)	1	Top $\delta = 11^o, \varphi = 2^o$	1.16	2.11	LEED	[17]
Pt(111)	c(4x2)	1/2	Top&	1.15	1.85	LEED	[45]
			Bridge	1.15	2.08		
	disordered	1/3	------	1.15	2.08	LEED	[46]
Rh(111)	(2x2)	3/4	2 Top	1.15	2.03	LEED	[8]
			1 Bridge	1.15	2.03		
	$(\sqrt{3}x\sqrt{3})R30^o$	1/3	Top	1.07	1.95	LEED	[7]
Rh(110)	p2mg(2x1)	1	Bridge $\delta = 13^o, \varphi = 11^o$	1.13	1.97	LEED	this work
Ru(0001)	$(\sqrt{3}x\sqrt{3})R30^o$	1/3	Top	1.09	2.00	LEED	[47]
	disordered	1/10	Top	1.10	2.00	LEED	[48]

* Θ(ML)= CO molecules/metal

δ = angle between the surface normal and the metal-C plane.

φ = angle between the metal-C plane and the C-O axis.

Table 3.2(continued): The structures of CO on various transition metal surfaces.

close proximity of the CO molecules induces large CO-CO repulsions that result in a tilting of the CO molecules away from the surface normal. In each case the metal-C-O bond is found to be non-linear. We refer to the metal-C tilt as the angle between the surface normal and the metal-C plane, and the C-O tilt as the angle between metal-C plane and the C-O axis. On Ni(110) the Ni-C tilt is 27° and the C-O tilt is 10° back towards the surface normal. On Rh(110) the Rh-C and C-O tilts are almost identical at approximately 12° each. For Pd(110) the CO is found to be top site bonded with a nearly linear Pd-C-O arrangement. The Pd-C tilt is 11° and the C-O tilt is 2° (within the error bars of 5° for the calculation). If we consider simply the CO-CO interactions as the dominant force resulting in the degree of CO tilting, then one may predict on the basis of the distances between CO molecules and the lattice parameters for each surface, that the smaller the lattice parameter, Ni(2.48Å)<Rh(2.69Å)<Pd(2.74Å), the greater the angle of tilt. If we consider the metal-C tilt as the indicator of this interaction this is consistent with the experimental results: Ni(27°)>Rh(13°)>Pd(11°). However, the same trend is not preserved for the tilt of the C-O axis with respect to the surface normal, Pd(13°)<Ni(17°)<Rh(24°). This tilting has also been examined by extended Hückel calculations for top site bonded CO on Pt(110). [33] In that work the effective CO radius of the system is correlated to the degree of tilting. Basing the effective CO radius on the carbon-carbon distance of two nearest neighbor CO molecules, given as 1/2 d(C1-C2), an effective CO radius of 1.49Å is reported for a tilt of 16° (Pt-C tilt is 16° and C-O tilt is 0°). So this also does not fit with the correlation between the metal-C tilt and the lattice parameter just presented.

Any correlation of the lattice parameter to the degree of tilting does not however explain why CO would choose bridge bonding on Rh(110) and top site bonding on Pd(110), the reverse behavior from the (111) surfaces of these metals. Electronic orbital calculations will be needed to explain these findings, similar to the comparison of CO bonding on the (111) surfaces of Ni, Pd, and Pt by extended Hückel calculations [34] which explained the adsorption site preference based on the orbital occupation probabilities.

3.6. Summary

From a LEED intensity analysis of the clean and CO covered Rh(110)-(1x1) surface, the structure of the clean surface has been confirmed to exhibit a top layer contraction of 0.09±0.02Å and a second layer expansion of 0.03±0.03Å relative to the bulk interlayer spacing of 1.345Å, with the third layer remaining bulk like, with an a goodness of fit given by Rp=0.17. Upon the adsorption of 1 monolayer of CO on the Rh(110) surface the molecules are arranged in a zig-zag fashion along the [-110] direction to produce the observed glide plane symmetry in the LEED pattern. The clean surface relaxations are removed, resulting in an expansion of the top two metal layers by 0.15Å, and the CO bonds in the short bridge site with the CO molecular axis oriented 24±4° from the surface normal. This bonding geometry results in a Rh-C bond length of 1.97±0.09Å and a C-O bond length of 1.13±0.09Å with an a goodness of fit given by Rp=0.31.

3.7 References

[1] M. Bowker, Q. Guo, and R.W. Joyner, Surf. Sci. 253 (1991) 33.

[2] M. Bowker, Q. Guo, and R.W. Joyner, Surf. Sci. 280 (1993) 50.

[3] A. Baraldi, V.R. Dhanak, G. Comelli, K.C. Prince, and R. Rosei, Surf. Sci. 293 (1993) 246.

[4] A. Baraldi, V.R. Dhanak, G. Comelli, M. Kiskinova, and R. Rosei, Appl. Surf. Sci. 68 (1993) 395.

[5] G. Comelli, V.R. Dhanak, M. Kiskinova, G. Paolucci, K.C. Prince, and R. Rosei, Surf. Sci. 269/270 (1992) 360.

[6] M. Bowker, Q. Guo, Y. Li, and R.W. Joyner, Catal. Lett. 18 (1993) 119.

[7] R.J. Koestner, M.A. Van Hove, and G.A. Somorjai, Surf. Sci. 107 (1981) 439.

[8] M.A. Van Hove, R.J. Koestner, J.C. Frost, and G.A. Somorjai, Surf. Sci. 129 (1983) 482.

[9] W. Nichtl, N. Bickel, L. Hammer, K. Heinz, and K. Müller, Surf. Sci. 188 (1987) L729.

[10] R.A. Marbrow and R.M. Lambert, Surf. Sci. 67 (1977) 489.

[11] V.R. Dhanak, A. Baraldi, G. Comelli, G. Paolucci, M. Kiskinova, and R. Rosei, Surf. Sci. 295 (1992) 287.

[12] C.M. Comrie and R.M. Lambert, JCS Faraday I 72 (1976) 1659.

[13] H.H. Madden, J. Küppers, and G. Ertl, J. Chem. Phys. 58 (1973) 3401.

[14] G. Ertl and P. Rau, Surf. Sci. 15 (1969) 443.

[15] K. Christmann and G. Ertl, Z. Naturforsch 28a (1973) 1144.

[16] D.J. Hannaman and M.A. Passler, Surf. Sci. 203 (1988) 449.

[17] A. Wander, P. Hu, and D.A. King, Chem. Phys. Lett. 201 (1993) 393.

[18] O. Knauff, U. Grosche, H.P. Bonzel, and V. Fritzsche, Molec. Phys. 76 (1992) 787.

[19] Z. Huang, Z. Hussain, W.T. Huff, and E.J. Moler, and D.A. Shirley, Phys.Rev. B 48 (1993) 1696.

[20] N. Pangher and J. Hasse, Surf. Sci. Lett. 293 (1993) L908.

[21] M.A. Van Hove, W. Moritz, H. Over, P.J. Rous, A. Wander, A Barbieri, N. Materer, U. Starke, and G.A. Somorjai, Surf. Sci. Rep. 19 (1993) 191.

[22] P.J. Rous and J.B. Pendry, Surf. Sci. 219 (1989) 355 and 373.

[23] P.J. Rous, Prog. Surf. Sci. 39 (1992) 3.

[24] M.A. Van Hove and S.Y. Tong, *Surface Crystallagrophy by LEED: Theory, Computation, and Structural Results,* Springer-Verlag, Berlin, Heidelberg, 1979.

[25] J.B. Pendry, J. Phys. C 13 (1980) 937.

[26] M.A. Van Hove, W.H. Weinberg, and C.-M.Chan, *Low-Energy Electron Diffraction: Experiment, Theory, and Surface Structure Determination,* Springer-Verlag, Berlin, Heidelberg, 1986.

[27] U. Starke, A. Barbieri, N. Materer, M.A. Van Hove, and G.A. Somorjai, Surf. Sci. 286 (1993) 1.

[28] W. Oed, H. Lindner, U. Starke, K. Heinz, K. Müller, and J.B. Pendry, Surf. Sci. 224 (1989) 239.

[29] A. Wander, M.A. Van Hove, and G.A. Somorjai, Phys. Rev. Lett. 67 (1991) 626.

[30] U. Starke, A. Barbieri, N. Materer, M.A. Van Hove, and G.A. Somorjai, Surf. Sci. 286 (1993) 1.

[31] N. Materer, A. Barbieri, D. Gardin, J.D. Batteas, M.A. Van Hove, and G.A. Somorjai, Phys. Rev. B 48 (1993) 2859.

[32] A.B. Anderson and M.K. Awad, J. Am. Chem.Soc. 107 (1985) 7854.

[33] M.I. Ban, M.A. Van Hove, and G.A. Somorjai, Surf. Sci. 185 (1987) 355.

[34] Y.T. Wong and R. Hoffmann, J. Phys. Chem. 95 (1991) 859.

[35] C.F. McConville, D.A. Woodruff, K.C. Prince, G. Paolucci, U. Chab, M. Suvman, and A.M. Bradshaw, Surf. Sci. 166 (1986) 221.

[36] S. Anderson and J.B. Pendry, J. Phys. C 13 (1980) 3547.

[37] L. Becker, S. Aminpirooz, B. Hillert, M. Pedio, J. Haase, and D.L. Adams, Phys. Rev. B 47 (1993) 9710.

[38] S.D. Kevan, R.F. Davis, D.H. Rosenblatt, J.G. Tobin, M.G. Mason, D.A. Shirley, C.H. Li, and S.Y. Tong, Phys. Rev. Lett. 46 (1981) 1629.

[39] L.G. Petersson, S. Kono, N.F.T. Hall, C.S. Fadley, and J.B. Pendry, Phys. Rev. Lett. 42 (1979) 1545.

[40] S.Y. Tong, A. Maldonado, C.H. Li, and M.A. Van Hove, Surf. Sci. 94 (1980) 73.

[41] M.A. Passler, A. Ignatiev, F. Jona, D.W. Jepsen, and P.M. Marcus, Phys. Rev. Lett. 43 (1979) 360.

[42] K. Heinz, E. Lang, and K. Müller, Surf. Sci. 87 (1979) 595.

[43] H. Ohtani, M.A. Van Hove, and G.A. Somorjai, Surf. Sci. 187 (1987) 372.

[44] R.J. Behm, K. Christmann, G. Ertl, and M.A. Van Hove, J. Chem. Phys. 73 (1980) 2984.

[45] D.F. Ogletree, M.A. Van Hove, and G.A. Somorjai, Surf. Sci. 173 (1986) 351.

[46] G.S. Blackman, M.-L. Xu, M.A. Van Hove, and G.A. Somorjai, Phys. Rev. Lett. 61 (1988) 2352.

[47] G. Michalk, W. Moritz, H. Pfnür, and D. Menzel, Surf. Sci. 129 (1983) 92.

[48] P. Piercy, P.A. Heimann, G. Michalk, and D. Menzel, Surf. Sci. 219 (1989) 189.

Chapter 4

The Bonding of Oxygen on Rh(110)

Oxygen is dissociatively chemisorbed on Rh(110) and forms an ordered (2x1) surface structure at one monolayer coverage. The automated tensor LEED approach has been applied to the determination of atomic positions in the Rh(110)-p2mg(2x1)-2O structure. The oxygen atoms are confirmed to be in a zig-zag fashion in the (110) troughs to produce the glide plane symmetry observed in the LEED pattern. The clean surface interlayer relaxations are reduced and the oxygen atoms are bound asymmetrically in the 3-fold fcc hollow-sites to the (111) facets of the steps. Two Rh-O bonds are formed to Rh atoms in the top metal layer with bond lengths of 1.86±0.11Å and a third Rh-O bond of 2.07±0.16Å is formed to a Rh atom in the second metal layer. A novel finding is that the second metal layer Rh atoms are found to shift towards the oxygen positions, introducing a zig-zag lateral displacement of the atoms in the row by 0.10±0.07Å.

4.1. Introduction

The adsorption and reaction of atoms and molecules at defect sites such as steps and kinks are of particular interest since these are the proposed "active sites" in many surface reactions. Some reactions have been observed to exhibit structure sensitivity when reaction rates are compared from different crystal planes. Under the conditions of low CO coverage, the catalytic reaction of CO and O on Rh surfaces to form CO_2 exhibits structure sensitivity. The rate of CO oxidation on Rh(110) has been shown to be higher than on the flat close-packed Rh(111) surface. [1] This may be related to the differences in bonding of CO and atomic O on these surfaces.

Oxygen chemisorption on Rh(110) has been examined by a variety of techniques including high resolution electron energy loss spectroscopy (HREELS) [2], low-energy electron diffraction (LEED)[3, 4], and scanning tunneling microscopy (STM) [5] to obtain bonding information for atomic oxygen on this surface. The chemisorption of 1/2 monolayer of oxygen on Rh(110) results in the formation of a p2mg(2x2) structure, where oxygen chemisorption induces a (1x2) missing-row reconstruction like that of the Pt, Ir, and Au(110)-(1x2) structure. (The p2mg refers to the surface space group symmetry which in this case consists of a mirror plane and a glide plane.) The oxygen atoms arrange in a zig-zag fashion on top of the ridges of these reconstructed rows. [4] Interestingly the (110) crystal planes of other face centered cubic metals (with open 5d shells), Ir, Pt, and Au, exhibit the (1x2) missing-row reconstruction when clean. The (110) crystal face of Rh (with an open 4d shell) reconstructs to form the same surface structure only in the presence of oxygen. STM results [5] show that as the oxygen coverage is increased, the number of missing rows decreases systematically, until at one monolayer coverage a p2mg(2x1) structure is formed in which the oxygen atoms are bonded on the unreconstructed (1x1) surface.

In this paper we report an automated tensor LEED intensity analysis for the Rh(110)-p2mg(2x1)-2O surface structure. Our results, confirm and refine the structure

determined earlier by fully dynamical LEED, in which automated tensor LEED was not used. [3] The oxygen atoms are found to induce an asymmetric cluster-like bonding to the 3-fold fcc hollow sites on the [111] microfacets of the surface with two Rh-O bonds to the top metal layer and a third Rh-O bond to the second metal layer. In the structure presented here lateral distortions of the metal surface induced by the adsorbed oxygen have also been found. We will describe the structure analysis and compare these results to those of oxygen structures on other Rh crystal faces and fcc(110) metal surfaces. The changes in the Rh(110) surface structure as a function of chemisorbed oxygen coverage are also described.

4.2. Experimental

All experiments were made under ultra-high vacuum conditions with a typical working pressure of 3 X 10^{-10} Torr. The LEED measurements were made with an Omicron 4-grid rear-view LEED system. The optics also functioned as a retarding field energy analyzer for Auger electron spectroscopy (AES). The Rh(110) crystal was cut from a boule of 99.999% purity and polished to within 0.5° of the [110] direction. The primary contaminants were B, C, and S which were removed by cycles of annealing at 1000 K in 10^{-4} Torr H_2 (1 h), sputtering in 10^{-5} Torr Ar at 300K (1 h), heating at 500K in 10^{-7} Torr O_2 (15 min.), followed by a final anneal to 1100K (5 min.) in vacuum. Residual oxygen was removed by the addition of CO at elevated temperatures. This was repeated until the sample was clean by AES. Oxygen and CO were supplied by Matheson with a purity of 99.9% and 99.5% respectively and used without further purification.

The structure of the clean surface was also verified to check the quality of the crystal and is described elsewhere. [6] LEED images and LEED I-V spectra were collected over the energy range of 50-200 eV for the oxygen structure. The data analysis used 9 symmetry inequivalent beams for a total energy range of 900 eV. This consisted of 5

integer and 4 fractional order beams. The (2x1) surface phase was prepared by the adsorption of oxygen at T = 190 K with an exposure of 10 L, based upon the uncorrected ionization gauge measurement. (1 L = 1 x 10^{-6} Torr•s) The sample was then flashed to 300 K to produce a sharp p2mg(2x1) pattern and then cooled back to 190 K for the LEED measurement. The LEED I-V spectra were obtained at normal incidence conditions as determined by the comparison of symmetry equivalent beams. Data acquisition was carried out with a Dage-MTI SIT-68 high sensitivity video camera coupled with a PC for rapid data acquisition and subsequent analysis of the integrated diffracted beam intensities. This method allowed for a complete set of images to be generated in approximately 300 s.

4.3. Theory

The surface structure of the p2mg(2x1) surface phase of oxygen was determined with an automated search method [7] based on the tensor LEED (TLEED) approximation [8, 9]. With this method only one fully dynamical calculation of the Van Hove-Tong type is required for each initial trial structural model. [10] This calculation provides a set of reference amplitudes and their dependence upon displacements for use in the TLEED search routine. In the automated TLEED routine the diffracted beam intensities for any model with a geometry within 0.3 - 0.4 Å of the reference geometry may be rapidly calculated. This routine is coupled to a search algorithm employing reliability factors (R-factors) to quantify the fit between the theoretical and experimental I-V spectra. In our calculations we have used the Pendry R-factor (Rp) which emphasizes peak positions in the spectra at the expense of intensities to quantify the fit between theory and experiment. [11] All calculations were carried out on an IBM RISC-6000 workstation. The reference structure calculations required approximately 1.5 h of CPU time and the full structural searches required approximately 200 s of CPU time.

In the reference structure calculations, two oxygen atoms and two metal atoms from the top three metal layers were prepared as a single composite layer using the Beeby matrix inversion scheme, which treats multiple scattering within a layer exactly [12]. The scattering between the layers and the bulk was computed using renormalized forward scattering (RFS) [12]. In all of the calculations, we employed a maximum angular momentum value of 6 which we have tested to be sufficient for the energy range examined (50 - 200 eV). The same Rh and O phase shifts were used as in our previous analysis of the Rh(110)-p2mg(2x1)-2CO structure. [6] Damping of the electrons was modeled with the imaginary part of the optical potential set to V_{0i} = -5 eV. The inner potential was initially set to V_0 = 10 eV and then fit to experiment. Thermal vibrations were modeled by using temperature dependent phase shifts where the Debye temperature of Rh was set to 480K. The O Debye temperature was fixed so as to have an equal amplitude of vibration with the Rh surface. Error bars in the calculation were estimated using Pendry's method [11, 13].

4.4. Structure Analysis

Three different models were tested for the Rh(110)-p2mg(2x1)-2O structure. Since on other Rh surfaces O has been found to bond in the highest coordination sites [14, 15] we tested two different 3-fold site models and the short bridge site as model geometries. These models are described here and illustrated in figure 1. For the short bridge site (model A) the O atoms were placed with Rh-O bonds of 2.0 Å and an O-O nearest neighbor distance of 2.8 Å. The two 3-fold site reference models were: O in fcc hollow sites on the facets coordinated to 2 Rh atoms in the top layer and 1 in the second (model B), and O in the hcp hollow sites on the facets coordinated to 1 Rh atom in the top metal layer and 2 in the second (model C). In model B the O was placed in the 3-fold fcc hollow site with equal Rh-O bonds of 2.0Å and an O-O nearest neighbor distance of 2.9 Å. In model C (similar

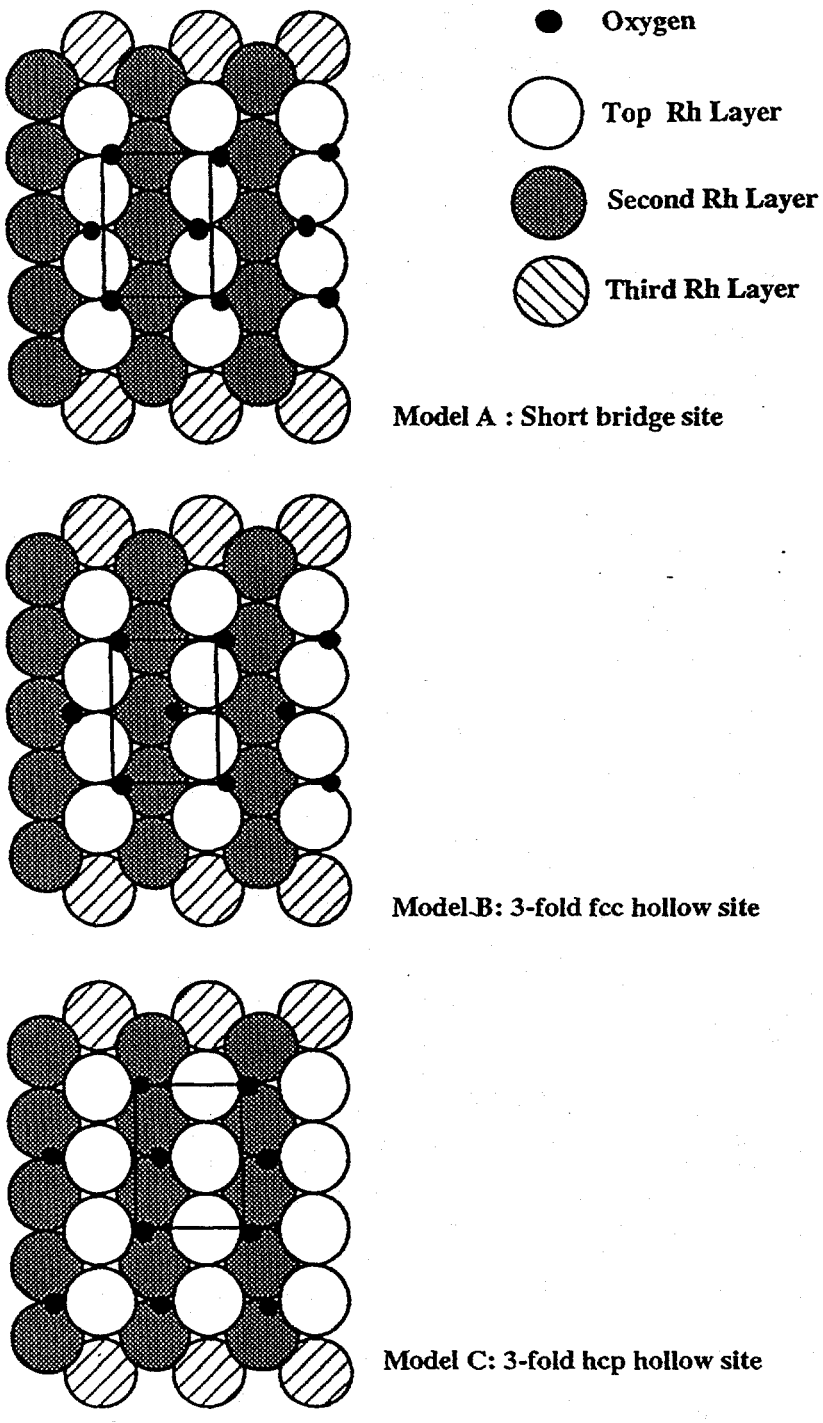

Figure 4.1: Model geometries tested for the Rh(110)-p2mg(2x1)-2O structure: model A: short bridge site, model B: 3-fold fcc hollow site, and model C: 3-fold hcp hollow site.

to an asymmetrical long bridge adsorption site) the O atoms were positioned in the hcp hollow sites with equal Rh-O bonds of 2.0 Å and had an O-O nearest neighbor distance of 2.7 Å. The optimum structure from a previous fully-dynamical LEED analysis of this structure was also tested.

The structure search was nominally restricted to maintain both the glide and mirror plane symmetries exhibited in the LEED pattern. This limited the number of parameters to be fit to six structural parameters. With full symmetry, these parameters include the O vertical position and lateral position in the [001] direction, the top layer Rh atoms vertical position, the second layer Rh atoms vertical position and lateral position in the [001] direction, and the third layer Rh atoms vertical positions. To test the reference structures, the search for the atomic positions of the two O atoms and top two metal layers was done by first optimizing the displacements perpendicular to the surface (to which LEED data collected at normal incidence is more sensitive) followed by the lateral displacements. The Pendry R-factor results for the best fits for models A, B and C were 0.56, 0.16, and 0.58 respectively. The structure of the best fit model B was further optimized by allowing the third metal layer atom positions to also vary, however there was no significant improvement of the R-factor and all of the bond distances remained unchanged within the error bars. This minimum in the R-factor in the structure search for model B was verified by starting a new search from this structure taken as a new reference structure and resulted in no change in the atomic positions. A check of he structure presented previously by Gierer et. al. resulted in Rp = 0.20, just on the edge of our error bars. A search using this structure as the reference structure finds the same minimum as our final structure. As a final check of the structure all of the symmetry was removed and the atomic positions did not change within the error bars of the calculations. We therefore report only the fully symmetrized structure. The theory-experiment fits for the 9 symmetry inequivalent I-V spectra employed are shown in figure 2.

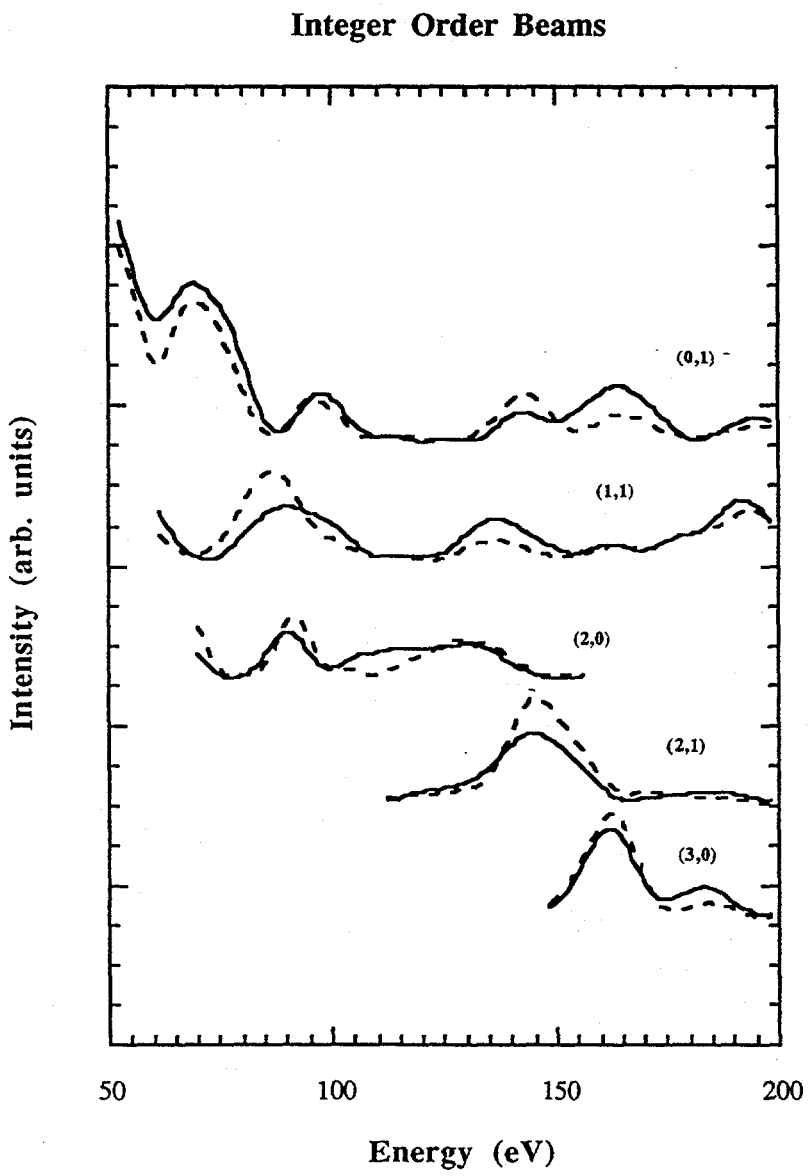

a)

Figure 4.2: The best fit I-V spectra for the Rh(110)-p2mg(2x1)-2O structure, which illustrate the agreement between the theory (——) and experiment (---) for the a) integer order diffraction beams.

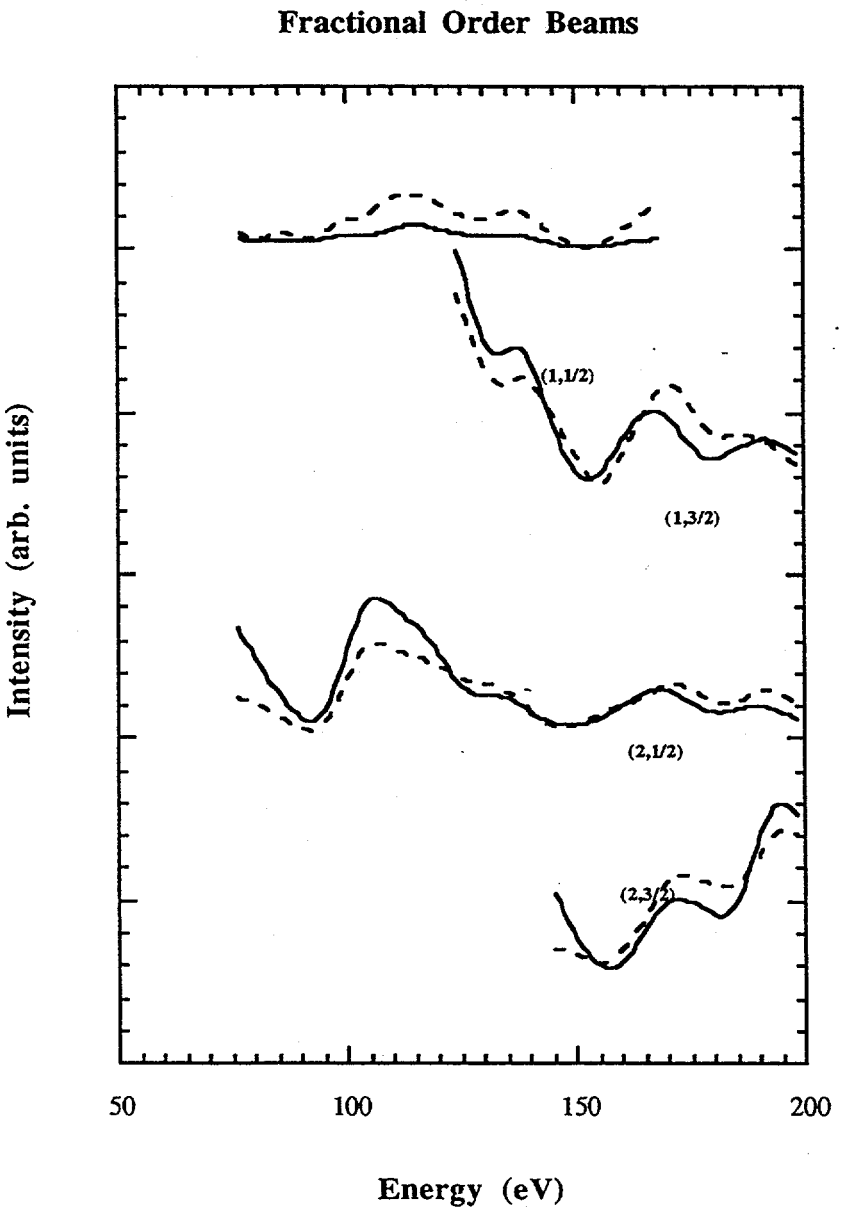

b)

Figure 4.2 (continued): The best fit I-V spectra for the fractional order diffraction beams.

The best fit structure for the Rh(110)-p2mg(2x1)-2O structure is shown in figure 4.3 and the atomic coordinates are tabulated in table 1. In this structure the atomic oxygen is bonded in the 3-fold fcc hollow site with two Rh-O bonds to the first metal layer of 1.86±0.11 Å and one Rh-O bond to the second metal layer of 2.07±0.16 Å. The O position is 0.60±0.03 Å above the top surface Rh atoms. The atomic geometry is like a Rh_3O cluster, which is reinforced by a reconstruction of the second metal layer Rh atoms, under the influence of the oxygen chemisorption, in which the metal layer is now distorted in a zig-zag fashion by 0.10±0.07 Å with the Rh atomic positions shifted towards the nearest O positions. The oxygen is in essence bound to the [111] microfacets in the Rh (110) crystal face.

4.5. Discussion

4.5.1 The Rh(110)-p2mg(2x1)-2O structure

By using the automated tensor LEED method, an exhaustive search of structural space can be obtained allowing for detailed refinements of a surface structure. We find that with the adsorption of one monolayer coverage of oxygen atoms on the Rh(110)-(1x1) surface the top metal interlayer spacing expands by 0.11 Å with respect to the clean surface. This result is similar to when the surface is saturated with other adsorbates such as CO or H. [6, 16] We have confirmed that the oxygen atoms are bound in the 3-fold fcc hollow sites on the Rh(110)-(1x1) surface, as reported in a recent fully-dynamical LEED analysis. [3] Some differences in the structural details however have been obtained. We have also identified a zig-zag lateral relaxation of the second metal layer of approximately 0.10 Å. These second layer Rh atoms move towards the nearest oxygen positions. This type of clustering of the Rh atoms about the O positions is also reported in an automated tensor LEED analysis of the missing-row Rh(110)-p2mg(2x2)-2O structure that is obtained

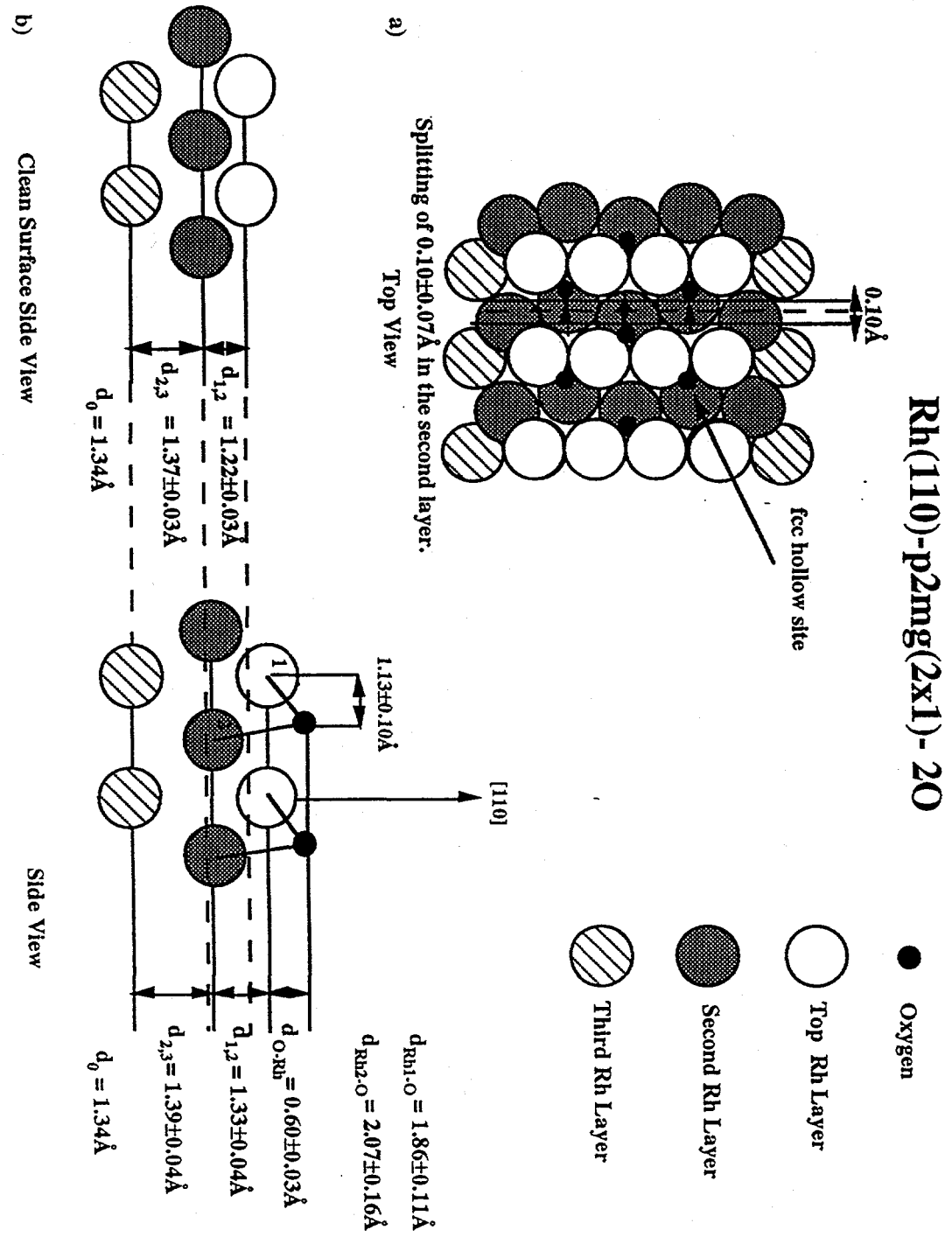

Figure 4.3: The a) top and b) side views of the Rh(110)-p2mg(2x1)-2O structure. The top view shows the splitting of the second layer metal atoms. The side view shown relative to the clean surface shows the expansion of the top two layer by 0.11Å for d_{12} and 0.02Å for d_{23}. The bulk interlayer spacing of Rh(110) is d_0 = 1.34Å.

Table 4.1:

	Lateral coordinates		Perpendicular coordinate
	X	Y	Z
Atomic coordinates			
O1	-1.13	2.69	0.00
O2	1.13	0.00	0.00
Rh1	0.00	1.34	0.60
Rh2	0.00	4.03	0.60
Rh3	1.85	0.00	1.93
Rh4	1.95	2.69	1.93
Rh5	0.00	1.34	3.32
Rh6	0.00	4.03	3.32
bulk repeat vector	1.90	1.34	1.34
2D repeat vectors	3.80	0.00	0.00
	0.00	5.38	0.00

Table 4.1: Table of Cartesian coordinates for the best fit Rh(110)-p2mg(2x1)-2O structure.

at 1/2 monolayer coverage of chemisorbed oxygen [4], in which the Rh atoms in the second metal layer nearest to the O positions were shifted up by 0.06 Å towards the O atoms. The relocation of metal atoms during oxygen chemisorption is consistent with the strong bonding of O to Rh. The lateral separation between the top layer Rh atoms and the O atoms was found to be 1.13 Å from this analysis, compared to 1.32 Å from the previous study. This close spacing results in a slightly asymmetric bonding for the oxygen atoms, with bond lengths of 1.86 Å to the metal atoms in the top layer, and 2.07 Å to the metal atoms in the second layer. This asymmetry of the oxygen bonding may be due to several factors. First, close range O-O repulsions may exist in the channels of the surface at saturation coverages which act to push the oxygen atoms apart. Also, the coordination of the Rh atoms may play a role, in that the top metal layer atoms are bonded to 7 other Rh atoms, and the second metal layer atoms are bonded to 11 other Rh atoms. When O is adsorbed on the surface some electron density is transferred from the metal to the O atoms, thus the metal atoms with fewer metal-metal nearest neighbors could contribute more electron density to the O, forming stronger, and thus shorter Rh-O bonds.

4.5.2 Coverage dependence of oxygen bonding on the Rh(110) surface

The study of oxygen adsorption on the Rh(110) surface as a function of coverage is a clear illustration of the interplay between adsorbate-adsorbate, adsorbate-substrate, and substrate-substrate interactions. The surface is at all times trying to minimize the surface free energy. Here we will describe how the metal surface structure changes with coverage of chemisorbed oxygen. The clean Rh(110)-(1x1) surface lowers its free energy by relaxations of the interlayer spacings. With the adsorption of 1/2 monolayer coverage of oxygen, at elevated temperatures, the metal surface reconstructs into the Rh(110)-(1x2) missing-row structure. This structure has oxygen adsorbed on top of the ridges of the (1x2) missing- row structure in fcc 3-fold hollow sites. The stability of this structure is

due to the formation of more [111] type facets and the capping of the lowest coordination Rh atoms at the surface layer by chemisorbed oxygen. The metal surface reconstruction may be maintained on the clean surface with the careful removal of the oxygen by hydrogen. However this clean surface reconstruction is metastable at 300K and only remains intact up to approximately 480 K, where it can revert back to the (1x1) clean surface structure. When the surface is saturated with oxygen at one monolayer coverage, below 300 K the oxygen atoms are bonded on the (1x1) surface. Thus the surface now prefers the more Rh-O bonds over more Rh-Rh bonds formed in the [111] facets of the missing-row structure.

STM studies [5] have shown that in between the 1/2 monolayer and one monolayer coverage, at elevated temperatures, c(2x2n) surface structures exist where oxygen is adsorbed on (1xn) type missing-row surface reconstructions. The trend that is observed in examining the structural changes with coverage show that beginning with the 1/2 monolayer coverage the [111] facets capped with oxygen stabilize the missing-row structure which is lower in surface free energy than the clean (1x1) surface. As more oxygen chemisorbs with increasing oxygen coverage, the Rh-Rh bonding energy gained by the formation of [111] facets in the (1x2) missing-row reconstruction is exchanged for more Rh-O bonds, restructuring the surface back to its (1x1) type surface structure. This occurs gradually with increasing oxygen coverage. At one monolayer below 300 K, the surface is saturated by oxygen on a (1x1) surface structure. In terms of the changes in the Rh substrate we first have no missing rows in the [001] direction, then every n^{th} row missing (n = 2, 3, 4, 5), returning to no missing rows at the saturation coverage of oxygen. These structural transformations as a function of oxygen coverage are illustrated in figure 4.

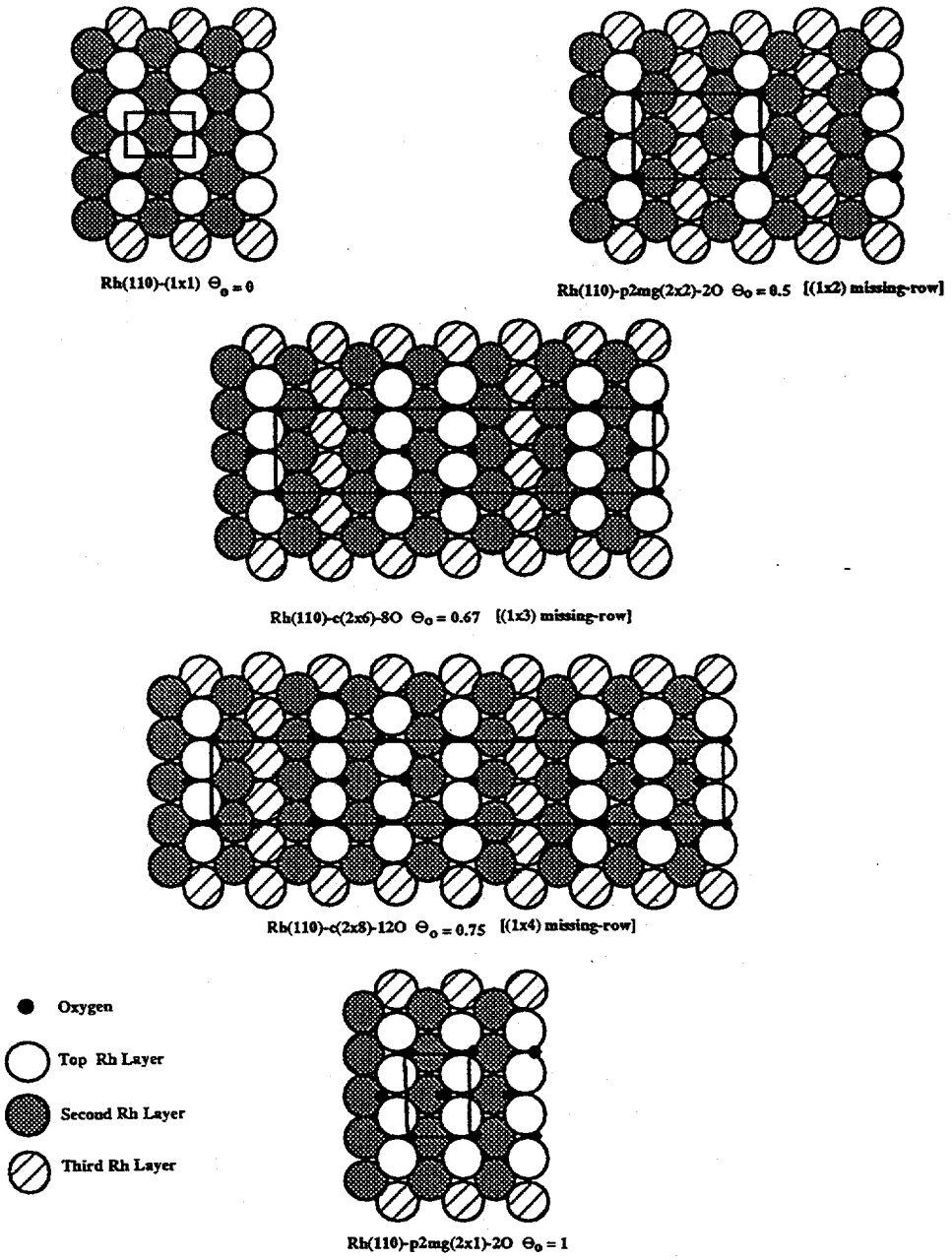

Figure 4.4: Changes in structure of the Rh(110) surface as a function of oxygen coverage. The initial structure is the clean Rh(110)-(1x1) surface. With oxygen adsorption the surface is reconstructed into a (1x2) missing-row, followed by a (1x3) and then a (1x4) missing-row structure with oxygen capping the lowest coordination Rh atoms at the surface. At saturation coverage of oxygen (one monolayer) the surface returns to the (1x1) type surface. [All structures are based on tensor LEED structure determinations with the exception of the Rh(110)-c(2x6)-8O structure and Rh(110)-c(2x8)-12O structure which are based on STM results on these surfaces assuming the oxygen positions are similar to those in the known oxygen structures.]

4.5.3 Comparison to oxygen adsorption on other Rh surfaces

For both the p2mg(2x1) and p2mg(2x2) oxygen structures on Rh(110), oxygen bonds in the 3-fold fcc hollow sites. The only other Rh surfaces for which oxygen adsorption structures have been examined in detail are the (111) and (100) crystal faces. On each of these surfaces oxygen has been shown to bond in the highest coordination site. On Rh(111) oxygen is bonded in the 3-fold fcc hollow site with a bond length of 1.98 Å. For oxygen adsorption on Rh(100) the oxygen is bonded in the 4-fold hollow site with a bond length of 2.13 Å.

4.5.4 Comparison to oxygen adsorption on other fcc(110) surfaces

The structural details of oxygen chemisorption have been examined for many other fcc(110) surfaces and are summarized in table 2. For the most part oxygen chooses to bond in the highest coordination surface site possible to make the most metal-O bonds. For Ag, Ni and Cu, added-row reconstructions upon oxygen adsorption appear to be the trend as observed for oxygen chemisorbed on Ag(110), Ni(110) and Cu(110). The oxygen atoms are bonded to 4 metal atoms: two metal atoms in the top layer, forming metal-oxygen-metal chains along the surface, and two metal atoms in the second layer. In the case of Rh(110) O is bonded in a 3-fold hollow site based on the two structures that have been determined so far. With Ir(110) a 2-fold bonded atomic oxygen species was reported. Further comparisons have been described in the literature. [4] The atomic O radius found in this work was 0.51 Å, assuming a hard sphere radius of 1.35 Å. This is smaller than the O radius found in the Rh(110)-p2mg(2x2)-2O structure, 0.65 Å, however it is within the range of O radii found on other fcc(110) surfaces, 0.34 -0.60 Å.

Table 4.2:

Surface	Structure	Θ(ML)*	Site	n.n. (Å)	2.n.n. (Å)	Technique	Ref.
Ag(110)	p(2x1)	0.50	long bridge	2.07	2.17	SEXAFS	[17]
		0.50	long bridge added row [001]	2.05	2.23	ICISS	[18]
		0.50	long bridge added row [001]	2.05	2.21	SEXAFS	[19]
Cu(110)	p(2x1)	0.50	long bridge added row [001]	1.81	2.01	LEED	[20]
				1.84	-----	SEXAFS	[21]
				1.62	1.90	ICISS	[22]
				1.81	2.00	LEIS	[23]
				1.84	1.85	XRD	[24]
Ir(110)	c(2x2)	0.50	short bridge	1.93	-----	LEED	[25]
Ni(110)	p(2x1)	0.50	long bridge added row [001]	1.78	-----	ALICISS	[26]
				1.85	2.19	SEXAFS	[27]
				1.77	1.86/2.04†	LEED	[28]
Rh(111)	(2x2)	0.25	3-fold hollow	1.98	-----	LEED	[15]
Rh(100)	(2x2)	0.25	4-fold hollow	2.13	-----	LEED	[14]
Rh(110)	p2mg(2x1)	1.00	3-fold hollow	1.97	2.04	LEED	[3]
	p2mg(2x1)	1.00	3-fold hollow	1.86	2.07	TLEED	this work
	p2mg(2x2)	0.50	3-fold hollow missing-row	2.00	1.88	TLEED	[4]

* Θ(ML)= O atoms/surface metal atoms.
n.n. = top metal layer nearest neighbor to the oxygen position.
2.n.n. = second metal layer nearest neighbor to the oxygen position.
----- = no value reported.
† Two values are given due to a reported asymmetry in the top layer bonding.

Table 4.2: Surface structural details for oxygen adsorbed on the (111) and (100) surfaces of Rh, as well as other fcc(110) surfaces.

4.6 References

[1] M. Bowker, Q. Guo, Y. Li, and R.W. Joyner, Catal. Lett. 18 (1993) 119.

[2] D. Alfé, P. Rudolf, M. Kiskinova, and R. Rosei, Chem. Phys. Lett. 211 (1993) 220.

[3] M. Gierer, H. Over, G. Ertl, H. Wohlgemuth, E. Schwarz, and K. Christmann, Surf. Sci. 297 (1993) L73.

[4] C. Comicioli, V.R. Dhanak, G. Comelli, C. Astaldi, K.C. Prince, A. Atrei, and E. Zanazzi, Chem. Phys. Lett. 214 (1993) 438.

[5] V.R. Dhanak, K.C. Prince, R. Rosei, P.W. Murray, F.M. Leibsle, M. Bowker, and G. Thornton, Phys. Rev. B 49 (1994) 5585.

[6] J.D. Batteas, A. Barbieri, E.K. Starkey, M.A. Van Hove, and G.A. Somorjai, Surf. Sci. 314 (1994) 341.

[7] M.A. Van Hove, W. Moritz, H. Over, P.J. Rous, A. Wander, A. Barbieri, N.Materer, U. Starke, and G.A. Somorjai, Surf. Sci Rep. 19 (1993) 191.

[8] P.J. Rous and J.B. Pendry, Surf. Sci. 219 (1989) 355 and 373.

[9] P.J. Rous, Prog. Surf. Sci. 39 (1992) 3.

[10] M.A. Van Hove and S.Y. Tong, *Surface Crystallagrophy by LEED: Theory, Computation, and Structural Results,* Berlin, Heidelberg: Springer-Verlag, 1979.

[11] J.B. Pendry, J. Phys. C 13 (1980) 937.

[12] M.A. Van Hove, W.H. Weinberg, and C.-M.Chan, *Low-Energy Electron Diffraction: Experiment, Theory, and Surface Structure Determination,* Berlin, Heidelberg: Springer-Verlag, 1986.

[13] W. Oed, H. Lindner, U. Starke, K. Heinz, K. Müller, and J.B. Pendry, Surf. Sci. 224 (1989) 239.

[14] W. Oed, B. Dötsch, L. Hammer, K. Heinz, and K. Müller, Surf. Sci. 207 (1988) 55.

[15] P.C. Wong, K.C. Hui, M.Y. Zhou, and K.A.R. Mitchell, Surf. Sci. 165 (1986) L21.

[16] W. Oed, W. Puchta, N. Bickel, K. Heinz, W. Nichtl, and K. Müller, J. Phys. C 21 (1988) 237.

[17] A. Puschmann and J. Hasse, Surf. Sci. 144 (1984) 559.

[18] M. Canepa, P. Cantini, F. Fossa, L. Mattera, and S. Terreni, Phys. Rev. B 47 (1993) 15823.

[19] L. Becker, S. Aminpirooz, A. Schmalz, B. Hillert, M. Pedio, and J. Hasse, Phys. Rev. B 44 (1991) 13655.

[20] S.R. Parkin, H.C. Zeng, M.Y. Zhou, and K.A.R. Mitchell, Phys. Rev. B 41 (1990) 5432.

[21] M. Bader, A. Puschmann, C. Ocal, and J. Hasse, Phys. Rev. Lett. 57 (1986) 3273.

[22] J.A. Yarmoff, D.M. Cyr, J.H. Huang, S. Kimm, and R.S. Williams, Phys. Rev. B 33 (1986) 3856.

[23] H. Dürr, T. Fauster, and R. Schneider, Surf. Sci. 244 (1991) 237.

[24] R. Feidenhans'l, F. Grey, R.L. Johnson, S.G.J. Mochrie, J. Bohr, and M. Nielsen, Phys. Rev. B 41 (1990) 5420.

[25] C.-M. Chan, K.L. Luke, M.A. Van Hove, W.H. Weinberg, and S.P. Withrow, Surf. Sci. 78 (1978) 386.

[26] H. Niehus and G. Comsa, Surf. Sci. 151 (1985) L171.

[27] K. Baberschke, U. Döbler, L. Wenzel, D. Arvanitis, A. Baratoff, and K.H. Rieder, Phys. Rev. B 33 (1986) 5910.

[28] G. Kleinle, J. Wintterlin, G. Ertl, R.J. Behm, F. Jona, and W. Moritz, Surf. Sci. 225 (1990) 171.

Chapter 5

Oxygen chemisorption on Rh(311)

The bonding of oxygen to the Rh(311) surface has been investigated by low-energy electron diffraction (LEED), temperature programmed desorption (TPD) and high-resolution electron energy loss spectroscopy (HREELS). The Rh(311) surface is densely stepped and consists of both (100) and (111) microfacets. Two ordered structures of oxygen have been found on this surface under oxygen chemisorption when the sample is annealed between 500-600 K. These structures can be described by the matrices $\begin{pmatrix} 3 & 0 \\ -2 & 1 \end{pmatrix}$ and $\begin{pmatrix} 2 & 0 \\ -3 & 2 \end{pmatrix}$ Based on the LEED and HREELS data models of the oxygen structures on the surface are presented. The oxygen atoms are proposed to be bonded to the top of the atomic ridges on the surface similar to that of oxygen chemisorption on Rh(110).

5.1. Introduction

Under high oxygen coverage conditions, Rh has been found to be structure sensitive for the oxidation of CO. [1-3] Little attention however has been given to the chemisorption of oxygen on more open, stepped surfaces of Rh. The Rh(311) surface is a densely stepped surface similar to Rh(110), however with both (100) and (111) microfacets at the surface. (Figure 5.1)

What is known about the chemisorption of oxygen on stepped Rh surfaces is briefly described here. To our knowledge the only other report of oxygen chemisorption on Rh(311) is a field ion microscopy (FIM) study of Rh tips under oxygen chemisorption [4] From these studies only the substrate periodicity could be examined and (1x3) and (1x2) type reconstructions of this surface was reported under oxygen chemisorption . In this work a (1x3) reconstruction of the surface as described in that work was not observed in the LEED patterns. However LEED patterns with streaks in the step direction have been observed and it is possible that both (1x3) and (1x2) reconstructed islands could co-exist on the Rh surface prior to the formation of the structure to be discussed. Oxygen chemisorption has also been examined on the Rh(711) surface. Based upon LEED, TPD and HREELS data both chemisorbed and sub-surface oxygen species were observed. This sub-surface oxygen was attributed to diffusion channels for oxygen into the bulk through the 4-fold hollow sites at the step edges on that surface.[5] These are similar to the 4-fold site on the Rh(311) substrate.

The surface closest in structure to the fcc(311) surface is the fcc(110) surface. Oxygen chemisorption has been extensively studied on this surface by LEED, AES, HREELS and STM [6-8]. On the Rh(110) surface oxygen is found to bond in the 3-fold fcc hollow sites in the troughs of the surface from dynamical LEED studies. The oxygen is bound strongly to the substrate and surface vibrational data confirms the O is bound in a 3-fold hollow site and finds a O-Rh stretching frequency of 555 cm^{-1}. While this is higher

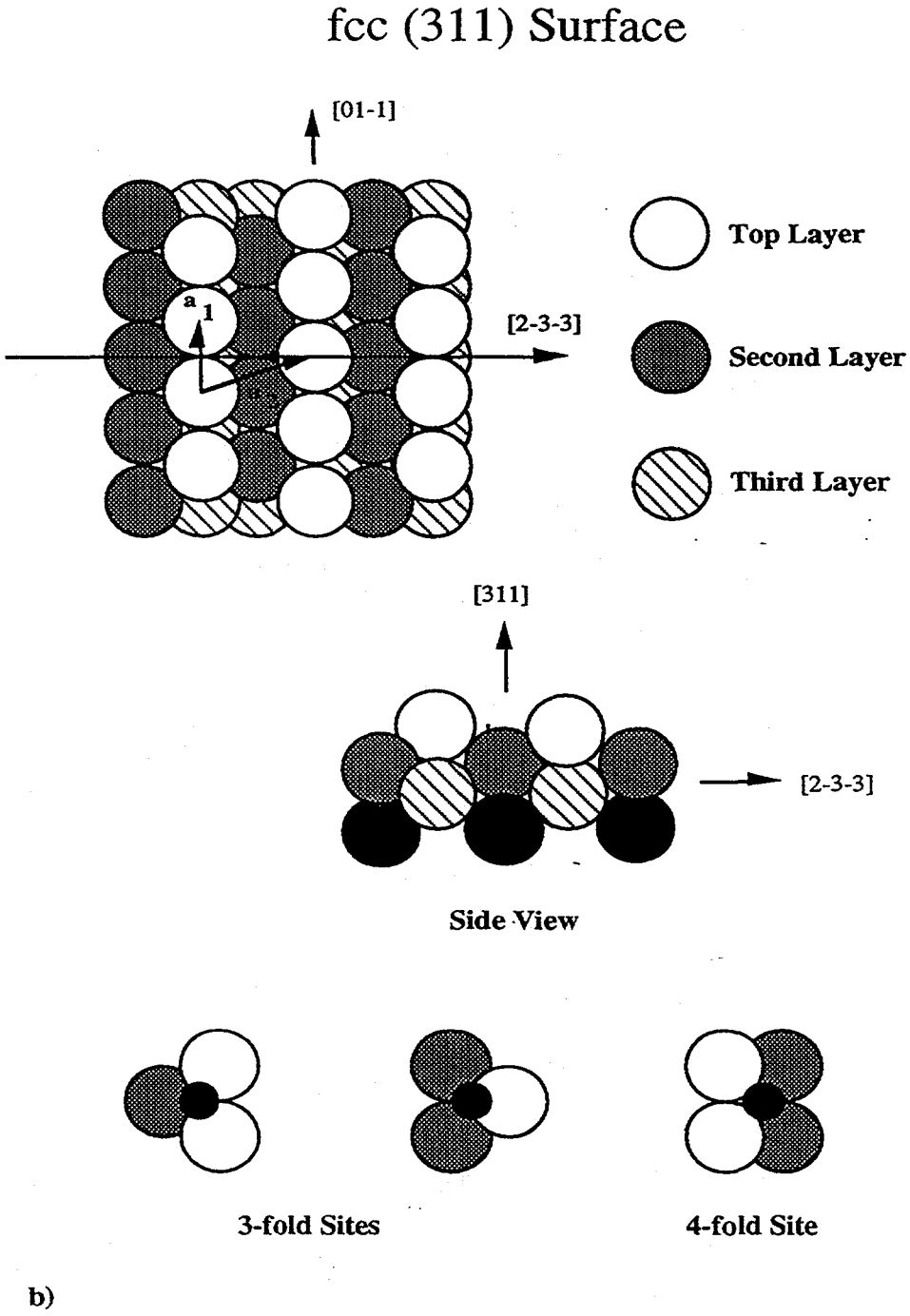

Figure 5.1: The top and side views of the fcc(311) surface showing the highest coordination surface sites.

than the typical 525 cm^{-1} found for O in fcc 3-fold hollow sites on Rh(111) this is understandable since on the (110) surface the oxygen is more strongly bound to the top of the atomic rows than to the Rh atoms in the second layer.

In this chapter the interactions of oxygen with the Rh(311) stepped surface are examined with combined LEED, TDS, and HREELS. Oxygen forms two ordered structures on the surface between 500 -600 K and coverages between 0.3 ML and 0.5 ML of saturation coverage. At 100 K oxygen adsorbs in a disordered fashion both molecularly and dissociated. Upon heating, the O_2 dissociates completely and forms two ordered structures depending on oxygen coverage. Based on these results structural models for oxygen chemisorption on the Rh(311) surface are presented.

5.2. Experimental

The Rh(311) crystal was cut from a boule of 99.999% purity and polished to within 1° of the [311] direction. The sample was cleaned and prepared in an ultrahigh vacuum chamber evacuated to 1.5 x 10^{-10} torr. Using Auger electron spectroscopy (AES) the primary contaminants were determined to be B, C, and S. These were removed by cycles of Ar^+ sputtering, O_2 treatments, and annealing in vacuum to 1100K. The cleanliness of the sample was monitored by both AES and HREELS. Temperatures above 1100 K were avoided as this results in a partially disordered (1x2) reconstruction which may only be removed by sputtering. [9] CO and O_2 were supplied by Matheson with a purities of 99.5% and 99.9% respectively and were used without further purification. All exposures are reported as the uncorrected ion gauge measurements. (1L = 1 x 10^{-6} torr•s)

The single crystal was mounted on the manipulator by Ta wires which allowed resistive heating of the sample. Sample cooling with liquid nitrogen cold fingers allowed for a minimum sample temperature of 100 K. Thermal desorption spectroscopy measurement were made with a UTI-100C quadrupole mass spectrometer at a heating rate

of 23 $K \cdot s^{-1}$. Low energy electron diffraction patterns were collected with a conventional Varian 4-grid LEED optics which also functioned as a retarding field energy analyzer for AES. The vibrational spectroscopy of surface adsorbates was carried out with a high resolution electron energy loss spectrometer. The spectrometer consists of two 127° cylindrical sectors and was designed [10] after current models in use. [11] The spectra were collected at an incident beam energy of 1.2 to 3.0 eV with a resolution of 7.3 to 12.4 meV (60 to 100 cm^{-1}). The elastic peak intensity in the specular direction ranged from 3 x 10^3 to 5 x 10^4 counts$\cdot s^{-1}$.

5.3. Results

5.3.1 LEED

After cleaning and preparing the Rh crystal, the clean surface exhibited a sharp (1x1) LEED pattern (fig. 2a). LEED I-V curves measured on the clean (1x1) surface compare readily with those given by a previous analysis of the clean surface structure.[9] Oxygen is dissociatively chemisorbed on the surface above 100 K. Two structures due to oxygen chemisorption have been observed as a function of oxygen exposure. A $\begin{pmatrix} 3 & 0 \\ -2 & 1 \end{pmatrix}$ structure is formed by an exposure of 1-3 L of O_2 at 100 - 300K, followed by flashing to 600 K. As the sample cools down, the ordered structures appears. A higher coverage structure given by the matrix $\begin{pmatrix} 2 & 0 \\ -3 & 2 \end{pmatrix}$ is formed from the adsorption of 6-20 L between 100 - 300K, followed by flashing to 600 K. The LEED pattern for the high coverage structure seems to indicate that a surface reconstruction has occurred. While heating this structure the intensity of the half-order diffraction beams, along the close direction of the diffraction pattern, remains intact, while the other fractional order beams disappear. This can be explained by the surface undergoing a (1x2) type reconstruction similar to Rh(110).

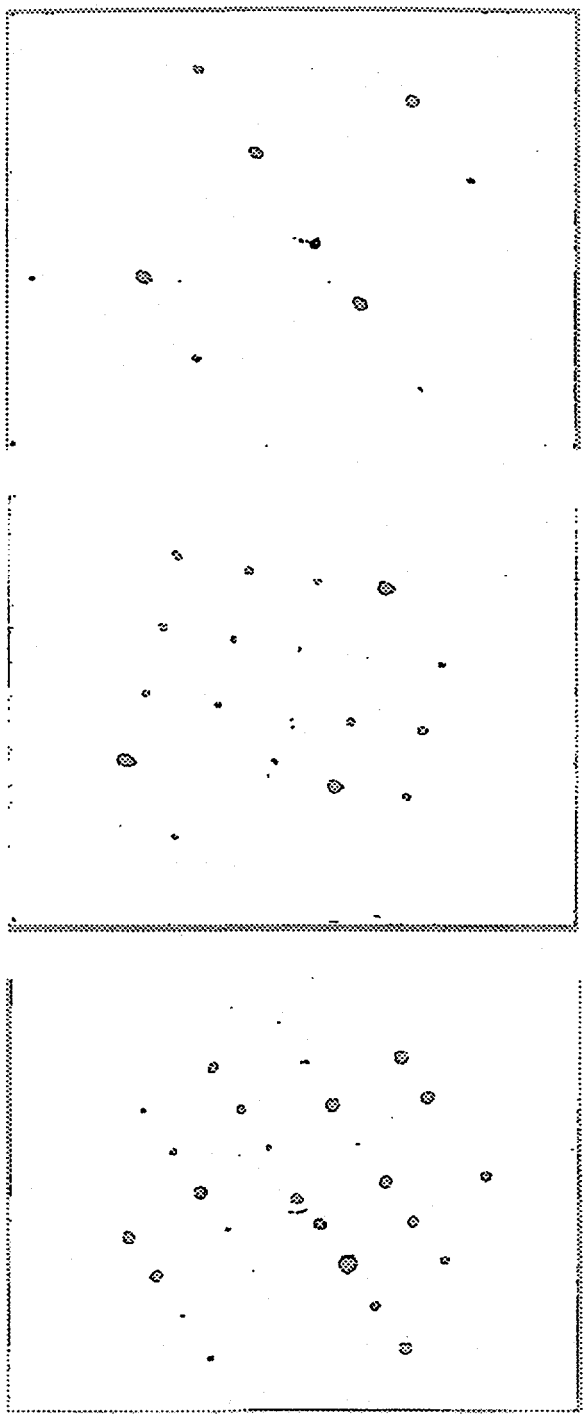

Figure 5.2: LEED patterns of the clean a) and oxygen covered b-c) Rh(311) surfaces.

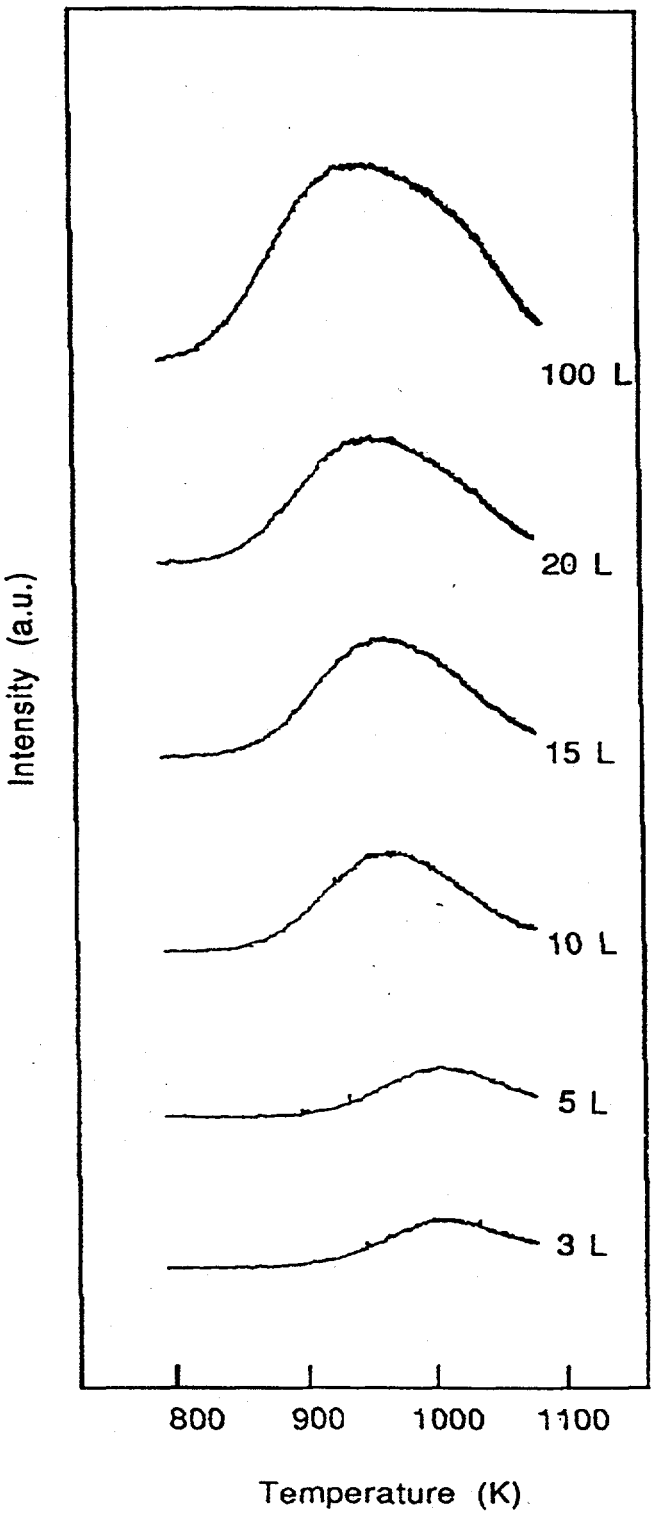

Figure 5.3: O_2 TPD spectra from Rh(311) as a function of O_2 exposure.

Thus the fractional order beams that decrease in intensity with increasing temperature are related to oxygen, while the others that remain are related to the reconstructed Rh, due to the differences in the Debye temperatures of oxygen and Rh.

5.3.2 TPD

The thermal desorption of O_2 has been monitored as a function of O_2 exposure and shown in figure 5.3. The desorption of oxygen from the surface is second order and has a shift in the peak rate of desorption from 1000 K at low coverage to 930 K at saturation. The heat of desorption changes from 61.2 to 56.6 kcal/mol with increasing oxygen coverage. Based upon the areas of the TPD peaks, the coverages of the two structures can assigned with respect to saturation. The coverage of the $\begin{pmatrix} 3 & 0 \\ -2 & 1 \end{pmatrix}$ structure is approximately 0.30 ML and the coverage of the $\begin{pmatrix} 2 & 0 \\ -3 & 2 \end{pmatrix}$ structure is approximately 0.50 ML.

5.3.3 HREELS

The vibrational spectroscopy of oxygen on Rh(311) has been investigated as a function of oxygen coverage and temperature. At 100 K oxygen adsorbs in a disordered fashion. The vibrational spectra of the ordered oxygen overlayers are shown in figure 5.4. At 100 K oxygen adsorbs in a disordered fashion and at 1 L exposure a vibrational band at 420 cm^{-1} is observed. This is consistent with dissociatively chemisorbed oxygen bonded in a 4-fold hollow site. With increasing oxygen exposure the vibrational band shifts to slightly higher frequency until at saturation the O-Rh stretch is observed at 485 cm^{-1}. A second, broad vibrational band appears weakly between 900-1000 cm^{-1} which is in the range of the O-O stretch of O_2 as observed with molecular O_2 absorbed on Rh(110) and (711). [5,8] Exposing the surface to 1-3 L of O_2 at 100 K and flashing to

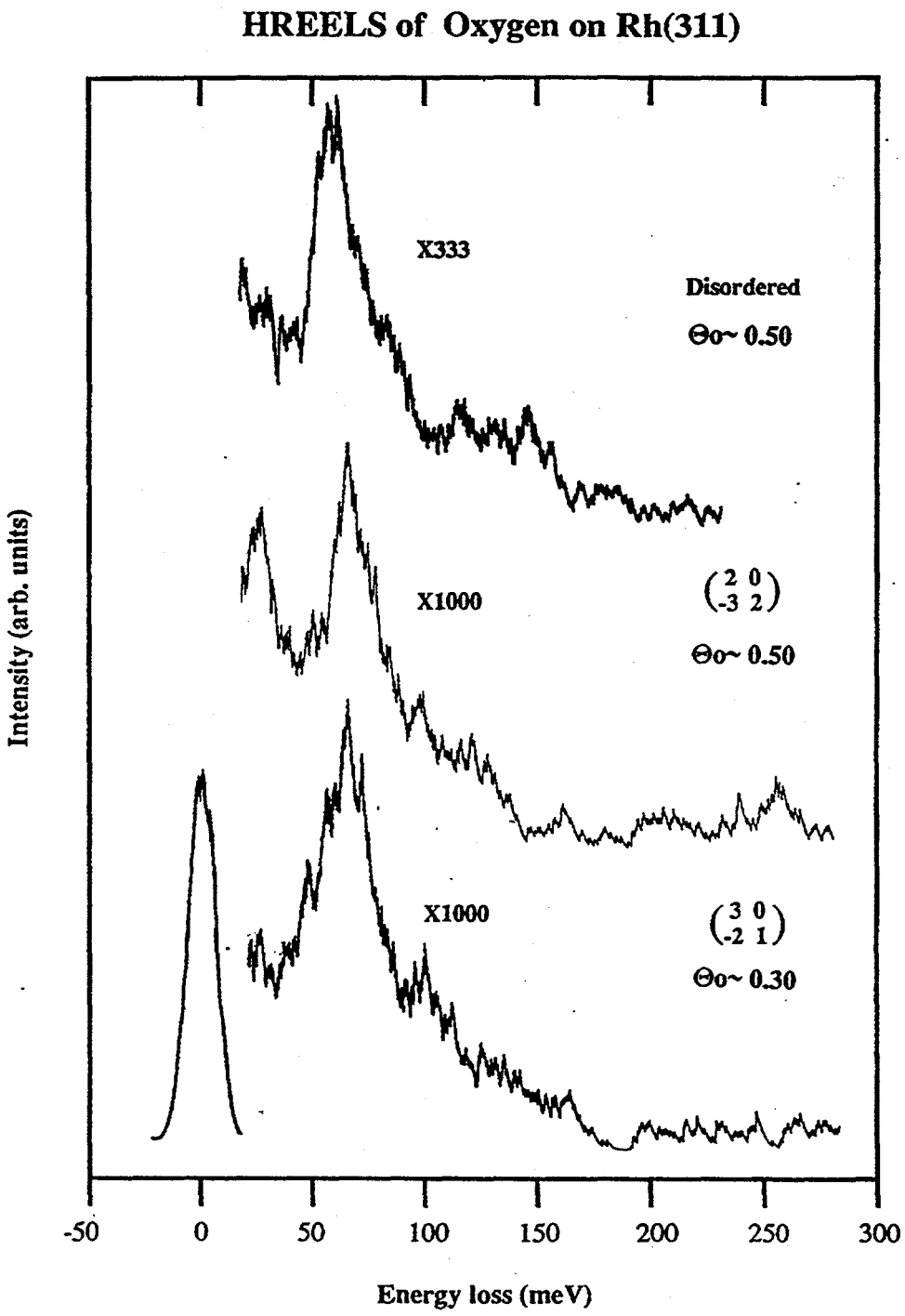

Figure 5.4: HREELS spectra for chemisorbed oxygen on Rh(311). Shown are the spectra from the two ordered oxygen structures and from disordered oxygen adsorbed at 100 K.

600 K results in the formation of the ordered O structure $\begin{pmatrix} 3 & 0 \\ -2 & 1 \end{pmatrix}$ and a shift in the O-Rh stretch to 553 cm^{-1} . This band is very broad ,~ twice the FWHM of the elastic peak, and thus may represent occupation of both 3-fold and 4-fold sites on the surface, or disorder in the overlayer. The same O-Rh band is found for the higher coverage $\begin{pmatrix} 2 & 0 \\ -3 & 2 \end{pmatrix}$ structure. This band however is much narrower than that of the low coverage structure which may be due to having a more well ordered structure on the surface. Additionally a low frequency mode appears around 200 cm^{-1}, which can be attributed to Rh phonons. The observation of these phonons may be activated by a reconstruction of the surface. This mode is similarly observed with oxygen chemisorption on Rh(110).

5.4. Discussion

The adsorption of oxygen on the Rh(311) surface results in two ordered oxygen structures, a $\begin{pmatrix} 3 & 0 \\ -2 & 1 \end{pmatrix}$ and a $\begin{pmatrix} 2 & 0 \\ -3 & 2 \end{pmatrix}$,at coverages 0.3 ML and 0.5 ML respectively. HREELS data on these two surfaces show Rh-O stretches in the range of 480 to 560 cm^{-1}. It is difficult to assign the oxygen to a given site on the surface given these Rh-O vibrational bands. The Rh(311) surface has both 4-fold and 3-fold coordination sites in the channels of the atomic rows on the surface. Oxygen has always been found to bond in the highest coordination sites on Rh. (See Chapter 4, Table 4.2) Thus we might expect that oxygen bonds in the 4-fold hollow site on Rh(311).

The Rh-O stretch for O in a 4-fold hollow site on the Rh(100) surface is at approximately 410 to 420 cm^{-1}.[12] On the Rh(111) surface the Rh-O stretch is found between 500 to 555 cm^{-1}. [13] On Rh(711), which is similar to Rh(311) except that the (100) facet on Rh(711) is 3 Rh atoms wider than on Rh(311), oxygen chemisorbs at the 4-fold hollow sites is identified by a Rh-O band between 434 to 483 cm^{-1}.

Based on this information it is suggested that in the disordered oxygen spectra, where the Rh-O stretch is found at 487 cm^{-1} near saturation, the oxygen may be bonded in the 4-fold hollow sites in the channels on the surface. The annealing of the surface shifts the Rh-O band in both structures to approximately 553 cm^{-1}. This is more consistent with oxygen chemisorption on Rh in a 3-fold coordinated site. This however is inconsistent with the trend for oxygen bonding in the highest coordination site on Rh.
Thus based on these previous results and the vibrational data shown here, the oxygen must be coordinated in a 3-fold hollow site. The breadth of the Rh-O band however does not exclude the possibility of domains of 3-fold coordination mixed with domains of 4-fold coordination.

Proposed models are presented in figure 5.5. For the low coverage structure, $\begin{pmatrix} 3 & 0 \\ -2 & 1 \end{pmatrix}$, no substrate reconstruction is expected and the oxygen atoms are placed in the fcc 3-fold hollow sites, much as in oxygen bonding on the Rh(110) surface. For the high coverage structure, $\begin{pmatrix} 2 & 0 \\ -3 & 2 \end{pmatrix}$, a (1x2) missing-row reconstruction is proposed based on the temperature dependence of the diffracted beams in the LEED pattern and the observation of a (1x2) missing-row on this surface under oxygen chemisorption by FIM. [4] The oxygen atoms in this structure are arranged along the tops of the atomic rows in an alternating fashion, as in the 0.50 ML oxygen induced missing-row structure on Rh(110). The mixture of 3-fold and 4-fold hollow sites explain the broad Rh-O band observed for this structure. Fully-dynamical LEED structure analyses of these structures will be required to determine the detailed structures.

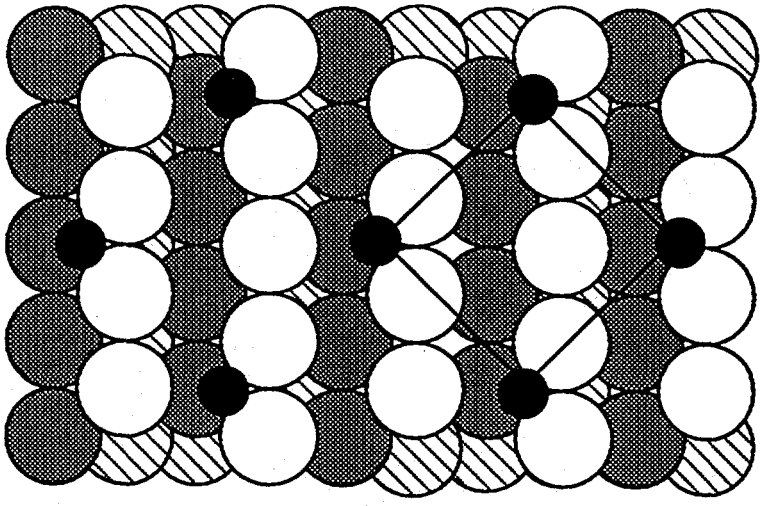

Rh(311)-$\begin{pmatrix} 3 & 0 \\ -2 & 1 \end{pmatrix}$-O Structure

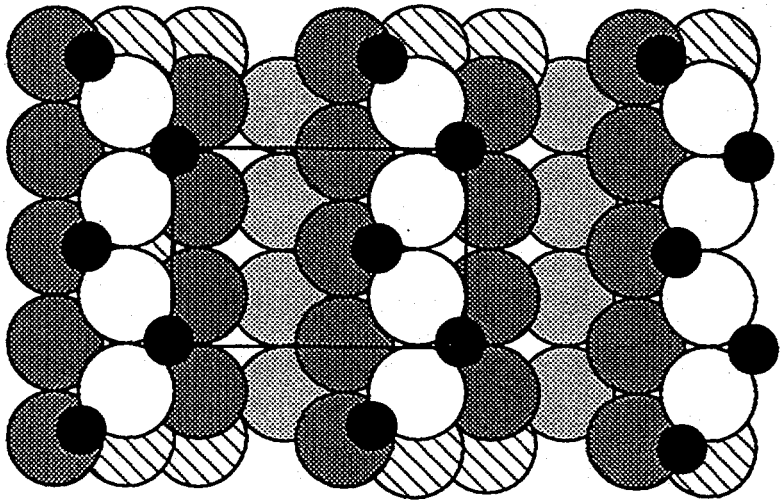

Rh(311)-$\begin{pmatrix} 2 & 0 \\ -3 & 2 \end{pmatrix}$-2O Structure

Figure 5.5: Proposed models for the ordered oxygen structures on Rh(311).

5.5 References

[1] S. H. Oh, G. B. Fisher, J. E. Carpenter and D. W. Goodman, J. of Catal. 100 (1986) 360.

[2] M. Bowker, Q. Guo, Y. Li, and R.W. Joyner, Catal. Lett. 18 (1993) 119.

[3] L.-W. H. Leung and D. W. Goodman, Catal. Lett. 5 (1990) 353.

[4] C. Voss, A. Gaussmann and N. Kruse, Appl. Surf. Sci. 67 (1993) 142.

[5] D.N. Belton, G.B. Fisher and C.L. DiMaggio, Surf. Sci. 233 (1990) 12.

[6] C. Comicioli, V.R. Dhanak, G. Comelli, C. Astaldi, K.C. Prince, A. Atrei, and E. Zanazzi, Chem. Phys. Lett. 214 (1993) 438.

[7] V.R. Dhanak, K.C. Prince, R. Rosei, P.W. Murray, F.M. Leibsle, M. Bowker, and G. Thornton, Phys. Rev. B 49 (1994) 5585.

[8] D. Alfé, P. Rudolf, M. Kiskinova, and R. Rosei, Chem. Phys. Lett. 211 (1993) 220.

[9] S. Liepold, N. Elbel, M. Michl, W. Nichtl-Pecher, K. Heinz, and K. Müller, Surf. Sci. 240 (1990) 81.

[10] C.M. Mate, Ph.D. Dissertation, University of California at Berkeley, 1986.

[11] H. Froitzheim, H. Ibach, S. Lehwald, Rev. Sci. Instrum. 46 (1975) 1325.

[12] L.H. Dubois, J. Chem. Phys. 77 (1982) 5228.

[13] T.W. Root, G.B. Fisher and L.D. Schmidt, J. Chem.. Phys. 85 (1986) 4687.

Chapter 6

CO chemisorption on Rh(311)

The bonding of CO on the stepped Rh(311) surface has been investigated by high resolution electron energy loss spectroscopy (HREELS), low-energy electron diffraction (LEED), and thermal desorption spectroscopy (TDS). At saturation coverage (estimated to be 1 monolayer) an ordered (2x2) surface structure is formed in the range of 120 to 270 K. Thermal desorption spectroscopy measurements (23 $K \cdot s^{-1}$) show first order desorption with a shift in peak temperature from 528 K at low coverage to 503 K at high coverage, accompanied by an additional peak at 388 K. The heat of desorption at low coverage is found to be 31.1 kcal/mol which is nearly identical to the heat of desorption of CO from Rh (110), (100), and (111) showing that CO bonding at low coverages is structure insensitive. From the HREELS spectra both the Rh-C and CO stretching frequencies are observed to shift from 524 to 443 cm^{-1} and 1935 to 2056 cm^{-1} respectively as a function of CO coverage. HREELS spectra of the (2x2) structure have a CO stretch at a frequency of 2056 cm^{-1} and a Rh-C stretch at 443 cm^{-1}, which indicates that the CO molecule is bonded to the top site of the step edges. Based on these results a structural model with CO top site adsorption is proposed.

6.1. Introduction

The chemisorption and surface structures of CO on flat close-packed surfaces of Rh such as the (111) and (100) crystal faces have been studied by many. [1-7] Because of the catalytic importance of Rh in reactions involving CO (hydrogenation and oxidation by NO) it is essential to examine CO chemisorption on defect sites, such as steps and kinks, which are the proposed sites of rapid surface reactions. Such sites are present in abundance on more open, rough high Miller Index surfaces. The Rh(311) surface is such a surface, it is densely stepped and consists of alternating (111) and (100) microfacets (fig. 1). This is somewhat similar to the (110) surface which only has (111)-type facets and which is 17% more close-packed than the (311) surface. Surface structural low-energy electron diffraction (LEED) analyses of the clean unreconstructed Rh(311) and Rh(110) surfaces have found relaxations in the top 4 metal layers, with a relaxation of the top interlayer spacing by -14.5% on the (311) surface [8], and by -6.9% on the (110) surface [9], relative to the bulk interlayer spacing. Because of the similarity between the surface structures of these two faces one might expect the bonding of CO on Rh(110) and Rh(311) to be similar.

Let us briefly review what is known about the bonding of CO to Rh(110). At saturation coverage (estimated at approximately 1 monolayer) CO forms a p2mg(2x1) structure in which the CO molecules are proposed to sit on top sites and to arrange in a zig-zag fashion to produce the observed glide-plane symmetry [10]. The thermal desorption spectroscopy (TDS) of CO from this surface shows first order desorption which in the low coverage limit has a heat of desorption of approximately 31 kcal/mol. No vibrational data and no structural analysis exists for this system to date; however an investigation of these properties are both currently underway in our laboratory. Information on structure and bonding is available for CO/Ni(110) however. A dynamical LEED analysis for p2mg(2x1)-CO on Ni(110) has found short bridge bonded CO molecules with a tilt angle

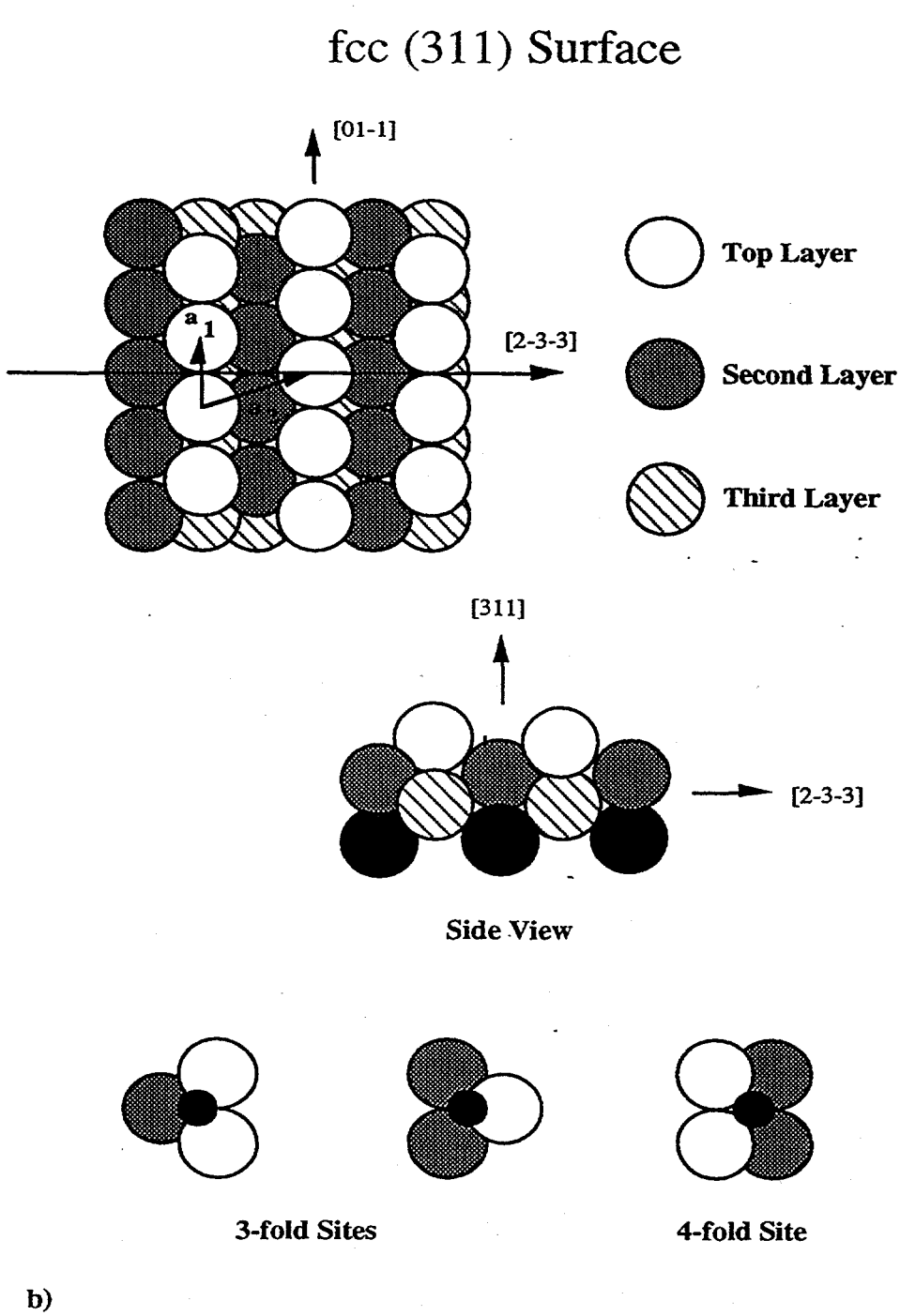

Figure 6.1: The top and side views of the fcc(311) surface .

of $17^{o} \pm 3^{o}$ from the surface normal. [11] Recent high resolution electron energy loss spectroscopy (HREELS) results presented by Ibach however find only top site adsorption for CO at high coverage on Ni(110). [12]

In this chapter the combined LEED, TDS, and HREELS results for CO bonding to the Rh(311) surface is described. We find that CO forms an ordered (2x2) surface structure at 270 K and below. At high coverage we find a Rh-C stretch at 443 cm^{-1} and a CO stretch at 2056 cm^{-1}. All of the evidence indicates that CO is occupying top sites on the surface and a model for the (2x2) structure is presented.

6.2. Experimental

The Rh(311) crystal was cut from a boule of 99.999% purity and polished to within 1^{o} of the [311] direction. The sample was cleaned and prepared in an ultrahigh vacuum chamber evacuated to 3×10^{-10} torr. Using Auger electron spectroscopy (AES) the primary contaminants were determined to be B, C, and S. These were removed by cycles of Ar^{+} sputtering, O_2 treatments, and annealing in vacuum to 1100K. The cleanliness of the sample was monitored by both AES and HREELS. Temperatures above 1100K were avoided as this results in a partially disordered (1x2) reconstruction which may only be removed by sputtering. [8] CO was supplied by Matheson with a purity of 99.5% and was used without further purification. All exposures are reported as the uncorrected ion gauge measurements. ($1L = 1 \times 10^{-6}$ torr•s)

The single crystal was mounted on the manipulator by Ta wires which allowed resistive heating of the sample. Sample cooling with liquid nitrogen cold fingers allowed for a minimum sample temperature of 120K. Thermal desorption spectroscopy measurement were made with a UTI-100C quadrupole mass spectrometer at a heating rate of 23 $K \cdot s^{-1}$. Low energy electron diffraction patterns were collected with a conventional Varian 4-grid LEED optics which also functioned as a retarding field energy analyzer for

AES. The vibrational spectroscopy of surface adsorbates was carried out with a high resolution electron energy loss spectrometer. The spectrometer consists of two 127° cylindrical sectors and was designed [13] after current models in use. [14] The spectra were collected at an incident beam energy of 3.3 to 3.5 eV with a resolution of 9.9 to 12.4 meV (80 to 100 cm^{-1}). The elastic peak intensity in the specular direction ranged from 3 x 10^3 to 1 x 10^4 counts•s^{-1}. The spectra were monitored as a function of CO exposure and detector angle.

6.3. Results

6.3.1 Low-energy electron diffraction studies of CO on Rh(311).

The ordering of CO on Rh(311) has been examined from 120 K to 550 K. After cleaning and preparing the Rh crystal, the clean surface exhibited a sharp (1x1) LEED pattern (fig. 2a). CO adsorbs in a disordered fashion resulting in increased background intensity. At low exposures of approximately 3L a weak (2x1) LEED pattern is observed, similar to that reported on Pd(311) [15], but is not well ordered resulting in diffuse diffraction beams. After an exposure of 40L between 120 and 270K, a well ordered (2x2)-CO structure is produced (fig. 2b). Only at saturation coverage could the diffraction pattern that corresponds to the (2x2) surface structure be formed. (The differences in background intensity shown in the figures are not due to partial disordering of the overlayer, but rather to a long exposure time in the LEED photo of the (2x2) pattern.) The (2x2) structure was found to be most stable below 220K. When CO was adsorbed at 270K the (2x2) pattern would be produced, but could only be maintained with a partial pressure of CO (5 x 10^{-9} torr) in the vacuum chamber. Upon removing the background pressure of CO the pattern degrades suggesting that the structure is electron beam sensitive and CO desorbs from the surface. Above 300K the pattern degrades rapidly

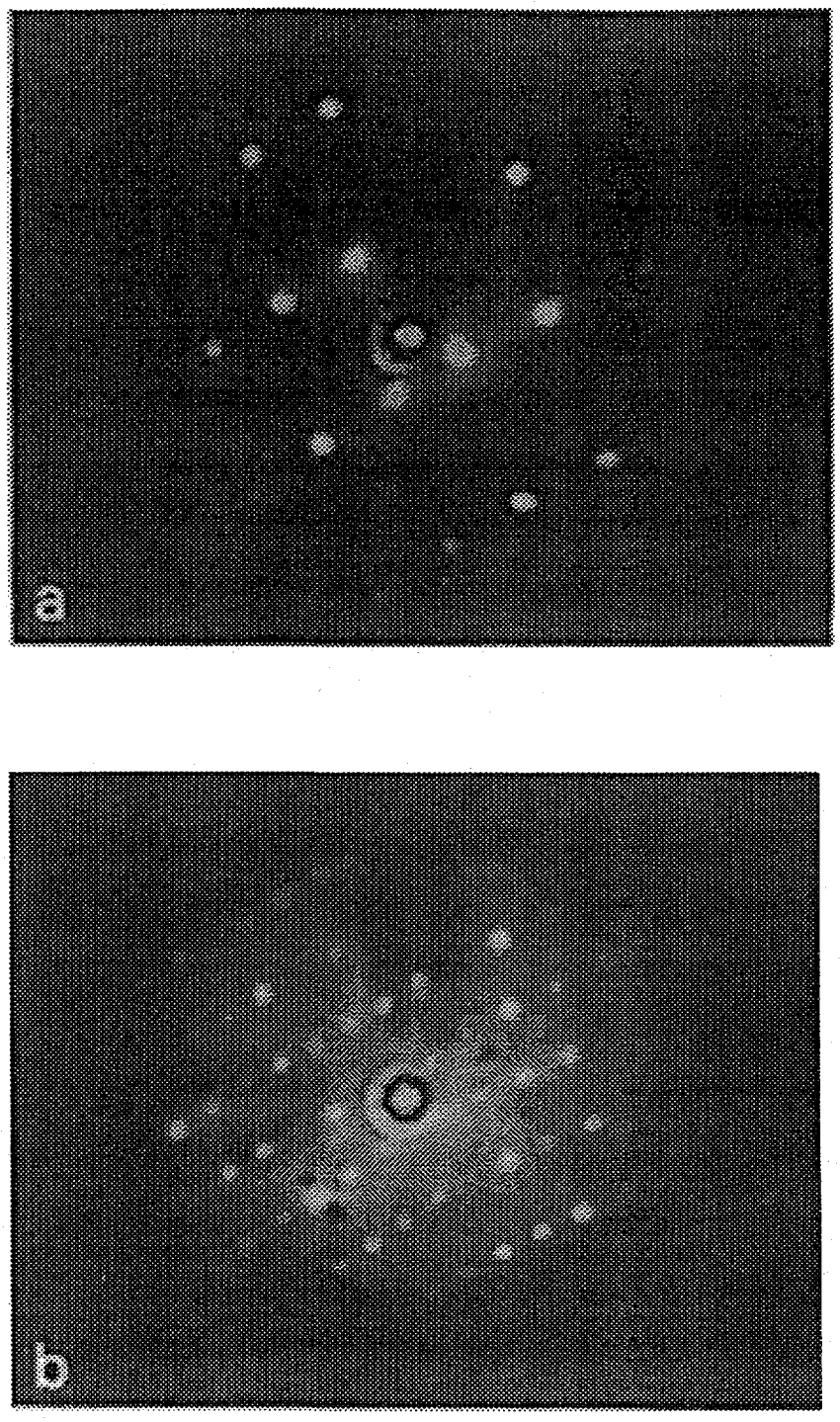

Figure 6.2: LEED patterns of the clean (1x1) surface (a) and (2x2)-CO (b) at 105 eV.

as CO begins to desorb from the surface. Only the (1x1) LEED pattern of the clean surface is observed past 550K.

6.3.2 The thermal desorption of CO from Rh(311).

The thermal desorption has been monitored as a function of CO exposure and is shown in figure 3. At low exposures there is only a single desorption state α_1 at 528K. With increasing exposure this state is observed to shift in temperature from 528K to 503K at 0.5 and 40L respectively. After 10L a second desorption state α_2 is observed with a peak temperature of 388K. Assuming first order desorption (based on HREELS results that show only molecular adsorption) and a pre-exponential factor of 10^{13} s^{-1} we have calculated the heat of desorption to range from 31.1 to 29.5 kcal/mol for the α_1 state at 0.5 and 40L respectively, and 22.3 kcal/mol for the α_2 state. We attribute this lowering of the heat of desorption to lateral interactions between CO molecules. The pre-exponential factor of 10^{13} s^{-1} was selected to allow for a comparison to the calculated heats of desorption from other surfaces for which the same pre-exponential was used. Shown in figure 4 we have correlated the heat of desorption as a function of coverage for the Rh (311), (110) [16], (111) [2], and (100) [4] surfaces. In the low coverage limit (given for exposures $\leq$ 0.5L) CO desorption from each surface approaches 30 to 31 kcal/mol. This shows that CO bonding at low coverages is structure insensitive suggesting that only the local metal atom is important for making the CO-Rh bond. At high coverages the TDS spectra for each face are different which may be due to differences in CO-CO interactions. The TDS results from the (110) face however most closely resembles that from Rh(311). Also, as small amounts of CO could be decomposed on the surface during heating, we looked for CO_2 and O_2 desorption, but did not detect any within the sensitivity of our mass spectrometer.

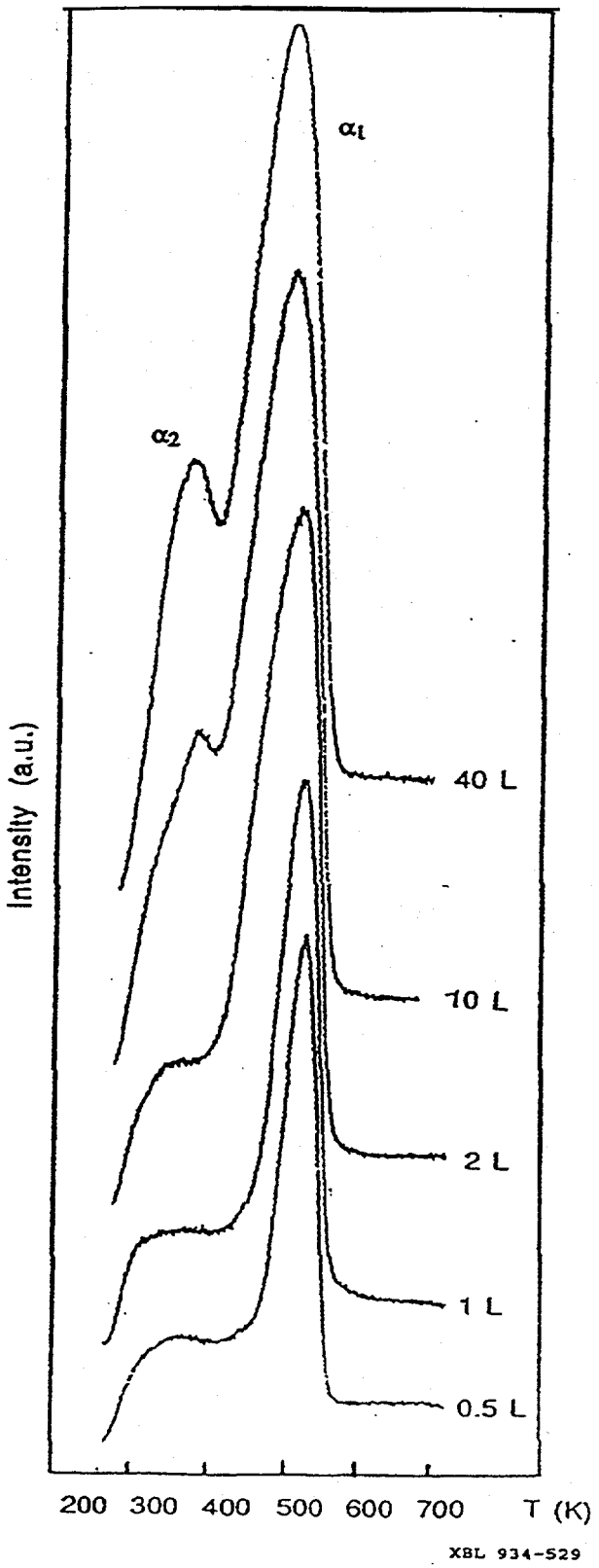

Figure 6.3: TDS as a function of CO exposure from Rh(311).

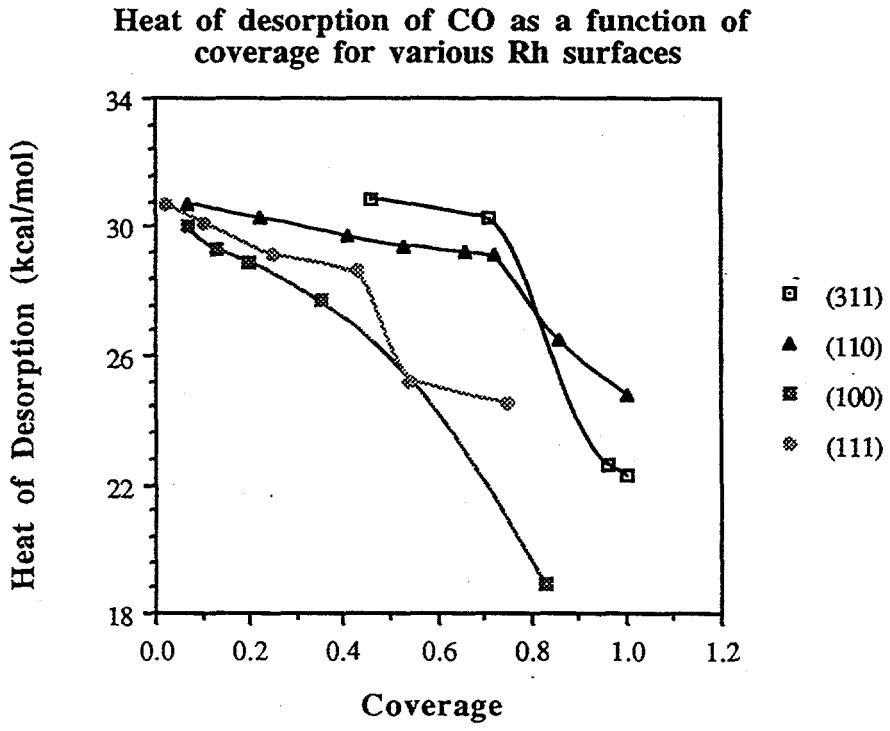

Figure 6.4: Change in heat of desorption of CO from various Rh surfaces as a function of coverage.

The absence of dissociative chemisorption of CO is consistent with an investigation of CO dissociation on Rh tips of (113) orientation. [17] From the similarities between the (311) and (110) crystal faces we can estimate the coverage of the (2x2) CO overlayer on Rh(311) to be at 1ML coverage, where 1ML is defined as 1 CO per Rh top site, based on a comparison of the coverage calibration of Bowker et. al. for CO/Rh(110). At saturation they find a coverage of 0.95 ± 0.05 ML. [16] The coverage values from the various exposures were then calculated from the total integrated TDS peak areas based on this assignment.

6.3.3 High resolution electron energy loss spectroscopy of CO adsorbed on Rh(311).

The vibrational spectroscopy of CO on the Rh(311) surface has been examined in the specular and off-specular directions. The spectra were collected at an incident beam energy of 3.3 to 3.5 eV with a resolution of 9.9 to 12.4 meV (80 to 100 cm^{-1}). The HREELS spectra in the specular direction are shown in figure 5 as a function of CO exposure. At 1L the Rh-CO stretching frequency is found to be 524 cm^{-1} and the CO stretch 1935 cm^{-1}. Although this is a typical CO stretching frequency for a bridge bonded species, the Rh-CO stretching frequency of 524 cm^{-1} would appear to be too high for a bridge bonded species. Such ambiguities have been recently observed when comparing vibrational site assignments to dynamical LEED structure calculations. An adsorption study of CO on Ni(110) by RAIRS [18] was used to assign bridge bonded species for a CO stretch of 1998 cm^{-1}, while in an HREELS study [12] top site adsorption was assigned to a CO stretch of 1984 cm^{-1}. The LEED structure calculation however found a bridged site. Also the structure of CO/Pd(110) was solved by LEED [19] finding a top site species, for which the CO stretching frequency was 2003 cm^{-1} [20]. It is therefore possible that at low exposures on Rh(311) the CO is bridge bonded.

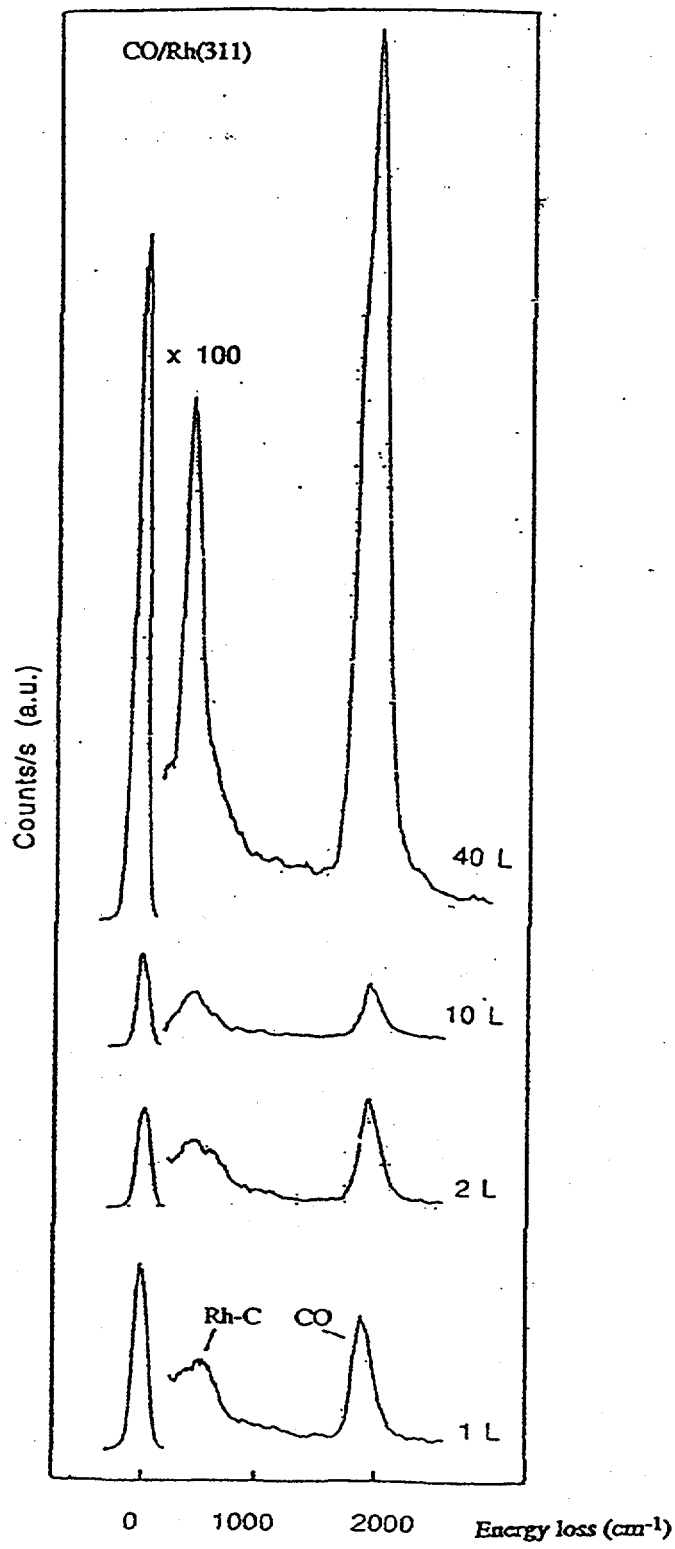

Figure 6.5: HREELS spectra of CO/Rh(311) in the specular direction as a function of CO exposure.

With increasing coverage both frequencies are observed to shift (fig. 6) until at 40L, where the (2x2)-CO structure is formed, we find a Rh-C stretch at 443 cm^{-1} and CO stretch at 2056 cm^{-1}. Few vibrational data exist for CO adsorbed on corrugated surfaces, however these frequencies are comparable to what is observed on other similar surfaces and with top site adsorption on Rh(111) and (100) (Table 1). The shift in stretching frequency with increasing coverage suggests that the CO-Rh bonding is changing as a function of coverage. As more CO is adsorbed on the surface, the Rh-C frequency decreases by 60 cm^{-1}. This is an indication of a weaker metal-carbon bond, which is consistent with the lowering of the heat of desorption with increasing CO coverage observed in the TDS results. The correlation between the heat of desorption and Rh-C stretching frequency is shown in figure 7. The 120 cm^{-1} increase in the CO stretch is a result of less 4d to $2\pi^*$ electron transfer, thus maintaining a stronger C=O bond.

Examining the HREELS spectra of the (2x2)-CO structure in the off-specular direction shows a decrease in the intensities of all modes as a function of the detector angle (fig. 8a,b) indicating that both the Rh-C and CO stretching modes are dipole active and that the CO molecule is oriented perpendicular to the surface normal. A unique feature to note is that at 10^o off-specular the CO stretch is broadened to lower frequency with a shoulder at 1955 cm^{-1} and the peak frequency is now observed at 2095 cm^{-1}. A similar splitting was observed for CO/Ni(110) where this was attributed to Davydov splitting resulting from in phase and out of phase vibrations of the multiple CO molecules in the unit cell [12]. Since a (2x2) unit cell on Rh(311) with 1ML of CO would consist of 4 CO molecules, it is reasonable that such an effect may be present.

6.4. Discussion

The adsorption of CO on Rh(311) results in the formation of a (2x2) surface structure. From thermal desorption spectroscopy the heat of desorption was found to

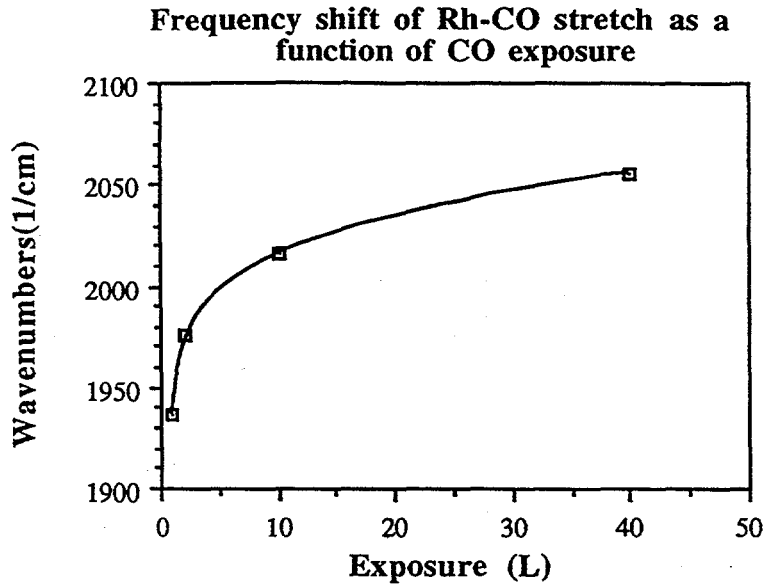

a)

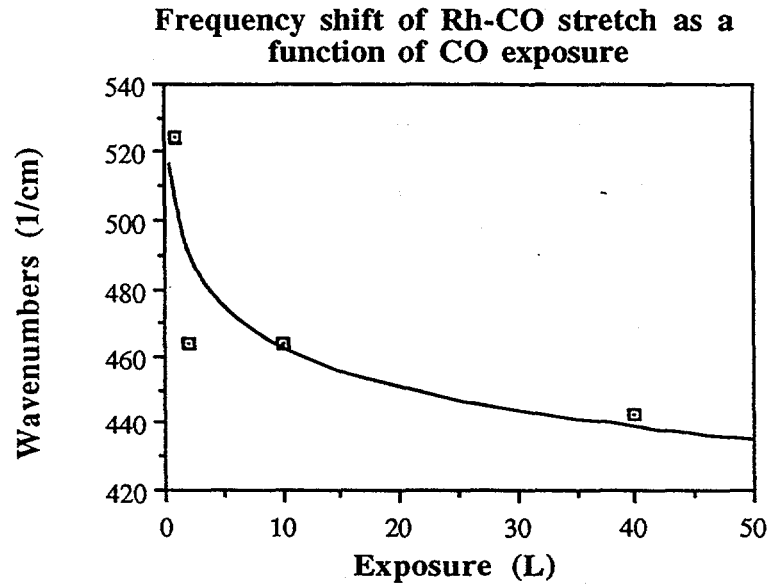

b)

Figure 6.6: Shifts in the CO (a) and Rh-C (b) stretching frequencies as a function of CO exposure. The curves are added to elucidate the trend in the shift.

Table 1: Vibrational frequencies * of CO on various transition metal surfaces.

Surface	Site	ν(M-CO) cm^{-1}	ν(C-O) cm^{-1}	Technique	Reference
Rh(311)	Top	443	2056	HREELS	this work
Rh(111)	Top	450	2065	HREELS	2
	Bridge	385	1855		
Rh(100)	Top	450	2020	HREELS	23
	Bridge	390	1930		
Rh(110)	-----	----	------		
Pd(110)	Top	----	2003	RAIRS	24
Cu(110)	Top	----	2094	IRAS	25
Ni(110)	Top	421	1984	HREELS	12
Ni(110)	Bridge	----	1998	RAIRS	18
Pt(110)	Top	475	2105	HREELS	27
	Top	----	2079	RAIRS	27
Fe(110)	Top	455	1890	HREELS	26

* All data are reported for high coverage except Fe(110).

Table 6.1: Vibrational data for CO on various transition metal surfaces.

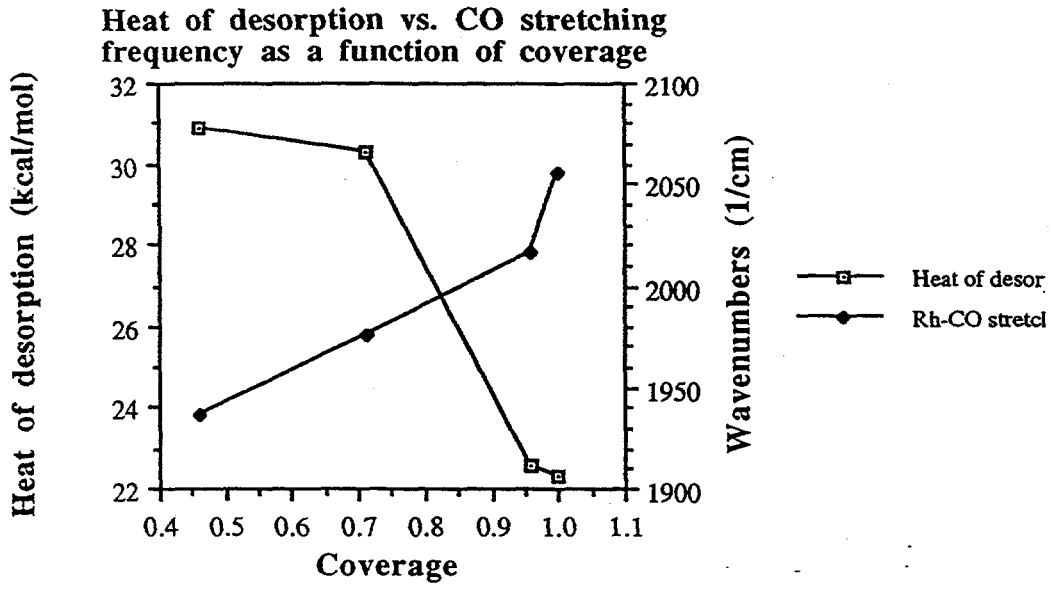

a)

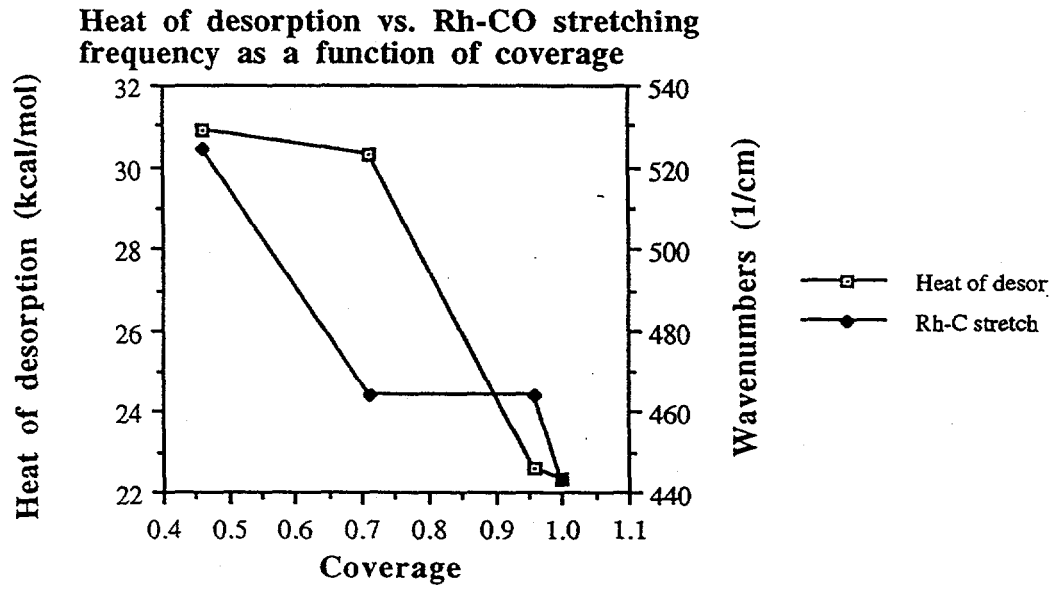

b)

Figure 6.7: Correlation of heat of desorption with the CO stretch (a) and the Rh-CO stretch (b).

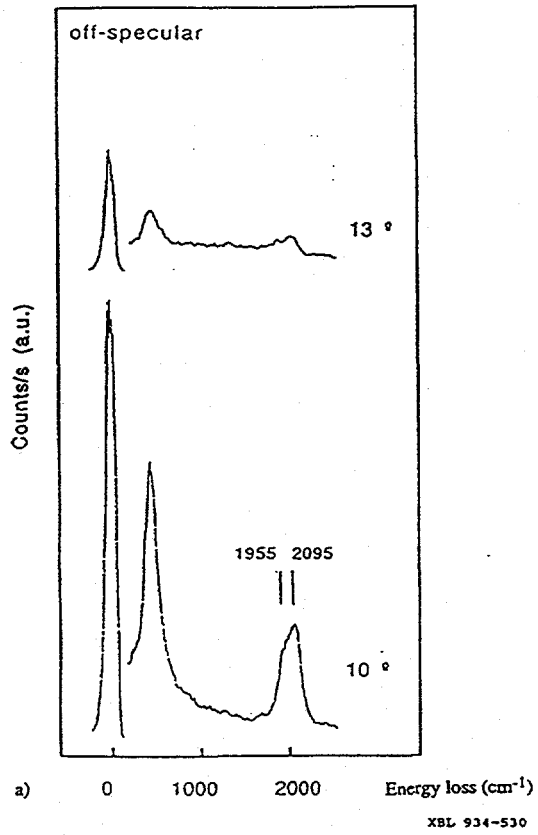

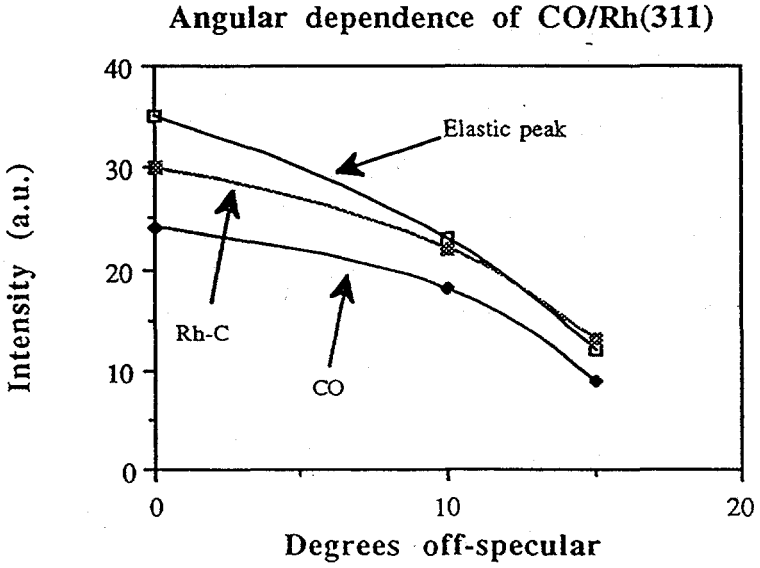

b)

Figure 6.8: Off-specular HREELS spectra of CO/Rh(311) (a) showing the angular dependence (b) of the loss features as compared to the elastic peak intensity.

decrease as a function of coverage from 31.1 kcal/mol to 22.3 kcal/mol. The initial heat of desorption is almost identical on the Rh (110), (100), (111) and crystal surfaces. The heat of desorption as a function of coverage is most similar to the (110) face. From the HREELS results we have found a Rh-C stretch at 443 cm^{-1} and a CO stretch at 2056 cm^{-1} which is nearly identical to the frequencies for top site adsorption on Rh(111) and (100). All of the data suggests that the (2x2) structure is formed with a ratio of 1 CO molecule to 1 Rh atom bonded in to a top site.

By collecting the facts discussed above it is possible to propose a model for CO adsorption on Rh(311). At saturation coverage we find heat of desorption and vibrational stretching frequencies found for a top site adsorption of CO that produces a (2x2) superstructure. The clean Rh(311) surface as discussed previously has essentially a bulk terminated structure with the exception of multilayer relaxations perpendicular to the [311] direction. Assuming 1ML coverage we can place 1 CO molecule per Rh atom and this would result in a (1x1) diffraction pattern. Introducing a zig-zag tilting arrangement in the CO overlayer such as the one found for CO/Ni(110), would produce a (2x1) diffraction pattern and since there is only one plane of symmetry on the surface no domain averaging can occur to produce a (2x2) pattern. Thus it is not possible to form a diffraction pattern corresponding to the (2x2) surface structure by maintaining the normal structure of the Rh surface. Considering that more open surfaces demonstrate a greater flexibility of the atomic positions in the top layers it is reasonable that the top metal layer in the Rh(311) surface may be reconstructed by molecular adsorption. CO has been shown to induce major reconstructions of metal surfaces, such as the (1x2) missing row reconstruction of CO/Pd(110). [21] It is therefore reasonable that the top layer of the metal may be reconstructed by the CO at high coverages. For our model we propose that like CO on fcc (110) surfaces, the molecules are bonded in a zig-zag arrangement along the rows. This produces the twofold periodicity in the [0,1,-1] direction. To produce the twofold periodicity in the [1,-1,-2] direction this could be accompanied by a "row-shifting"

reconstruction of every other row to form pairs of a (110) like surface (fig. 9a). This is similar to the proposed faceting model for the (1x2) reconstructed phase of H/Rh(311) at 1ML coverage. [22] Figure 9b illustrates the resulting possible (2x2) structure. However the confirmation and details of our model must await a complete dynamical LEED analysis of the I-V spectra.

6.5. Summary

The adsorption of CO on Rh(311) has been examined by LEED, TDS, and HREELS. From vibrational spectroscopy, at high coverage CO has been found to adsorb on the top site of the (311) step edges to produce a (2x2) surface structure. We propose that the adsorption results in a "row-shifting" reconstruction of the top layer to produce a more (110)-like substrate. The heat of desorption form the surface has been found to be approximately 31 kcal/mol. This is consistent with desorption from Rh(110) , (100), and (111) at low coverages where CO is bound to the top site as well. A complete LEED I-V structural analysis of the (2x2) structure is currently underway.

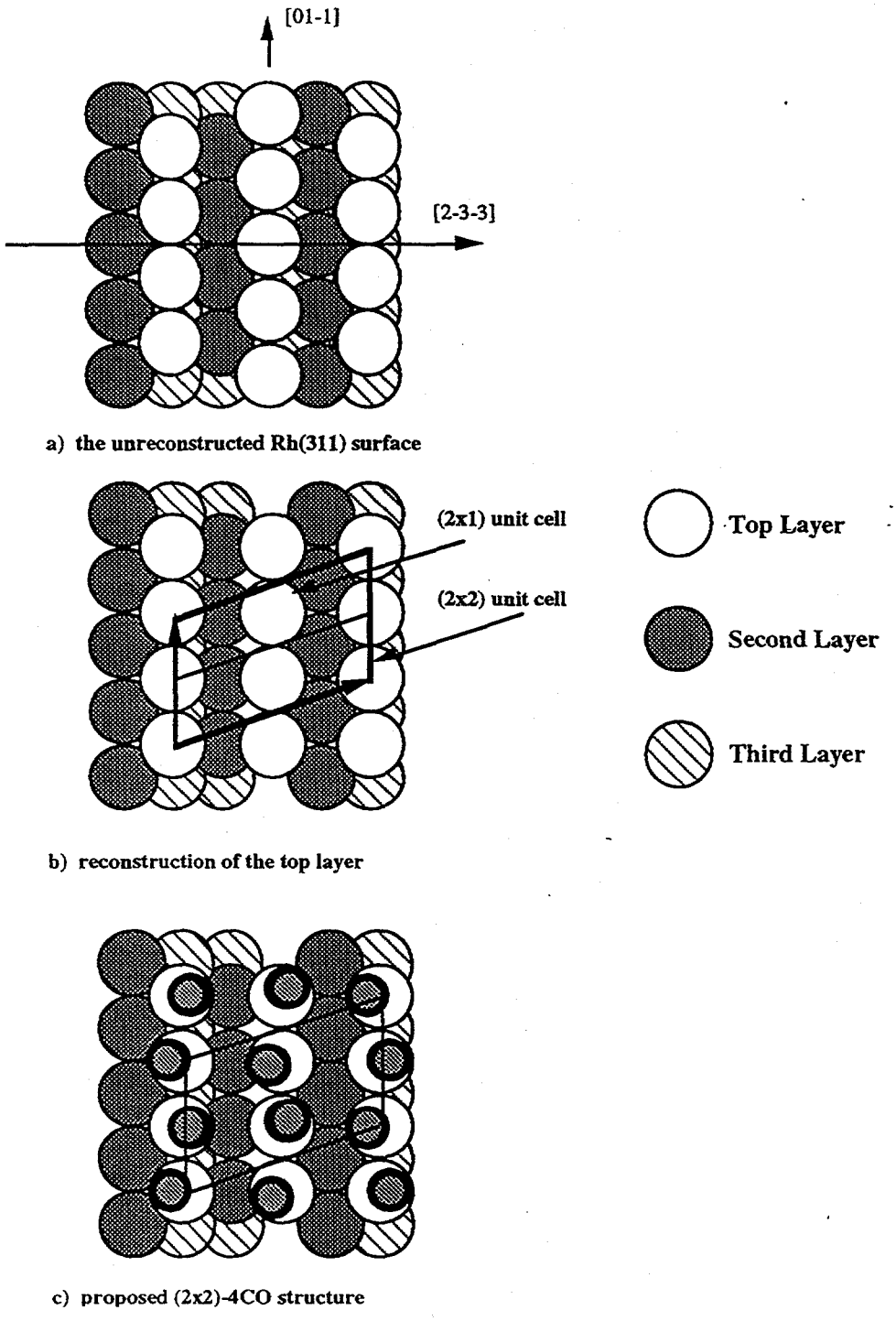

Figure 6.9: Possible model for the Rh(311)-(2x2)-4CO structure showing the clean unreconstructed surface (a), proposed substrate reconstruction (b), and a possible adsorbate geometry on the surface(c).

6.6 References

[1] J.T. Yates, Jr., E.D. Williams, and W.H. Weinberg, Surf. Sci. 91 (1980) 562.

[2] L.H. Dubois and G.A. Somorjai, Surf. Sci. 91 (1980) 514.

[3] L.A. DeLouise and N. Winograd, Surf. Sci. 138 (1984) 417.

[4] D.G. Castner, B.A. Sexton, and G.A. Somorjai, Surf. Sci. 71 (1978) 519.

[5] P.A. Thiel, E.D. Williams, J.T. Yates, Jr., and W.H. Weinberg, Surf. Sci. 84 (1979) 54.

[6] Y. Kim, H.C. Peebles, and J.M. White, Surf. Sci. 114 (1982) 363.

[7] B.A. Gurney, L.J. Richter, J.S. Villarrubia, and W. Ho, J. Chem. Phys. 87 (1987) 6710.

[8] S. Liepold, N. Elbel, M. Michl, W. Nichtl-Pecher, K. Heinz, and K. Müller, Surf. Sci. 240 (1990) 81.

[9] W. Nichtl, N. Bickel, L. Hammer, K. Heinz, and K. Müller, Surf. Sci. 188 (1987) L729.

[10] R.A. Marbrow and R.M. Lambert, Surf. Sci. 67 (1977) 489.

[11] D.J. Hannaman and M.A. Passler, Surf. Sci. 203 (1988) 449.

[12] B. Voigtländer, D. Bruchmann, S. Lehwald, and H. Ibach,
Surf. Sci. 225 (1990) 151.

[13] C.M. Mate, Ph.D. Dissertation, University of California at Berkeley, 1986.

[14] H. Froitzheim, H. Ibach, S. Lehwald, Rev. Sci. Instrum. 46 (1975) 1325.

[15] H. Conrad, G. Ertl, J. Koch, and E.E. Latta, Surf. Sci. 43 (1974) 462.

[16] M. Bowker, Q. Guo, and R. Joyner, Surf. Sci. 253 (1991) 33.

[17] K. Kiu and D.M. Ren, Surf. Sci. 232 (1990) 323.

[18] S. Haq, J.G. Love, and D.A. King, Surf. Sci. 275 (1992) 170.

[19] A. Wander, P. Hu, and D.A. King, Chem. Phys. Lett., 201 (1993) 393.

[20] R. Raval, M.A. Harrison, and D.A. King, Surf. Sci. 211/212 (1989) 61.

[21] P. Hu, L. Morales de la Garza, R. Raval, and D.A. King,
Surf. Sci. 249 (1991) 1.

[22] W. Nichtl-Pecher, W. Stammler, K. Heinz, and K. Müller,
Phys. Rev. B 43 (1991) 6946.

[23] L.H. Dubois, J. Chem. Phys. 77 (1982) 5228.

[24] R. Raval, S. Haq, M.A. Harrison, G. Blyholder, and D.A. King, Chem. Phys. Lett. 167 (1990) 391.

[25] D.P. Woodruff, B.E. Hayden, K. Prince, and A.M. Bradshaw, Surf. Sci. 123 (1982) 397.

[26] W. Erley, J. Vac. Sci. and Tech. 18 (1981) 472.

[27] S. R. Bare, P. Hofmann, and D.A. King, Surf. Sci. 144 (1984) 347.

Chapter 7

Interactions of CO and Oxygen on Rh(311)

The reaction dynamics for CO oxidation on the Rh(311) surface has been investigated by low-energy electron diffraction (LEED), high resolution electron energy loss spectroscopy (HREELS) and temperature programmed desorption (TPD). Both CO and oxygen form well ordered structures on this surface as described in previous chapters. The interaction of CO with the two ordered phases of oxygen on this surface shows two distinct reaction pathways for the formation of CO_2. First a reaction limited case with a peak rate of desorption at approximately 200 K and second, a diffusion limited case with a peak rate of formation at approximately 350 K. Based on a comparison of the bonding of CO and oxygen on this surface with the well characterized surface structures of CO and oxygen on other Rh surfaces, the influence of the surface steps on the reaction and a possible reaction geometry can be described.

7.1 Introduction

The oxidation of CO to CO_2 on Rh has been shown to be structure sensitive in the regime of high oxygen surface coverages. [1-3]. In the previous chapters the structure and bonding of oxygen and CO on Rh have been described. This chapter addresses the interactions of oxygen and CO on the densely stepped Rh(311) surface. Much work has been done on the characterization of CO oxidation on other stepped metal surfaces. The major features of this reaction on stepped metal surfaces is the low temperature formation of CO_2 from the surface. This has been observed on several systems, including Pt(335) [4] , Pt(112) [5,6] and Rh(110) [7]. This low temperature formation has been attributed to the stepped nature of the surface.

In this chapter the interaction of CO and oxygen on the Rh(311) surface will be described. These interactions have been examined by LEED, TPD and HREELS experiments. A low temperature reaction channel for the formation of CO_2 has been observed and is associated with a weakly bound CO molecular state on the surface as confirmed by vibrational spectroscopy. Based on this evidence and the structure analyses in the previous chapters, a model of the reaction dynamics and the reaction geometry is proposed.

7.2 Experimental

The Rh(311) crystal was cut from a boule of 99.999% purity and polished to within 1° of the [311] direction. The sample was cleaned and prepared in an ultrahigh vacuum chamber evacuated to 1.5×10^{-10} torr. Using Auger electron spectroscopy (AES) the primary contaminants were determined to be B, C, and S. These were removed by cycles of Ar^+ sputtering, O_2 treatments, and annealing in vacuum to 1100 K. The cleanliness of the sample was monitored by both AES and HREELS. Temperatures above 1100 K were

avoided as this results in a partially disordered (1x2) reconstruction which may only be removed by sputtering. CO, CO_2 and O_2 were supplied by Matheson with purities of 99.5%, 99.9% and 99.9% respectively and were used without further purification. All exposures are reported as the uncorrected ion gauge measurements. ($1L = 1 \times 10^{-6}$ torr•s)

The single crystal was mounted on the manipulator by Ta wires which allowed resistive heating of the sample. Sample cooling with liquid nitrogen cold fingers allowed for a minimum sample temperature of 100K. Thermal desorption spectroscopy measurement were made with a UTI-100C quadrupole mass spectrometer at a heating rate of 15-23 $K \cdot s^{-1}$. Low energy electron diffraction patterns were collected with a conventional Varian 4-grid LEED optics which also functioned as a retarding field energy analyzer for AES. The vibrational spectroscopy of surface adsorbates was carried out with a high resolution electron energy loss spectrometer. The spectrometer consists of two 120° cylindrical sectors and was designed after current models in use. The spectra were collected at an incident beam energy of 1.2 to 3.5 eV with a resolution of 7.3 to 12.4 meV (60 to 100 cm^{-1}). The elastic peak intensity in the specular direction ranged from 3×10^3 to 5×10^4 counts•s^{-1}.

7.3 Results

7.3.1 Low-energy electron diffraction (LEED)

The ordered oxygen overlayers were prepared by the adsorption of 1-20 L of O_2 between 100 -300 K. For an exposure of 1-6 L of O_2, followed by annealing to 600 K for 30 s, the 0.30 ML $\begin{pmatrix} 3 & 0 \\ -2 & 1 \end{pmatrix}$ structure is formed. The sample was then cooled back to 100 K and CO co-adsorbed on the surface. The addition of CO is seen in the surface vibrational spectrum as described below. The LEED pattern under the addition of CO does not change, other than an increase in the background intensity, indicative of disordered

adsorption of CO on top of the ordered oxygen structure. The surface was subjected to exposures of CO between 1-20 L with no change in the surface structure as observed in the LEED pattern. The $\begin{pmatrix} 2 & 0 \\ -3 & 2 \end{pmatrix}$ structure was likewise formed by an exposure of 20 L of O_2 between 100 - 300 K followed by annealing to 600 K. Similarly the structure remained intact under CO co-adsorption . The fact that the initial O LEED patterns remain intact with CO adsorption suggests that the CO is bonded on top of the ordered O structures.

7.3.2 Temperature programmed desorption (TPD)

The reaction of co-adsorbed CO and oxygen on the Rh(311) surface was monitored by TPD to examine the desorption of CO_2 from the surface. Desorption of CO_2 was first monitored from the molecular adsorption and desorption of CO_2 from the surface. CO_2 was adsorbed at 100 K and the TPD spectrum of CO_2 shows a maximum between 130-140 K. At large exposures of CO_2, some CO desorption was detected at 350 K, suggesting the possibility of dissociation on the surface, however the amount detected was not greater than that which could be accounted for by the cracking of CO_2 in the mass spectrometer.

The formation of CO_2 from the reaction of co-adsorbed CO and oxygen on the surface was found to occur at much higher temperatures than for molecularly adsorbed CO_2. The formation of CO_2 from the reaction of CO with both the ordered O structures and for disordered chemisorbed O are shown. For both ordered structures two distinct reaction pathways occur. The first is a low temperature pathway with a peak rate of formation at approximately 200-210 K. A higher temperature reaction pathway is also observed with a peak rate of formation at approximately 350 K. This higher temperature for CO_2 desorption is consistent with the formation of CO_2 from other Rh surfaces [1,3,7]. The TPD profiles from the ordered oxygen structures are very similar, however when oxygen is initially adsorbed in a disordered fashion, the CO_2 desorption profile becomes broad an more uniform between 150 - 400 K. Assuming a unimolecular desorption state

for CO_2 from the surface, the upper limits for the CO_2 formation energies on the surface for the two reaction pathways may be calculated from the desorption data. These are 12 kcal/mol for the low temperature channel and 20 kcal/mol for the high temperature channel, assuming a pre-exponential of 10^{-13} s^{-1}. At lower exposures if CO, only the high temperature desorption state of CO_2 is observed.

7.3.3 High resolution electron energy loss spectroscopy (HREELS)

The vibrational spectra for independently chemisorbed CO and oxygen on Rh(311) have been described in the previous chapters. Briefly, a single Rh-O vibrational mode is observed between 400-560 cm^{-1}. Both of the ordered oxygen structures show a Rh-O vibrational mode centered at 553 cm^{-1}. For chemisorbed CO, two vibrational modes are observed with increasing coverage, a Rh-CO stretch between 400-500 cm^{-1} and a C-O stretch between 1875-2056 cm^{-1}. In the (2x2) CO structure formed at saturation coverage the Rh-CO stretch is 420 cm^{-1} and the C-O stretch is 2056 cm^{-1}. As a function of coverage, only a single C-O stretch mode is observed in the specular direction.

At 100 K, CO can be co-adsorbed with oxygen on the surface. In the presence of oxygen, i.e. the 0.30ML structure, two distinct C-O vibrational modes are observed with the addition of ~ 0.25 ML of CO to the surface. The vibrational spectrum of the mixed overlayer is shown in figure 7.1. The two modes observed are a low frequency mode at 1975 cm^{-1} and a high frequency mode at 2117 cm^{-1}. the 1975 cm^{-1} mode is within the range of C-O stretching frequencies observed for CO on the clean surface. The high frequency mode however is ~ 60 cm^{-1} higher that observed at saturation CO coverages, and must be due to the influence of the pre-adsorbed oxygen.

The evolution of the spectra as a function of temperature will now be discussed. At 100 K, two distinct C-O vibrational modes are observed at 1975 and 2117 cm^{-1}. As the sample is heated to ~ 250 K, the high frequency mode disappears and the 1975 cm^{-1} mode

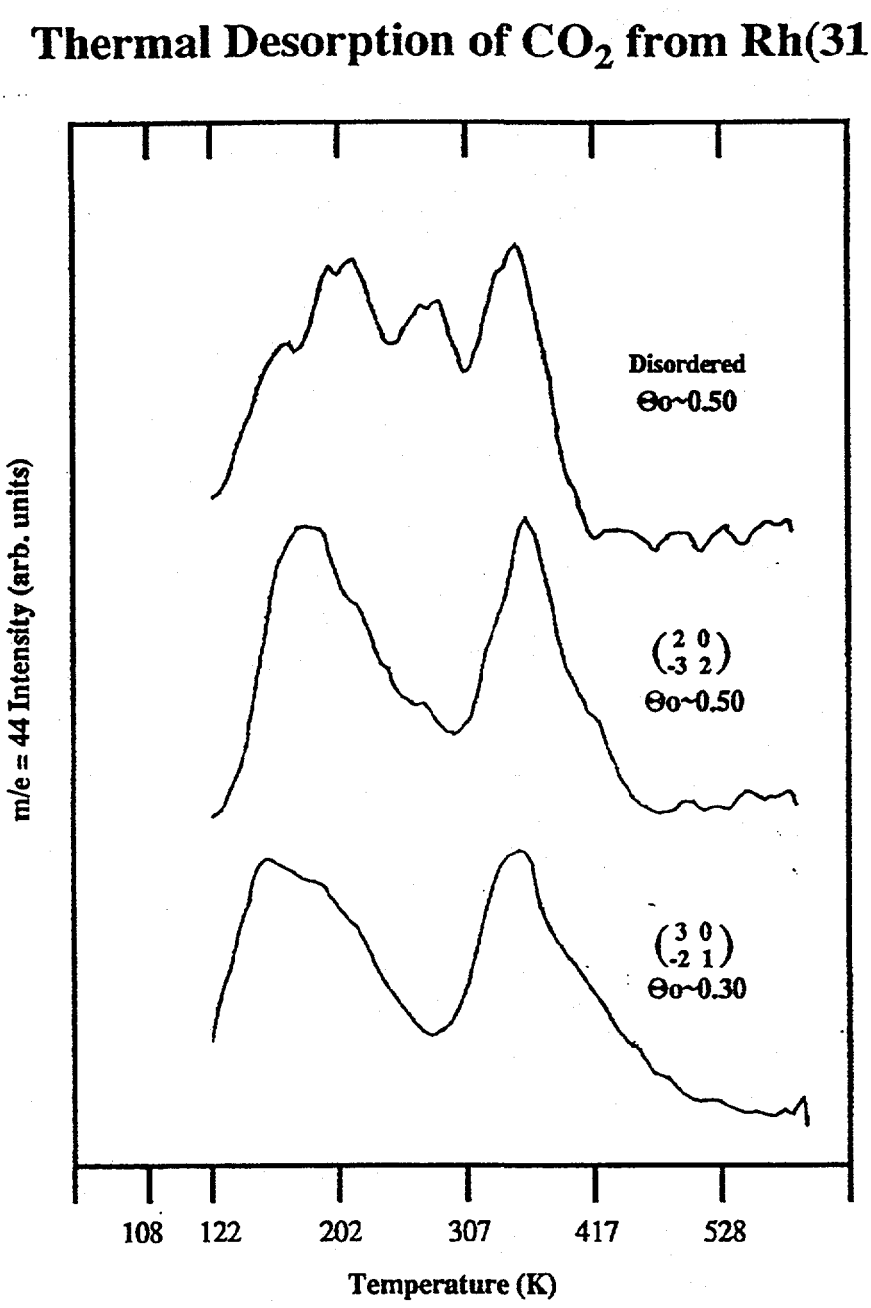

Figure 7.1: The formation of CO_2 on the Rh(311) surface as a function of oxygen coverage.

remains. The dissipation of this mode is concurrent with the formation and desorption of CO_2 from the surface. Annealing the surface to greater than 400 K results in the removal of the low frequency mode, again concurrent with CO_2 formation and desorption from the surface.

7.4 Discussion

7.4.1 Model for the CO oxidation reaction dynamics on Rh(311)

By combining the LEED, TPD and HREELS results, a model for the interaction between co-adsorbed CO and oxygen on the surface may be developed. The LEED results indicate that CO adsorbs in a disordered fashion on top of the ordered oxygen overlayer. The vibrational spectrum of this co-adsorbed layer indicates that two C-O vibrational bands appear, one at 1975 cm^{-1} and the other at 2117 cm^{-1}. The low frequency mode is within the range of C-O stretches for CO adsorbed on the clean surface. The higher frequency mode may be explained by the interaction between CO and the locally bonded O atoms. When O is chemisorbed on the surface, the local d-band electron density is decreased as electrons are transferred to the O from the metal. CO chemisorption occurs via a bonding/back-bonding mechanism where the lone pair electrons of the C bond to the metal and d electrons from the metal are transferred back to the $2\pi^*$ orbitals of the CO, which acts to weaken the C-O bond. Near a chemisorbed oxygen the local d electron density is reduced. This reduces the amount of back-bonding to the CO which may occur, thus maintaining a stronger C-O bond, and thus observing a higher C-O stretching frequency. Similar modification of the CO vibrational bands by co-adsorbtes, such as hydrogen or oxygen has been described on Pd(100) [8] and Ni(111) [9]. This modification of the local electron densities on surfaces near electronegative adsorbates has also been described theoretically. [10-11]

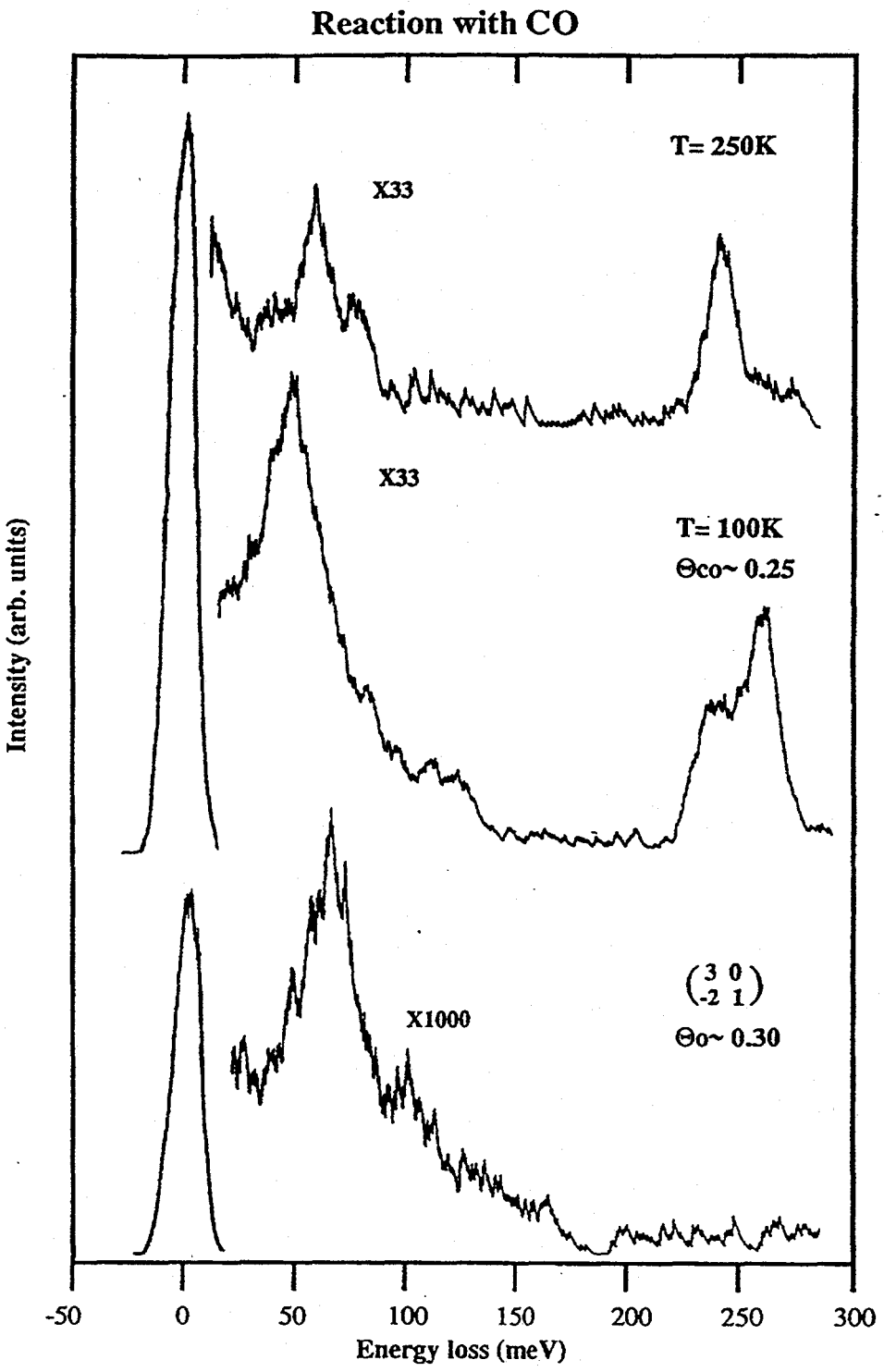

Figure 7.2: HREEL spectra showing the interactions between CO (~ 0.25 ML) and oxygen (~ 0.30 ML) on the Rh(311) surface as a function of temperature.

With increasing temperature from 100-400 K, the reaction between the CO and O proceeds via initial reaction of CO with nearest neighbor bonded O atoms (within 3 Å). The desorption of CO_2 between 100-250 K is reaction limited, with a maximum at ~ 200 K. Between 250 - 300 K the desorption of CO_2 drops off until CO gains enough energy to diffuse across a larger range of the surface. Thus at T > 250 K, CO must diffuse relatively longer distances than initially until it finds more O leading to an increase in the desorption of CO_2 from the surface. This process produces the two reaction pathways observed in the TPD results and is outlined in figures 7.3 and 7.4. This low temperature desorption process is consistant with reactions at step edges as described on Pt(335) and (211) [4-6].

7.4.2 Proposed model of the reaction geometry

Based on the known adsorption structures for CO and O on other Rh surface, the large low temperature desorption state can possibly be explained geometrically, in terms of the nearest neighbor O-CO distances and the O-CO bond angles that can be attained on stepped surfaces. The bonding parameters of CO and O on Rh(111),(100) and (110) surfaces are shown in table 7.1. Based upon the known adsorbate geometries determined from fully-dynamical LEED structure analyses, the nearest neighbor O-CO bond lengths and bond angles have been approximated for given reaction geometries. Assuming that the oxygen atomic positions during reaction are consistent with their LEED structures (i.e. the O diffusion barrier is large and thus the O atoms stay near their equilibrium positions) a limit on the O-CO bond lengths and bond angles may be approximated. These estimated bond lengths and bond angles show that overall, on an open surface such as Rh(110) (and thus Rh(311)) the O and CO can get closer together than on the close-packed surfaces, because O blocks no sites for CO chemisorption. The topmost atoms on the (110) surface are free for chemisorption, whereas on the (111) and (100) surfaces, the O-CO distances are on the order of 0.2-0.5 Å longer. Also of interest is the O-CO bond

2 CO Stretching Frequencies

2 Desorption States

CO = 1970 cm^{-1} CO* = 2100 cm^{-1}

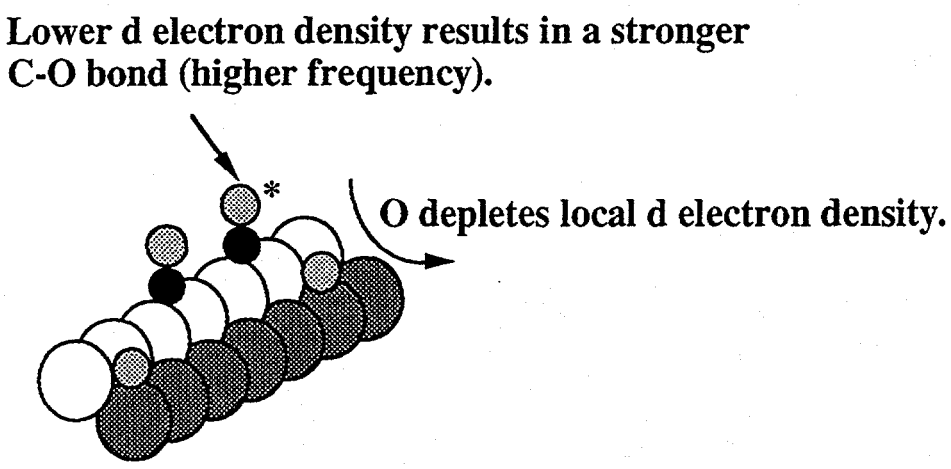

Figure 7.3: Model of CO adsorption states on oxygen covered Rh(311).

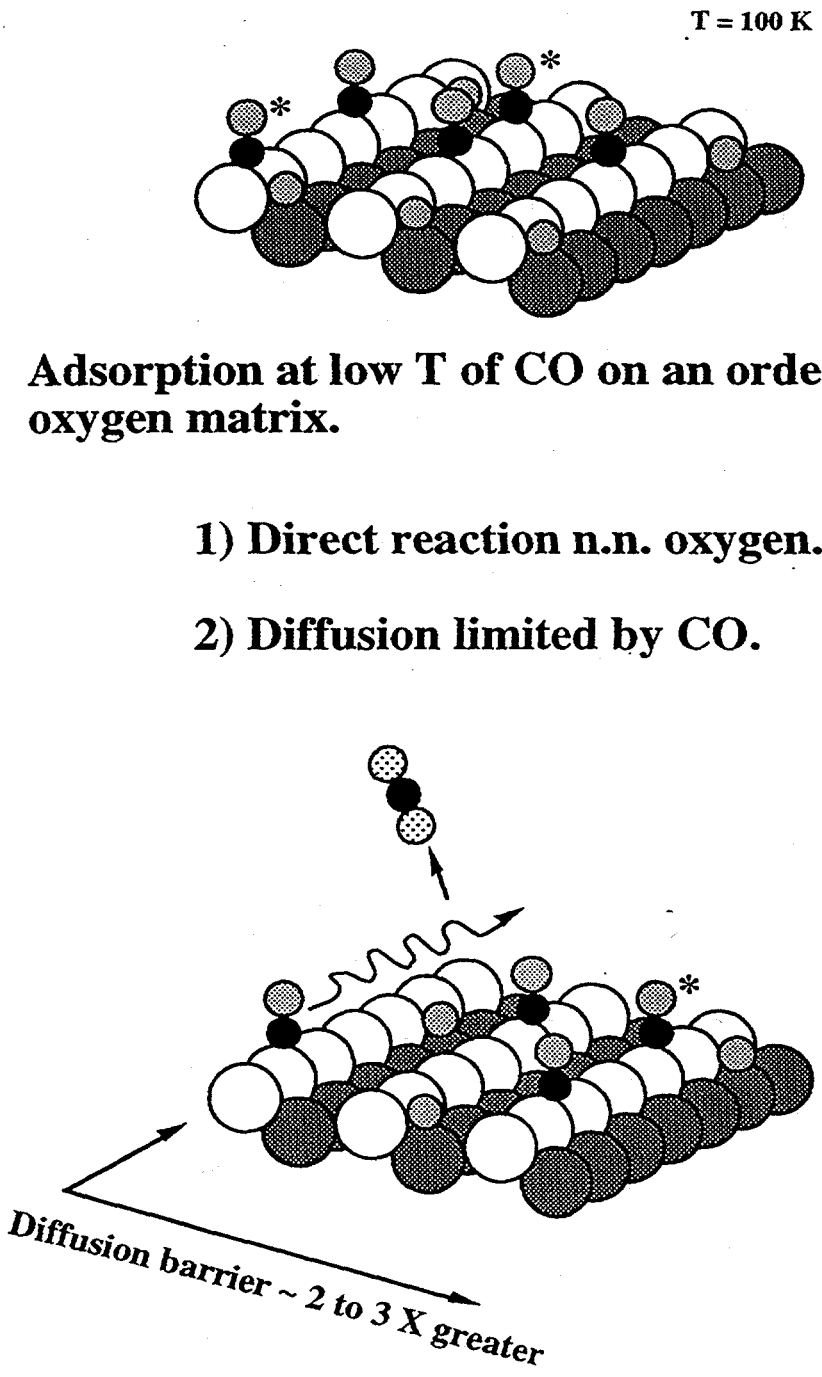

Figure 7.4: Model of the CO oxidation reaction dynamics on Rh(311).

System	O---C-O distance (Å)	O---C-O bond angle (degrees)
Gas phase CO_2	1.16	180
Rh(111)	2.06 (top site CO)	117
	1.86 (bridge site CO)	107
Rh(100)†	2.14 (top site CO)	117
	1.98 (bridge site CO)	107
Rh(110)*	1.65 (tilted 24°)	176
	1.38 (normal to surface)	152

† Since no CO structures have been determined on Rh(100), the CO bond lengths are assumed, for the basis of comparison.

* The CO molecule is in the short bridge site in both cases. (See Chapter 3)

Table 7.1: Estimated bond lengths and bond angles for CO and oxygen in nearest neighbor sites on various Rh surfaces. The bond lengths and bond angles are based on known structural parameters for CO and oxygen on these surfaces.†

angles predicted. On the (111) and (100) surfaces, this angle is near 110°, while on (110) this value approaches 150-170°, in the range of the predicted CO_2^- intermediate (152°) [12-13] in CO oxidation, and the final CO_2 product of 180°. These geometries are induced by the corrugated nature of the surface and may explain the high reactivity of the surface.

7.5 References

[1] S. H. Oh, G. B. Fisher, J. E. Carpenter and D. W. Goodman, J. of Catal. 100 (1986) 360.

[2] M. Bowker, Q. Guo, Y. Li, and R.W. Joyner, Catal. Lett. 18 (1993) 119.

[3] L.-W. H. Leung and D. W. Goodman, Catal. Lett. 5 (1990) 353.

[4] J. Xu and J.T. Yates, J. Chem. Phys. 99 (1993) 725.

[5] T. Matsushima, Y. Ohno and A. Rar, Surf. Sci. 293 (1993) 145.

[6] A. Szabó, M.A. Henderson and J.T. Yates, J. Chem. Phys. 96 (1992) 6191.

[7] T. Matsushima and Y. Ohno, Catal. Lett. 23 (1994) 313.

[8] Z. Xu, L. Surnev, K. J. Uram and J. T. Yates, Surf. Sci. 292 (1993) 235.

[9] E. M. Stuve, R. J. Madix and C. R. Brundle, Surf. Sci. 146 (1984) 155.

[10] P. J. Feibelman and D. R. Hamann, Surf. Sci. 149 (1985) 48.

[11] J. M. Maclaren, J. B. Pendry, R. W. Joyner and P. Meehan, Surf. Sci. 175 (1986) 263.

[12] B. Bartos, et al., Surf. Sci. 179 (1987) 59.

[13] F. Solymosi and G. Klivényi, Catal. Lett. 22 (1993) 337.

Chapter 8

Ethylene dehydrogenation on Rh(311)

The adsorption and thermal decomposition of ethylene was examined on the Rh(311) stepped surface by AES, LEED, TPD, and XPS in order to obtain a better understanding of the reactivity of atomically roughened surfaces. Ethylene is adsorbed in a disordered fashion at 200K. Upon annealing the surface to 600K a partially disordered (1x3) graphite overlayer is observed. X-ray photoelectron spectroscopy (XPS) is utilized to examine the temperature dependence of the C(1s) peak, in the range of 300K to 800K, to differentiate between surface species. The C(1s) peak undergoes a shift in binding energy from 284.1 eV to 284.9 eV at 300K and 750K respectively. The binding energies are compared to reported results on Rh(111) and Rh(331) to propose a decomposition pathway and assign surface species to the observed LEED patterns. The XPS results suggest a stable $C_{2,ads}$ species between 400 -550K and a graphitic overlayer between 600-700K. These temperatures correspond to finding C_2 and graphite at $\approx$ 100K lower than on the Rh(111) surface. This is consistent with the concept that rougher surfaces are more reactive. The stability of the C_2 species is attributed to the stepped nature of the surface.

8.1. Introduction

In order to gain a better understanding of the catalytic reactivity of surfaces, greater attention has been given to stepped and kinked surfaces. Surfaces of this nature contain defect sites which are the proposed sites of surface reactions. To study a surface of this nature we have selected the Rh(311) surface. The surface is densely stepped and consists of troughs of alternating (111) and (100) microfacets. This offers the adsorbate several highly coordinated sites for bonding, consisting of 2 distinct 3-fold sites as well as a 4-fold site in the troughs. Considering the roughness of the surface, one would expect the surface chemistry to reflect this in the reactivity of the surface with various adsorbates. Also, the mixture of highly coordinated sites in close proximity may aid to stabilize intermediate species on the surface where the species may receive bonding contributions from both 3-fold and 4-fold sites.

On Rh(111) and Rh(100) [1] ethylene has been found to adsorb intact at low temperatures. Ethylene undergoes dehydrogenation at elevated temperatures to form the ethylidyne species, which remains stable to above 300K on these surfaces. Molecular dynamics simulations by modified extended-Hükel theory on Pt(111) and Pt(100) [2] clearly demonstrate that $CCH_{3,\,ads}$ is highly stable in the 3-fold sites of the (111), while unstable in the 4-fold hollow site of the (100). The ethylidyne structure on Rh(111) as solved by LEED [3] also finds a 3-fold hcp site coordination. Considering that 3-fold sites on the (311) surface are in the troughs, this may present a unique bonding situation for ethylene.

The decomposition chemistry of ethylene on Rh(111) and Rh(100) has been studied by high resolution electron energy loss spectroscopy (HREELS). [4] The results indicate that on Rh(111) ethylene dehydrogenates to ethylidyne at 270K, followed by subsequent hydrogen loss to form $C_2H_{,ads}$ and possibly $CH_{,ads}$ at 400K. Further heating results in graphitic carbon above 750K. On Rh(100) ethylidyne is unstable at $\Theta < 0.5$ ML and

metastable at $\Theta > 0.5$ ML. The primary intermediate on Rh(100) also appears to be $C_2H_{,ads}$, with the possibility of a $C_2H_{2,ads}$ species. Complete dehydrogenation occurs at T > 500K.

The application of X-ray photoelectron spectroscopy (XPS) to examine decomposition products on surfaces has been applied to several systems such as C_2H_4 on Pt(111)[5], C_6H_6 on Ni(110) [6], C_2H_2 and C2H4 on Ir(111) [7], and CO on Pt(111) [8]. Shifts in the core level binding energies reflect changes in the local electronic environment of the adsorbed atom or molecule. In the absence of a vibrational technique this can be a powerful tool to examine reactions on surfaces. By studying the C(1s) peak binding energy and the full width at half maximum (FWHM) as a function of annealing temperature, Levis et. al. [9] describes the decomposition of ethylene on Rh(111) and Rh(331) and assigned various decomposition species to given binding energy ranges. In their experiments they found that all decomposition species (such as CH, C_2H and graphite) on Rh(331) are formed 50-100K below that on Rh(111). We can apply their assignments to a study of the decomposition chemistry of C_2H_4 on our surface and determine the effects of the steps on the decomposition pathway.

8.2. Experimental

8.2.1 Sample preparation

The single crystal was prepared from a Rh boule of high purity. It was oriented using Laue X-ray back reflection and cut to within 1^o of the (311) plane by spark erosion. One face of the crystal was then polished to 0.1 mm with an alumina slurry. The sample was then cleaned and prepared in an ultrahigh vacuum chamber evacuated to 5×10^{-10} torr. By using Auger electron spectroscopy (AES) the primary contaminants were determined to be C, B, and S. These species were removed by Ar^+ bombardment in 5 X

10^{-7} torr Ar at T=300K and T= 800K (10-30 minutes) as well as by thermochemical treatment with 5 X 10^{-7} torr O_2 from T=600K-800K (5-10 minutes), followed by annealing at 1100K for 1-2 minutes. After the surface was completely cleaned, traces of C from ethylene or residual gases could be removed by treating with O_2 at 5 X 10^{-8} torr for 2 - 3 minutes followed by annealing at 1100K for 1-2 minutes. This procedure was used during the XPS measurements.

8.2.2 Low energy electron diffraction and Temperature programmed desorption

Low energy electron diffraction (LEED) measurements were carried out using a conventional Varian 4-grid LEED optics with an off-axis electron gun. This also functioned as an RFA for AES measurements. LEED patterns and Intensity vs. Energy curves were measured using a Dage-MTI SIT-68 high sensitivity video camera which could image the LEED screen and process that image to a PC for data acquisition and analysis. An Auger uptake of ethylene was prepared by measuring the relative peak heights of the C (272 eV) and Rh (256 eV) peaks as a function of exposure to determine surface coverages relative to saturation.

Temperature programmed desorption (TPD) measurements were made with a UTI 100C quadrupole mass spectrometer. The sample was spotwelded to the manipulator on Ta plates and could be heated resistively. Sample cooling was carried out with liquid nitrogen cold fingers from which cooling was directed to the sample by Cu braids. A minimum temperature of 180K could be obtained. Desorption measurements were made at a heating rate of 17 $K \cdot s^{-1}$.

8.2.3 X-ray photoelectron spectroscopy

Measurements of the C(1s) spectra by XPS were made with a PHI 5400 small spot ESCA. The sample was prepared in an additional chamber, attached to the main XPS chamber, equipped with electron beam heating and variable leak valves for gas introduction. A transfer arm is then used to move the sample under vacuum (7×10^{-10} torr) into the XPS chamber for analysis. The sample was cleaned and prepared as described above and background spectra measured to determine cleanliness. The sample was then exposed to 5×10^{-8} torr C_2H_4 for 200s (10 L) at 300K. All exposures are given as the uncorrected ion gauge measurements. ($1L = 1 \times 10^{-6}$ torr·s) The sample was then annealed for 75 s at the given temperature.

The C(1s) spectra were measured over the binding energy range of 282eV to 288eV using the MgKα line (1253.6eV) as the excitation source. The spectra were then background subtracted to remove satellite peaks. The measurements were made with a hemispherical analyzer set to a constant pass energy of 8.95eV which provided the spectrometer with a resolution of 0.22eV. All binding energies are referenced with respect to the Rh Fermi level which places the Rh $3d_{5/2}$ peak at 307.3eV. From these spectra were obtained the peak binding energy and the full width at half maximum (FWHM) as a function of annealing temperature.

8.3. Results

8.3.1 Low energy electron diffraction

By applying LEED to the surface analysis the substrate periodicity as well as any adsorbate ordering on the surface could be studied. The surface coverages relative to saturation were determined by an Auger uptake curve prepared as described above. For the

adsorption of ethylene as a function of exposure at 270K, we find that surface saturation occurs for exposures >3L (Fig. 1). We will assign this as 1 ML coverage. Coverages reported for the LEED experiments are based on this curve. After preparing the crystal as described, the clean surface exhibited a well ordered (1x1) with low background. I-V curves for the diffracted beams compared readily with those previously reported for the clean surface. [10]

Ethylene was adsorbed in a disordered fashion at 200K with a coverage of 0.33ML. The observed LEED pattern was a (1x1) with an increased background due to the adsorption. Annealing the sample to 420K produced a weak overlayer periodicity with a high background. With further annealing of the sample to >500K we begin to observe streaking in the LEED pattern along the surface vector perpendicular to the step edges. This would seem to be indicative of surface diffusion perpendicular to the steps. Once the surface is annealed to >600K a distinct (1x3) pattern is observed with some streaking perpendicular to the step direction, but not along a surface unit vector (Fig. 2). Heating to temperatures greater than 800K results in a return to the (1x1) as C begins to dissolve into the bulk.

Exposing the surface to 10L of ethylene at low temperature also produced a (1x1) pattern with an increased background. No ordering was found however until 600K when again the (1x3) pattern was observed. However, no ethylene was desorbed by annealing. The C(272eV)/Rh(252eV) peak ratio following annealing was found to be within 5% of saturation which we consider to be within the experimental error. At saturation coverages the additional streaking found at lower exposures was not as apparent.

On the Rh(111) surface ethylene is decomposed to form a graphite basel plane at 750K. This results in a (12x12) coincidence lattice not observed on the Rh(311) surface. The LEED patterns suggests that if graphite is being formed that it probably forms in the channels on the (111) terraces to produce a (1x3) pattern. The streaking is the result of a

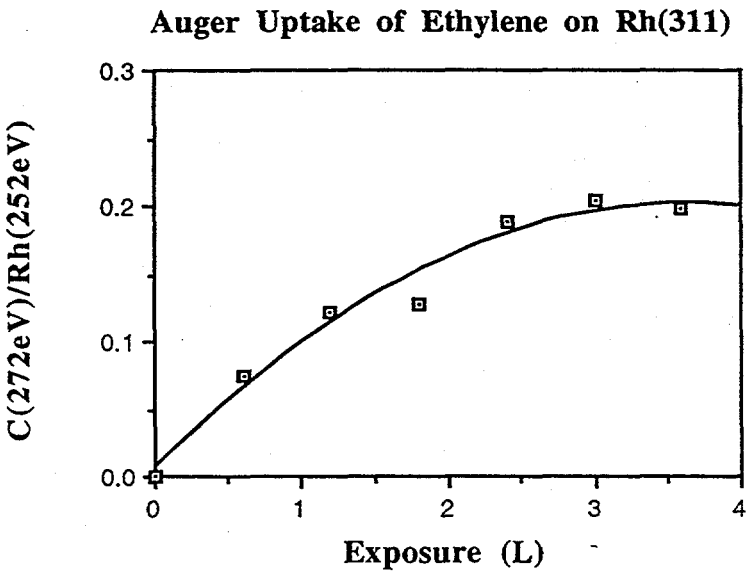

Figure 8.1: The Auger uptake of ethylene on the Rh(311) surface at 270K.

partial disordering of this overlayer. This is similar to what is observed on the Rh(331) surface whose (111) terrace is 1 atom larger than in the (311) case.[11]

8.3.2 Temperature programmed desorption

The desorption spectra of H_2 from the pre-adsorbed ethylene has also been examined as described above to aid in determining the surface chemistry. The desorption spectrum (Fig. 3) shows two peaks at 250K and 420K. The 250K peak would appear to be desorption limited as it is seen for H_2 desorption from the clean Rh(311) surface. [12] After background subtraction to account for trace background hydrogen from the manipulator, the peak areas were found to correspond to be $\approx$ 2.9:1 for the 250K and 420K peaks respectively. This would suggests than the 420K peak corresponds to desorption from a $C_2H_{,ads}$ species. The 250K peak is not observed on Rh(111), but is found on Rh(100). This suggests that hydrogen is desorbing from the 4-fold site.

8.3.4 X-ray photoelectron spectroscopy

C(1s) spectra vs. temperature

When considering the C(1s) spectroscopy we are primarily interested in two features, the binding energy (to describe the chemical species) and the FWHM to gain an idea of the local electronic environment of the carbons in association with the metal. The broadening of the spectra may be accounted for by additional decomposition products, or carbon atoms in different electronic environments, on the surface. This results in a spectrum that contains one or more unresolved peaks contributing to the spectral width.

By following the changes in the C(1s) spectrum as a function of annealing temperature we have been able to observe different chemical species on the Rh(311) surface

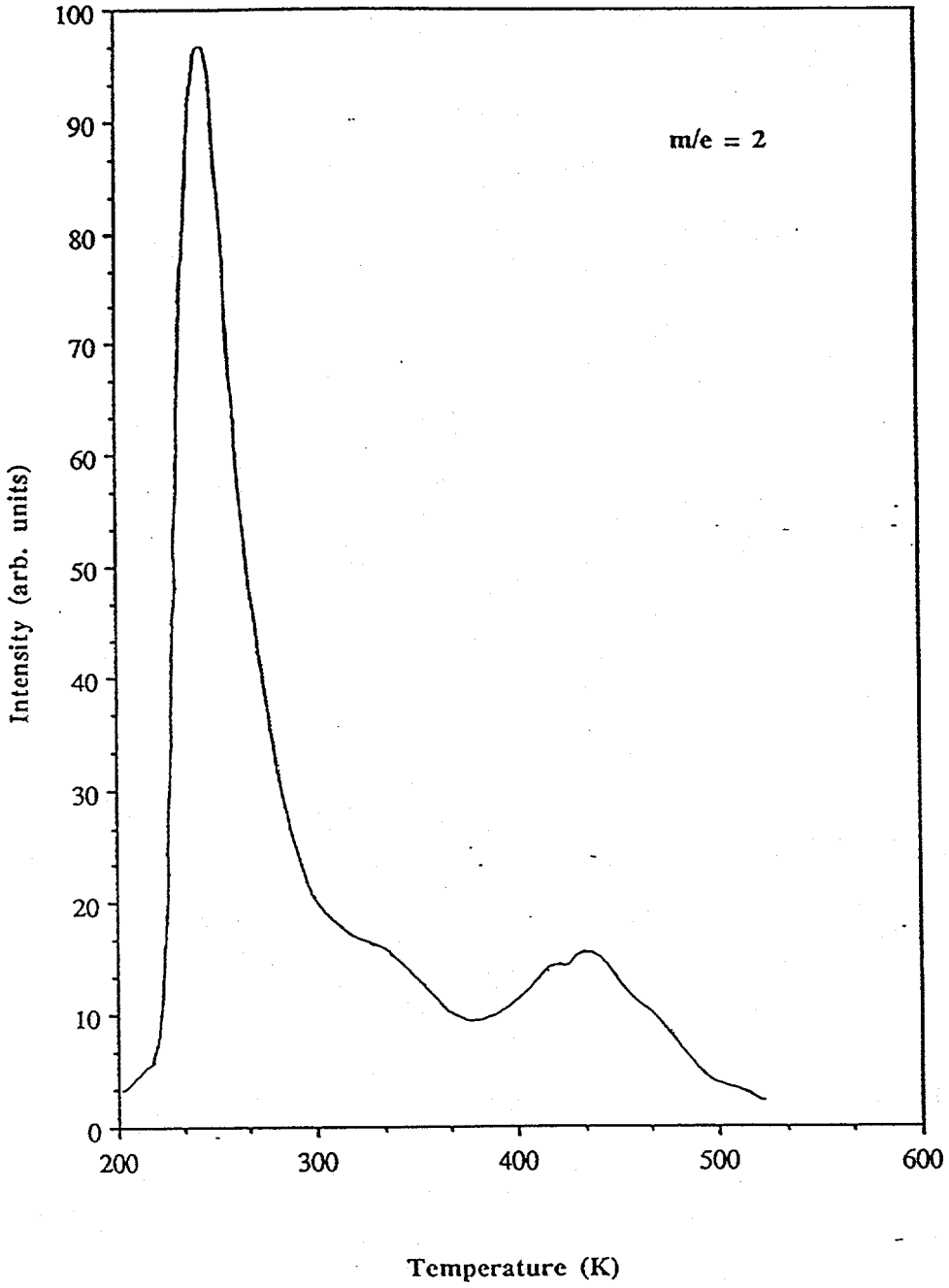

Figure 8.2: Uncorrected TPD spectrum of H_2 from pre-adsorbed C_2H_4.

from the dehydrogenation of ethylene. The adsorption of a saturation coverage of ethylene at 300K results in a peak binding energy of 284.1eV, with a FWHM of 1.2eV. Annealing to higher temperatures results in a shift in the spectrum to higher binding energies and a subsequent broadening at intermediate temperatures (Fig. 4a). The C(1s) spectra are shown along with their difference spectra in order to elucidate the variation between consecutive spectra. In the temperature regime of 400-550K, very little change is observed in the binding energy or FWHM. The binding energy is approximately constant at 284.3-284.4eV, with a FWHM of 1.63-1.7eV. The initial increase from 284.1eV to 284.3eV along with the dramatic broadening from 1.21eV to 1.63eV coincides with the final hydrogen desorption from the surface, resulting in a C_2,ads species. This is consistent with the binding energy for C_2,ads on Rh(331). By 600K the binding energy has risen to 284.7eV and the FWHM returned to a lower value of 1.32eV. This shift appears with the ordering of the (1x3) on the surface as observed by LEED. Further annealing results in a final binding energy of 284.9eV and a FWHM of 1.14eV, this is consistent with graphite formation of Rh(331) as will be discussed below. The slight broadening at 750K may be attributed to carbon beginning to dissolve into the bulk. The results of the spectral temperature dependence are summarized in Figure 5.

Comparison to Rh(111) and Rh(331)

In order to make any direct comparisons to the results of ethylene decomposition reported by Levis et. al. on Rh(111) and Rh(331), we must first subtract 0.2eV from the binding energies reported for our spectra. We find the Rh 3d5/2 peak at 307.3eV, while Levis et. al. reports a binding energy of 307.1eV for this transition. This difference of 0.2eV is most probably due to differences in spectrometer work functions. After taking this into account the following points may be made. while we observe the same trends found on Rh(111) and (331), there is an overall lowering of the binding energies with

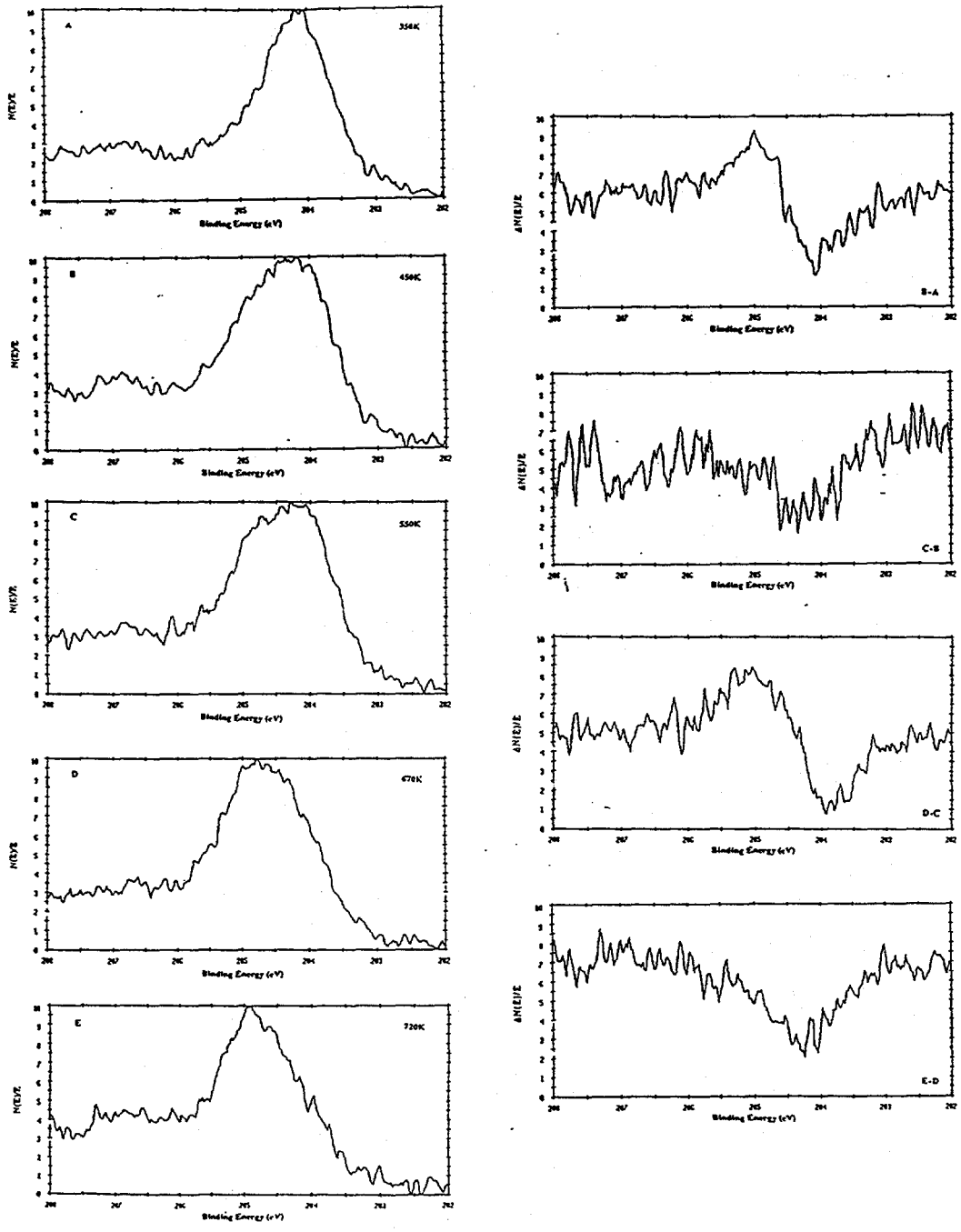

a) b)

Figure 8.3: a) C(1s) spectra as a function of annealing temperature. (Normalized to peak intensity.) b) Differences between the consecutive spectra.

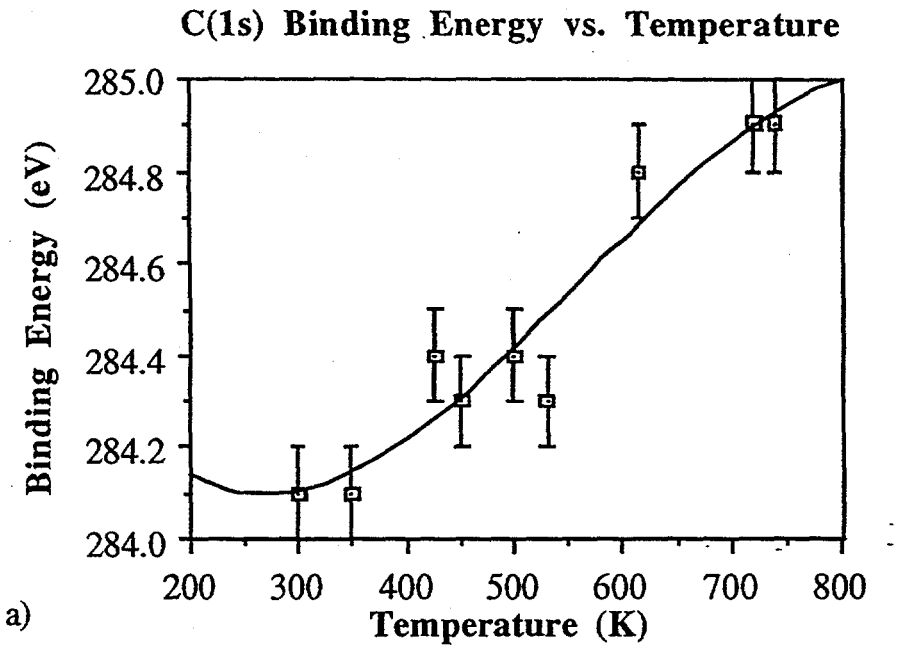

a)

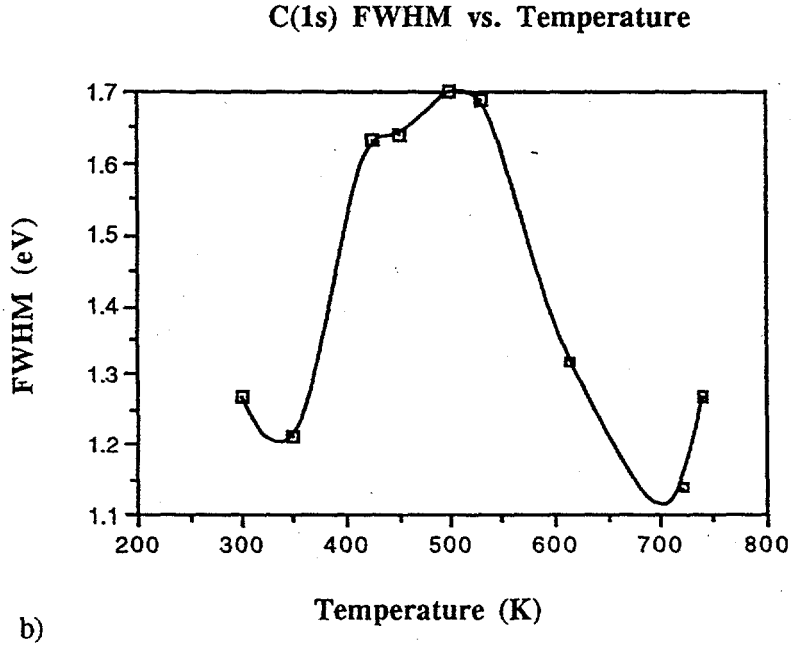

b)

Figure 8.4: a) C(1s) binding energy vs. temperature. The smooth curve is provided to indicate the trend in the data. (Error bars are given in terms of the absolute spectrometer resolution.) b) C(1s) FWHM vs. temperature.

respect to the (111) and narrower peaks. These two features suggest that the adsorbates are in intimate contact with the surface, i.e. lying in the troughs, and therefor receive a strong electronic contribution from the surface to lower the binding energy. (It is also important to note that our XPS experiments begin at 300K, between the regions of hydrogen desorption. We are therefore beginning with the C_2H,ads species, whereas on Rh(111) and (331), the initial adsorbate is ethylidyne.)

Upon adsorption we find a peak binding energy 0.2eV lower than on the (111) surface. Also, our FWHM is only 1.2eV, while it is 1.6eV on the (111) This broad peak on the (111) has been attributed to the different electronic environments of the ethylidyne carbons. One is bound to 3 metal atoms, while the other to 3 hydrogens. If the absorbates were placed in the troughs on our surface, both carbons would be close to the metal surface and this would lower the binding energy and FWHM as is observed. This is consistent with the (331) surface which also shows a narrower peak binding energy of 283.9eV and FWHM of 1.4eV at 300K. At elevated temperatures we find a final binding energy of 284.7eV, which is consistent with graphite formation on the Rh(331) surface. This is 0.2eV lower than on the Rh(111) surface. The peak widths are also consistently lower on our surface than on the (111) and (331).

8.3.5 Surface vibrational spectroscopy (preliminary results)

The thermal decomposition of ethylene on the Rh(311) surface was monitored in a separate chamber by high resolution electron energy loss spectroscopy. The surface was exposed to 10 L of C_2H_4 at 100 K. The surface vibrational spectra compares well with that of molecularly π-bonded ethylene on Rh(100). [13] The changes in the HREELS spectra (not shown) were then monitored as a function of annealing temperature. Heating the sample to 300 K, just above the first H_2 desorption peak, the spectrum is shown to change dramatically. This spectrum at 300 K is consistent with that of a mixture of C_2H and CH

species, similar to those observed on Rh(111) and Rh(100) [13], at higher temperatures. Heating the sample to temperatures greater than 450 K results in a spectrum consisting of primarily C species on the surface. The HREELS data confirms that no ethylidyne species is formed on the surface and that at room temperature the ethylene is already partially dehydrogenated.

8.4 Discussion

XPS has been used in conjunction with HREELS, LEED and TPD to explore the decomposition chemistry of C_2H_4 on the Rh(311) stepped surface. Ethylene adsorbs in a disordered fashion at T < 200K. Based upon the hydrogen desorption spectrum, $\approx$ 75% of the hydrogen is lost from the molecule by 300 K, resulting in C_2H_{ads} and CH_{ads} species. This has been confirmed by XPS and HREELS. The C(1s) spectra between 400-550 K shows evidence of little change and suggests that following final hydrogen loss, a stable C_2, ads species remains. We propose that this stability is the results of the stepped nature of the surface. Only recently metallized C_2 complexes have been synthesized that are composed of 3 and 4 metal atoms bound to the ends of the C_2. [14] This is very similar to the structural geometry of our surface. The combination of 3-fold and 4-fold site may aid to stabilize the adsorbate.

In the decomposition chemistry we find lower temperature dehydrogenation prior to C-C bond breaking. This was also reported by Ibach et. al. on Ni stepped surfaces for ethylene decomposition. [15] That work reported that hydrogen loss on the stepped surfaces occurred at lower temperatures compared to the Ni(111) surface. Also, the stepped surface was found to produce a metastable C_2 as found by HREELS. HREELS data in this work indicate that no ethylidyne formation occurs, probably due to the close proximity of the step edge to the 3-fold sites on the surface.

At T > 600 K, a partially disordered (1x3) graphite overlayer is formed. This formation occurs ≈ 100K below that on the (111) surface, and ≈ 50K below the (331). Annealing to T > 750 K we find the surface returns to the (1x1) as C begins to dissolve into the bulk. The thermal decomposition path described by our results is given in the following diagram.

8.5 References

[1] A.J. Slavin, B.E. Bent, C.-T. Kao, and G.A. Somorjai, Surf. Sci. 206 (1988) 124.

[2] P.D. Ditlevsen, M.A. Van Hive, and G.A. Somorjai, Phys. Rev. B (Submitted).

[3] A. Wander, M.A. Van Hove, and G.A. Somorjai, Phys. Rev. Lett., 67 (1991) 626.

[4] A.J. Slavin, B.E. Bent, C.-T. Kao, and G.A. Somorjai, Surf. Sci. 206 (1988) 124.

[5] N. Freyer, G. Pirug, and H.P. Bonzel, Surf. Sci., 126 (1983) 487.

[6] D.R. Huntley, S.L. Jordan, and F.A. Grimm, J. Phys. Chem., 96 (1992) 1409.

[7] Ts.S. Marinova and K.L. Kostov, Surf. Sci., 181 (1987) 573.

[8] P.R. Norton, J.W. Goodale, and E.B. Selkirk, Surf. Sci., 83 (1979) 189.

[9] R.J. Levis, L.A. DeLouise, E.J. White, and N. Winograd, Surf. Sci, 230 (1990) 35.

[10] S. Liepold, N. Elbel, M. Michl, W. Nichtl-Pecher, K. Heinz, and K. Müller,

Surf. Sci., 240 (1990) 81.

[11] D.G. Castner and G.A. Somorjai, Surf. Sci., 83 (1979) 60.

[12] W. Nichtl-Pecher, W. STammler, K. Heinz, and K. Müller, Phys. Rev. B, 43 (1991) 6946.

[13] B.E. Bent, Ph.D. Dissertation, University of California at Berkeley, 1986.

[14] M. Akita, S. Sugimoto, M. Tanaka, and Y. Moro-oka, J. Am. Chem. Soc., 114 (1992) 758.

[15] S. Lehwald and H. Ibach, Surf. Sci., 89 (1979) 425.

Chapter 9

In Situ Scanning Tunneling Microscopy of Model Catalyst Surfaces

The coadsorption of sulfur (S) and carbon monoxide (CO) on a vicinal Pt(111) surface has been examined *in situ* by scanning tunneling microscopy (STM). The sulfur chemisorbs forming a p(2x2) structure on the terraces, and a doubling of the atomic step heights on the surface occurs. Upon adsorption of CO the sulfur overlayer is compressed and the surface restructures where the double height steps split into two single atom height steps, via Pt diffusion from the step edges, to form new sulfur free Pt terraces where further CO adsorption occurs. The step density on the surface is now increased and CO and sulfur are predominantly segregated onto separate single atomic height terraces. This work presents the first direct evidence for a mechanism by which a surface covered with an unreactive, strongly chemisorbed overlayer, can restructure to provide new sites for bonding and reactions. This novel surface phenomenon and its implications in catalysis are described.

9.1 Introduction

Under catalytic reaction conditions, most surfaces are covered by a strongly chemisorbed unreactive overlayer. For example during hydrocarbon reactions, over 80% of the surface is typically covered by a carbonaceous layer. [1] In hydrodesulfurization reactions of thiophene to butenes, the surface is covered by both carbon and sulfur. [2, 3] The atomic details of many catalytic reactions have been examined using single crystal metal surfaces that proved to be excellent model catalysts and also operate in the presence of an unreactive adsorbate overlayer. Thus one of the major puzzles in metal catalysis is how do surface reactions occur when the surface is covered with a strongly chemisorbed, unreactive overlayer, such as carbon or sulfur, which acts to block sites during reactions and poison the catalyst? [4]

The restructuring of metal surfaces upon the chemisorption of atoms or molecules has been well documented (adsorbate induced restructuring). [5] Restructuring of surfaces can occur locally, by forming cluster-like bonds between the displaced metal surface atoms and the adsorbate, or more dramatically, to reconstruct, forming a spatially extended surface structure much different from that of the clean substrate. This leads to the description of the surface as being flexible, constantly changing its structure with the adsorption and desorption of gases. [6] Even the clean close-packed (111) surface of Pt, which is the most thermodynamically stable surface plane, is known to reconstruct under certain conditions when additional Pt is added to the surface. [7, 8]

The scanning tunneling microscope (STM) allows for the examination of the structure of model catalyst surfaces *in situ*. This *in situ* analysis has lead to the discovery of the structural changes and high adsorbate mobility on surfaces in the elevated pressure and temperature regime where real catalysts are used. [9] By examining the interactions between coadsorbed species by STM, one mechanism for achieving catalytic activity on a crowded, unreactive adsorbate covered surface has been found. Coadsorption of carbon

monoxide occurs on Re(0001) and Pt(111) crystal surfaces that are covered by an ordered overlayer of sulfur (25% of a monolayer) by compressing the sulfur layer locally to higher coverages thereby allowing CO to adsorb. As long as the bond energy of the reacting adsorbates is large enough, lateral compression of the sulfur layer provides metal sites for bonding and reactions. [10, 11]

In this report we present evidence for a novel surface restructuring mechanism which occurs on a surface during coadsorption that provides new sites for adsorption or reactions. In this work the vicinal Pt(111) surface is initially covered with an unreactive overlayer of sulfur, and CO is coadsorbed on the surface. Coadsorbate induced compression of the sulfur is observed and an additional restructuring of the surface is found where new terraces of Pt, that are free of sulfur, are generated at the step edges, providing new adsorption sites on the surface. The step density on the surface doubles, and segregation of the sulfur and CO onto separate terraces is observed. Following the molecular desorption of CO, the surface returns to the initial sulfur covered structure and the newly created steps recede. This restructuring mechanism demonstrates the "flexibility" of the surface, and has many implications in metal surface catalytic reactions.

9.2 Experimental

All of the experiments were carried out in an ultra-high vacuum (UHV) chamber (base pressure < 7 x 10^{-10} Torr) where a vicinal (stepped) Pt(111) single crystal was cleaned and maintained. The single crystal was cut at an angle of 10° from the (111) direction. Sulfur was added to the surface via an electrochemical source ($Ag/AgI/Ag_2S$) [12] under UHV conditions, at room temperature. The surface was then annealed to 600°C for 30 s. Upon cooling the surface exhibited a well ordered p(2x2) structure as determined by examining the low-energy electron diffraction (LEED) pattern. The surface was then examined by scanning tunneling microscopy (STM) in the same chamber which showed

that the Pt(111) surface is uniformly covered by this sulfur structure. CO is next added to the vacuum chamber via a leak valve at a pressure of 1 x 10^{-6} Torr and the changes in the surface structure are monitored with the scanning tunneling microscope in the CO ambient. The typical STM tunneling conditions were 1 nA of tunneling current and 100-200 meV negative sample bias.

9.3 Coadsorption of sulfur and CO on a vicinal Pt(111) surface

STM topographic images of the clean Pt surface, prior to sulfur adsorption, show single atomic height steps of approximately 2.20 Å and terraces widths on the order of 20 - 30 Å. Following the deposition of sulfur on the Pt surface, the sample was annealed to 600°C and cooled to 25°C forming an ordered p(2x2)-S structure (figure 1) on the surface. A topographic image of the sulfur covered surface, shown in figure 2a, indicates that step doubling has occurred, as shown by the height difference between terraces which is now measured to be approximately 4.60 Å. This is accompanied by a widening of the terraces on the surface to approximately 40 - 50 Å. The doubling of steps induced by sulfur on stepped Pt surfaces and the simultaneous increase in terrace widths is a well known effect. [13] This structure is found to be uniform over the surface.

The addition of a background pressure of CO (1 x 10^{-6} Torr) at room temperature produced a dramatic change in the structure of the original sulfur covered surface. (figure 2b) STM images now show that the original double atomic height steps have split into two monoatomic steps separated by small terraces, on the order of 10 - 20 Å in width as shown in figure 3. These steps and terraces appear smoother and dimmer than the original terraces and alternate with wider (40 - 50 Å) terraces that show higher contrast. Based on a previous study of the coadsorbate induced compression of sulfur on Pt by CO [11], it was found that the contrast of the sulfur covered portions of the surface is higher than that of the CO covered areas. Thus, we attribute the contrast of the bright terraces to compressed

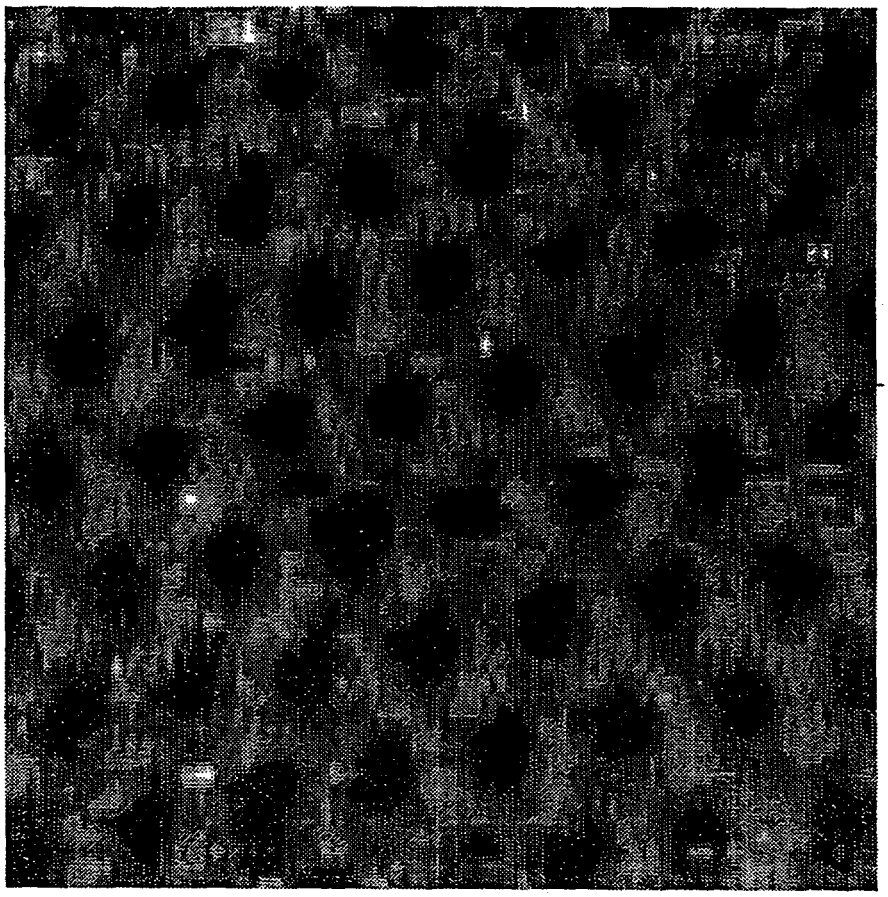

Figure 9.1: a) Current image (40 Å x 40 Å) of the p(2x2)-S structure on the terraces of the vicinal Pt(111) surface.

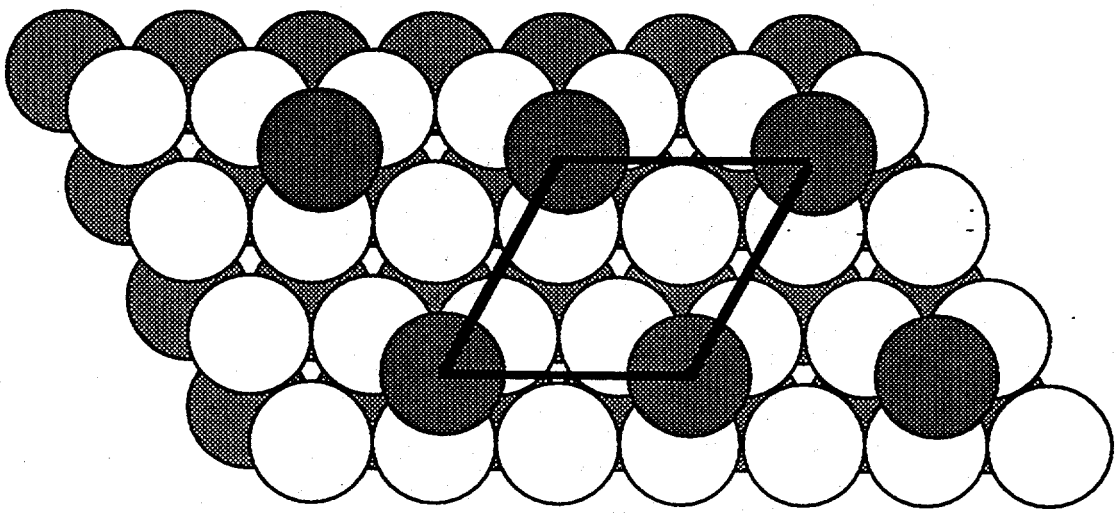

Figure 9.1 (continued): Model of the p(2x2)-S structure on the Pt(111) surface, showing the S (black top spheres) atoms in the fcc 3-fold hollow sites.

a)

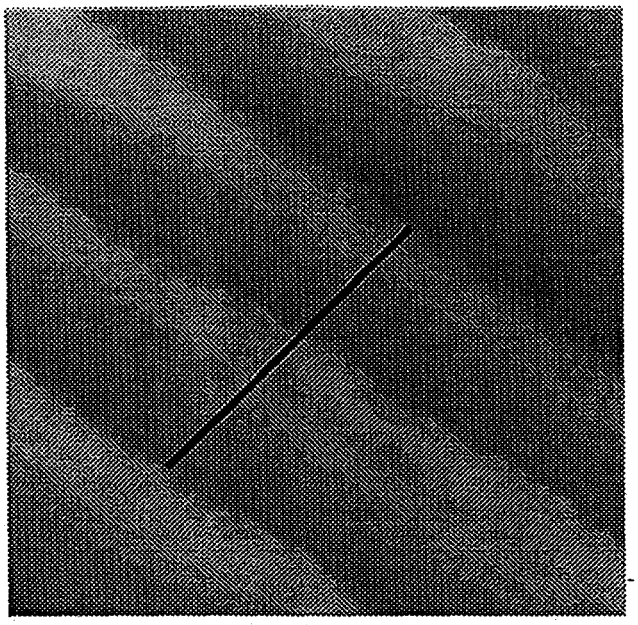

b)

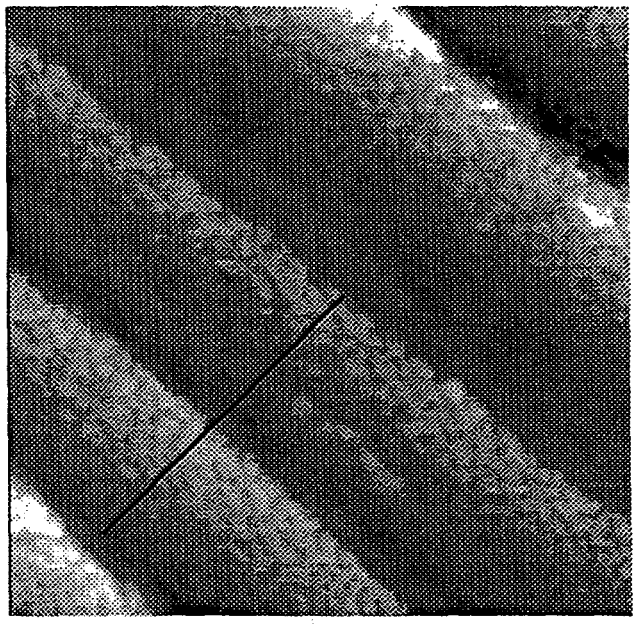

Figure 9.2: a) Topographic image (180 Å x 200 Å) of the Pt(111)-p(2x2)-S structure. b) Topographic image (200 Å x 200 Å) of the surface in a background pressure of 1 x 10^{-6} Torr of CO. The bright regions are compressed S on the surface separated by dimmer regions of new small Pt terraces where CO has adsorbed.

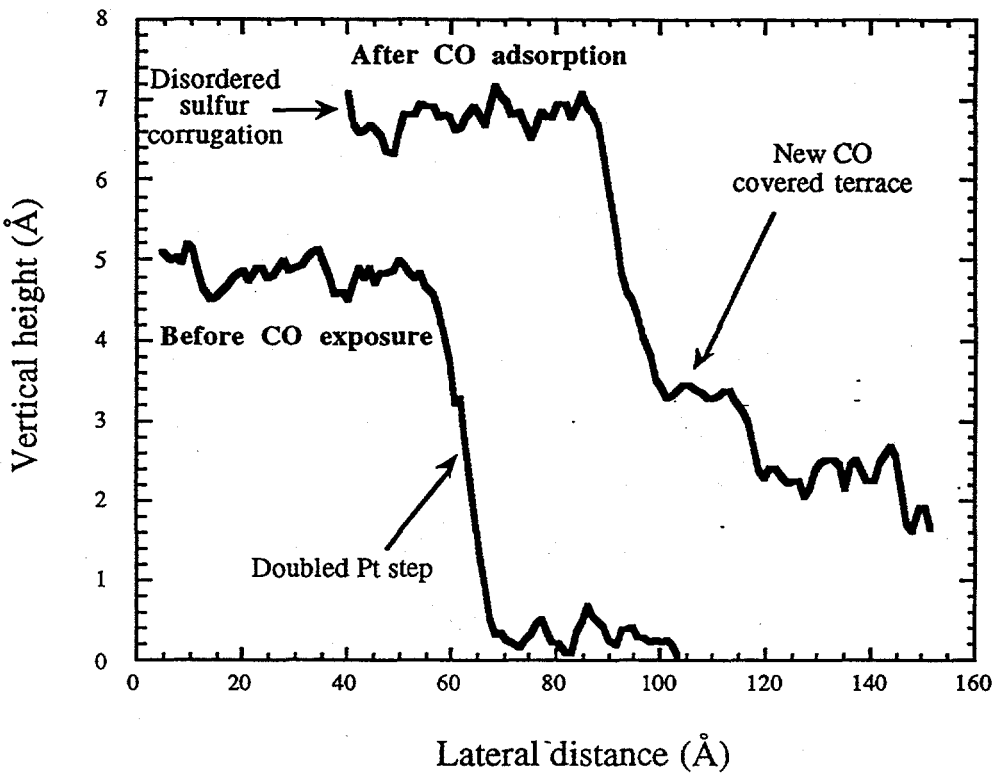

Figure 9.3: The bottom curve is a cross-section of the middle two terraces of the surface shown in figure 1a, indicating double atomic height steps. The top curve is a cross-section of the middle three terraces of the restructured surface shown in figure 1b, indicating the change to single atomic height steps. The height between the upper terrace and the new CO terrace is approximately 3.60 Å, the height of the Pt step, plus the S height on the surface (shown to be approximately 1.60 Å from dynamical LEED analyses of the Pt(111)-($\sqrt{3}$ x $\sqrt{3}$)R30°-S structure). (19)The height between the new CO terrace and the bottom step is a Pt step height minus the S height on the surface, which is approximately 0.90 Å.

sulfur islands. Atomic resolution images on the compressed areas (figure 4) show many maxima due to sulfur atoms compressed from 5.50 Å, in their original p(2x2) structure, to distances closer to 4.80 Å ($\sqrt{3}$ times the Pt lattice distance). [11] These correspond to distances found in higher coverage sulfur structures. We attribute the low contrast, newly formed terraces, to be Pt covered by CO. No atomic details on these terraces were obtained however. CO is known to diffuse too rapidly on Pt at room temperature and thus cannot be imaged by STM. [14] STM images of the CO covered surface taken in our STM, in the absence of sulfur, exhibit either the clean (1x1) periodicity of the Pt or the atomic structure is not resolved at all, depending on the tip conditions. Following CO desorption from the surface by heating the crystal to 600°C for a few seconds, the surface returns to the p(2x2)-S structure with the steps returning to their original two atom height, indicating that the CO induced restructuring of the sulfur covered stepped Pt surface is reversible.

9.4 A new surface restructuring mechanism

We have shown evidence that the vicinal Pt(111) surface restructures in the presence of coadsorbed sulfur and CO, as compared to its structure in the presence of one or the other adsorbates. This is the first reported coadsorbate induced restructuring of a metal surface. The proposed mechanism by which this reconstruction occurs is shown in figure 5 and described as follows. First the p(2x2)-S structure is formed and the step heights double on the surface. Normally steps are repulsive, however the formation of double height steps has been previously attributed to the long range energy gain from the ordered sulfur overlayer which prefers to have large uninterrupted domains. [15] As CO is added to the surface it initially bonds to step edges where the Pt-CO bonding is the strongest [16], and compression of the sulfur overlayer occurs away from the step edges, due to the repulsive interactions between sulfur and CO. This compression plays two roles, it disorders the sulfur structure, removing the long range energy gain which

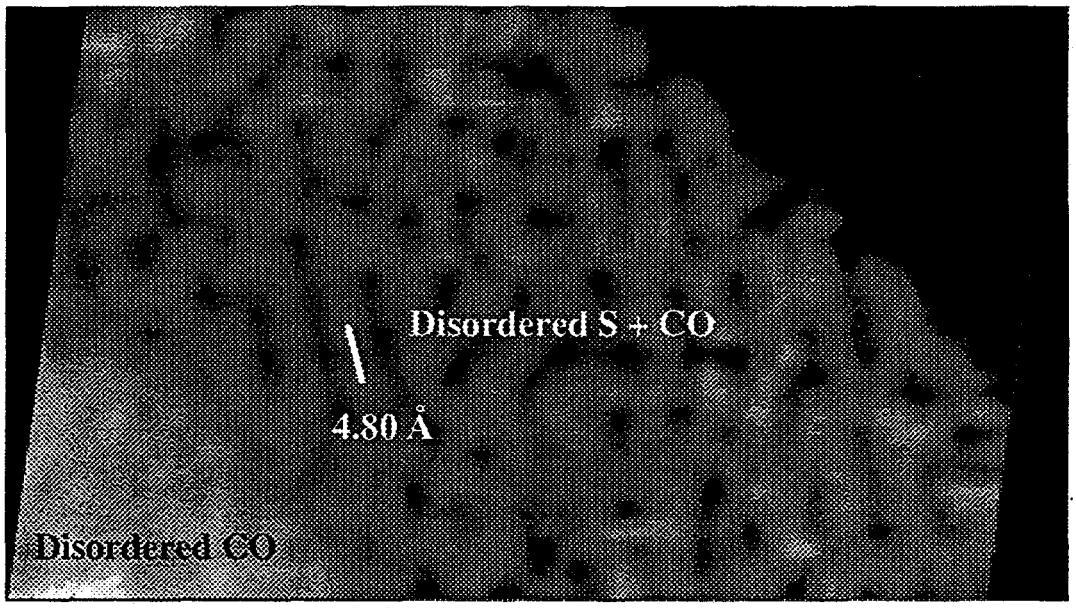

Figure 9.4: Close up topographic image (56 Å x 93 Å) of a CO covered terrace and a sulfur covered terrace showing the disordered arrangement of the compressed sulfur atoms.

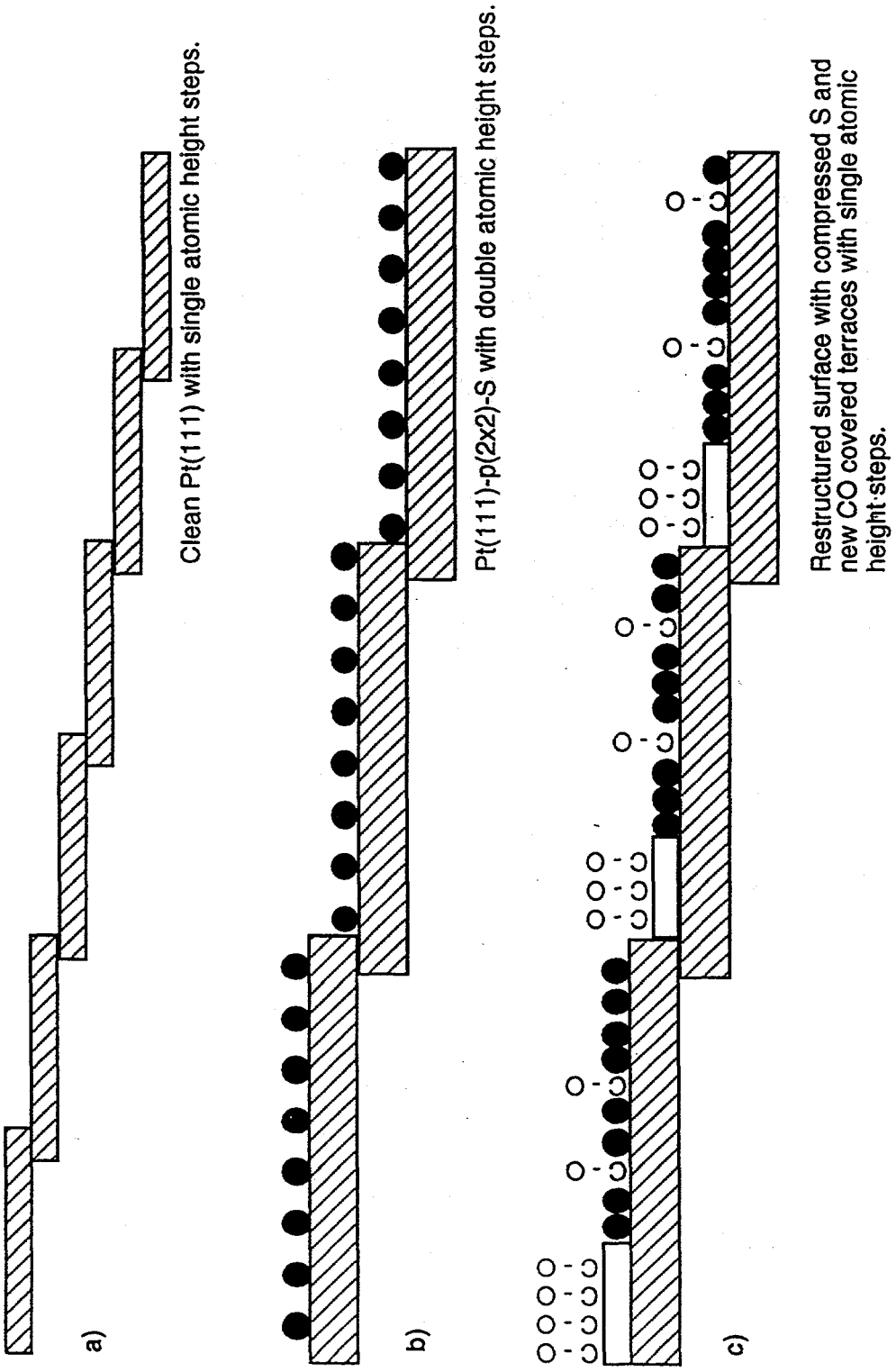

Figure 9.5: Proposed mechanism for the coadsorbate induced restructuring.

stabilized the doubled steps, and it frees the bottom sites of the step edges where further CO can adsorb on the surface. With the long range order lost, the steps are energetically driven apart and the adsorption of CO acts to promote Pt diffusion from the tops of the step edges forming the additional small (10-20 Å wide) (111) terraces that are covered by CO. The enhancement of Pt diffusion by CO has been previously shown in the Pt(110)-(1x2) to (1x1) reconstruction and the Pt(100)-(1x5) to (1x1) reconstruction in which large amounts of Pt are transferred at the surface. [14, 17] These new terrace widths are consistent with the amount of surface area which is freed up by the compression of the sulfur overlayer from its original p(2x2) (5.50 Å S-S distances) structure to sulfur atoms at distances of 4.80 Å.

9.5 Implications for catalysis

One of the puzzles of surface chemistry is how reactions can occur on surfaces in the presence of a strongly chemisorbed, unreactive overlayer, which blocks sites for adsorption or reactions to take place. Previous work of CO coadsorption on sulfur covered Re and Pt surfaces have shown that compression of sulfur induced by repulsive interaction with CO allows for CO to adsorb reversibly. This work presents the first direct evidence for a different mechanism by which a surface covered with a strongly chemisorbed overlayer can "make" new sites on the surface for reactions by surface restructuring. These results also indicate that while the initial surface is covered by sulfur, the adsorption of a reacting species only occurs on a fraction of the surface. The results demonstrate that steps at surfaces can reconstruct to provide new clean metal surface sites for bonding and reactions to occur. This restructuring is driven by the energy gain from the heat of adsorption of the reacting species on the surface.

These results point to the necessity of accurate *in situ* measurement of the total number of sites on the surface. Restructuring induced by reactant adsorption changes the

number of surface sites, thus changing the total concentration of sites where turnovers may take place. The rate of surface reactions are usually computed by determination of the total number of surface atoms measured by adsorption, *ex situ*. Since changes of site concentration occur during coadsorption (or reaction) and the surface returns to its original state after the reaction, the surface site densities measured by adsorption *ex situ* may be inaccurate by an order of magnitude or more. Further, the sulfur-carbon monoxide interaction weakens the CO bonding to the metal surface. [18] Such lowering of the heats of adsorption imply decreased surface residence times which can lead to higher turnover rates during catalytic reactions. Thus, low coverage coadsorbed sulfur may accelerate some reactions by weakening the bonds of the coadsorbed species to the surface.

9.6 Preliminary reaction with oxygen

In order to examine the reactivity of the "new" terraces on the surface, oxidation of the CO on the surface was attempted. After the formation of the restructured surface (as determined by STM) by the introduction of 1 x 10^{-6} Torr CO, the CO pressure was removed and a background pressure of 1 x 10^{-5} Torr, of oxygen was introduced into the chamber with the sample in the STM. The oxidation of CO on Pt is known to occur at room temperature. The surface structure was observed to change. The new terraces which originally had little to no observable corrugation due to the rapidly diffusing CO, now showed atomic resolution features. Shown in figure 9.6 is the surface in the oxygen environment. Atoms which are probably sulfur (as oxygen is typically observed as a slight depression) are observed to have some local ordering into chains of atoms on both the "new" terrace and the terrace where the sulfur was originally compressed. It appears that the CO was removed by the oxygen, and the sulfur atoms diffused over the step edges to spread out again. The step height between the two terraces shown in figure 9.6 is measured to be approximately 2.20 Å, indicating that atoms on both terraces are similar.

Figure 9.6: Topographic image (95 Å x 50 Å) of the interaction of the "new" terraces with oxygen at 1 x 10^{-5} Torr, showing the newly enhanced corrugation on the steps. The step height is found to be approximately 2.20 Å, one Pt atom high.

9.7 References

[1] S. M. Davis, F. Zaera, G. A. Somorjai, *J. Catal.* **77**, 439 (1982).

[2] A. J. Gellman, D. Neiman, G. A. Somorjai, *J. Catal.* **107**, 92 (1987).

[3] A. J. Gellman, M. E. Bussell, G. A. Somorjai, *J. Catal.* **107**, 103 (1987).

[4] G. A. Somorjai, *Langmuir* **7**, 3176 (1991).

[5] P. R. Watson, M. A. V. Hove, K. Hermann, *NIST Surface Structure Database Ver. 1.0*NIST Standard Reference Data Program Gaithersburg, MD, 1993).

[6] G. A. Somorjai, *Annu. Rev. Phys. Chem.* **45**, 721 (1994).

[7] M. Bott, M. Hohage, T. Michely, G. Comsa, *Phys. Rev. Lett.* **70**, 1489 (1993).

[8] A. R. Sandy, S. G. J. Mochrie, D. M. Zehner, G. Grübel, K. G. Huang, D. Gibbs, *Phys. Rev. Lett.* **68**, 2192 (1992).

[9] B. J. McIntyre, M. Salmeron, G. A. Somorjai, *J. Vac. Sci. Tech.* A **11**, 1964 (1993).

[10] J. C. Dunphy, B. J. McIntyre, J. Gomez, D. F. Ogletree, G. A. Somorjai, M. B. Salmeron, *J. Chem. Phys* **100**, 6092 (1994).

[11] B. J. McIntyre, M. Salmeron, G. A. Somorjai, *Surf. Sci.* **323**, 189 (1995).

[12] C. Wagner, *J. Chem. Phys.* **21**, 1819 (1953).

[13] A.-M. Lanzillotto, S. L. Bernasek, *J. Chem. Phys.* **84**, 3553 (1986).

[14] T. Gritsch, D. Coulman, R. J. Behm, G. Ertl, *Phys. Rev. Lett.* **63**, 1086 (1989).

[15] J. C. Dunphy, C. Knight, P. Sautet, D. F. Ogletree, G. A. Somorjai, M. B. Salmeron, *Surf. Sci.* **280**, 313 (1993).

[16] S. M. Davis, Ph.D., Univ. of California at Berkeley (1981).

[17] B. Lang, R. W. Joyner, G. A. Somorjai, *Surf. Sci.* , 454 (1972).

[18] D. G. Kelly, A. J. Gellman, M. Salmeron, G. A. Somorjai, V. Maurice, M. Huber, J. Oudar, *Surf. Sci.* **204**, 1 (1988).

[19] K. Hayek, H. Glassl, A. Gutmann, H. Leonhard, M. Prutton, S. P. Tear, M. R. Welton-Cook, *Surf. Sci.* **152**, 419 (1985).

Chapter 10

Overview of surface chemical bonding

This chapter focuses on the structures of surfaces at the atomic scale. Surfaces and films play a key role in areas such as heterogeneous catalysis, microelectronics, and tribology, and are of interest to those who use surfaces for their unique chemical, physical, and electronic properties. In heterogeneous catalysis for example, metal and oxide surfaces are used in a variety of ways, from the reforming of fuels to the removal of toxic gases such as NO_x from automotive exhausts. This chapter is set to provide an overview of the field of surface chemical bonding that the work in this thesis is now a part of. A brief review of other techniques used in surface structure determinations is provided. This is followed by the current understanding of surface chemical bonding for clean and adsorbate covered surfaces, which primarily contain few defects. While this is much different than the surfaces described in this dissertation, however the groundwork of our current understanding is outlined.

10.1 The importance of monolayer surface structures

The ability to actively control surface properties would enable the design of products on the atomic scale. To obtain this control, details of molecular bonding and structure of surfaces are required. Such information has been attained through the development of surface sensitive techniques over the past 25 years. These techniques can probe surface electronic and vibrational states, elemental composition, and the atomic structure of surfaces and adsorbed species. Here we shall focus on the structures of surfaces. First we will briefly review the techniques that help us understand surface structure, in particular low-energy electron diffraction (LEED) from which almost half of the detailed surface structures have been obtained. Next a description of the structures of clean surfaces and how surface atoms exhibit different properties from their bulk counterparts will be introduced through the concepts of surface relaxation and reconstruction. We will then describe the nature of the surface chemical bond based upon detailed structures of atomic and molecular species on surfaces, followed by a description of mixed overlayers and the co-adsorption phenomena. The chapter concludes with a summary of what has been learned about surface bonding and an outlook for the future.

10.2 Techniques for the determination of monolayer structures.

A summary of the techniques employed in the determination of surface structures and the information they provide is listed in table 10.1. Much surface structural information has been obtained by techniques in which either photons, electrons, ions, or atoms are scattered and/or diffracted from single crystal surfaces under ultra-high vacuum conditions (pressures on the order of 10^{-10} torr) and analyzed as a function of energy or scattering angle. Vibrational spectroscopy has also made a significant contribution to the understanding of surface bonding of monolayers and how molecules rearrange on surfaces.

Direct observations of surface structure have been obtained through developments in the scanning probe microscopies (SPM). These advances in SPM have lead to the ability to actively manipulate surface atoms, [1], study the surfaces of organic films [2], and to atomically examine surfaces under real catalytic conditions of elevated temperatures (150 °C) and pressures (2 atm). [3]

10.2.1 Low-energy electron diffraction.

Almost half of the detailed surface structures known have been obtained from the dynamical analysis of low-energy electron diffraction (LEED) data from single crystal surfaces. When electrons are scattered from a surface they interact only with the top few atomic layers of the material due to the strong interactions between electrons and matter. This interaction makes electrons useful probes of the structure of surfaces. Electrons in the range of 20 to 300 eV have de Broglie wavelengths comparable to the lattice spacings in crystals. By scattering low-energy electrons from well ordered single crystals, diffraction patterns may be obtained. The diffracted beam intensities as a function of energy contain information on the surface structure. The surface structure may be determined by fitting a theoretical model to these experimental intensity vs. energy (I-V) curves

Table 1: Summary of Surface Sensitive Structural Techniques.

Technique	Description	Information
Atomic Diffraction	A beam of monoenergetic neutral atoms is scattered from the topmost surface layer and detected as a function of energy and angle.	Atomic surface structure.
X-ray Adsorption Fine Structure	This involves the ejection of a core level electron wave which may then be back-scattered from a neighboring atom producing an interference which is structurally and chemically sensitive.	Local atomic surface structure.
Scanning Probe Microscopy	Consists of both scanning tunnelling microscopy (STM) and atomic force microscopy (AFM). The surface topography is mapped by scanning a probe over the surface and measuirng either electron charge densities (STM) or surface interactions (AFM).	Provides Å resolution surface topographic information.
Photoelectron Diffraction	A monoenergetic beam of photons is used to excite core level electrons whose interference and diffraction provide surface structural information.	Atomic surface structure
X-ray Diffraction	Normal X-ray diffraction employed at extreme glancing angles to increase surface sensitivity.	Atomic surface structure
Ion Scattering	High energy ion (~ 1MeV) beams are directed along bulk crystal axes in solid surfaces. The "blocking" and "channeling" of the beams are dependent upon the structure of the crystal surface.	Atomic surface structure
Surface Vibrational Spectrocsopy	Measured either with typical infra-red absorption techniques or by measuring the inelastic losses from (1-5eV) electrons scattered from the surface.	Intramolecular and surface bonding.
Field Ion Microscopy	A sharp metal tip with a radius of ~ 1000A at a potential of ~10kV is placed in a low pressure of gas (He). The gas, polarized by the field is attracted to the tip, ionized and projected onto a phosphor screen where they produce an image of the high field regions of the tip.	Atomic surface structure and surface diffusion.
Electron-Stimulated Ion Angle Distribution	An electron beam incident upon the surface can excite electrons in chemical bonds into non-bonding states, inducing decomposition. This accelerates an ion fragment along the direction of the broken bond resulting in the angular distribution of signal.	Molecular orientation of species on the surface.
Low-Energy Electron Diffraction	Electron in the range of 30-300eV are back-scattered from the surface. The diffracted intensities as a function of energy and angle are analyzed to provide structural information.	Atomic and molecular surface structure.

Table 10.1: A summary of surface sensitive techniques used in the determination of surface structures.

The current state-of-the-art experimental approach involves two different experimental methods for the detection of diffracted electrons, the "video-LEED" technique and the "digital-LEED" technique. In the "video-LEED" technique shown in figure 10.1a, electrons are backscattered from the single crystal sample and passed through energy selecting grids which allow only the elastically scattered electrons to pass through. The electron impacts are monitored on a fluorescent screen where the diffraction pattern is observed. This pattern is then recorded by a high sensitivity video camera and digitized by a computer. The electron beam energy is varied over a given energy range with images collected every 2-3 eV. From these images the integrated intensities as a function of energy for various diffracted beams may be measured to produce experimental I-V curves as a database for structure calculations.

In the "digital LEED" technique shown in figure 10.1b, electrons are again backscattered from the single crystal sample and passed through energy selecting grids which allow only the elastically scattered electrons through. This method however uses a detector designed to measure the impact positions of *single* electrons. A pair of multichannel plates is used to generate a charge cloud from each electron impact. This charge cloud is detected by a wedge and strip anode (or a resistive anode) and used to generate the LEED pattern in a histogram memory. An important advantage to this approach is the very low electron beam current used (~ 1 pA). This minimizes electron induced dissociation or desorption of surface species. The images are also processed by a computer to generate I-V curves for each diffracted beam for use in the structure calculation.

The modeling of the surface structure to obtain bond lengths and bond angles requires a fully dynamical LEED intensity analysis of experimental LEED I-V curves. The details of the surface structure are contained in these I-V curves, however no direct method of obtaining this information is available as in X-ray crystallography, due to the strong electron-atom interactions which cause complex multiple scattering events in the surface.

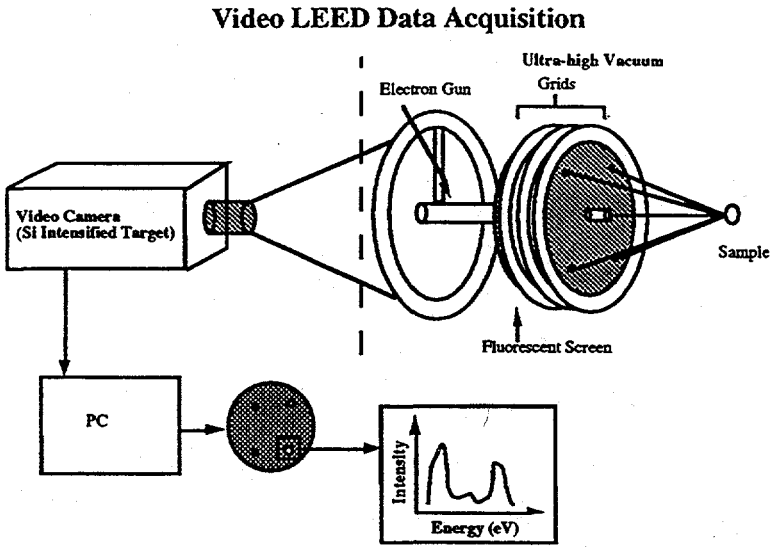

a)

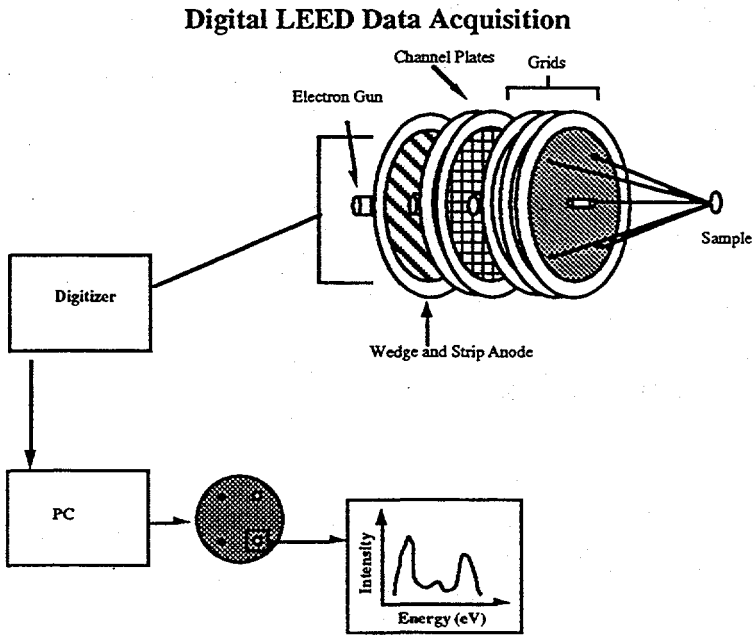

b)

Figure 10.1: Schematic diagram of the video LEED (shown for a rear-view LEED optics) method for the acquisition of electron diffraction data from single crystal surfaces.

To obtain structural information from electron diffraction data the exact scattering paths of the electrons must be calculated for a series of model structures producing theoretical I-V curves. These models are based upon the symmetry of the LEED pattern, and any information available from other techniques. The I-V curves for these structures are calculated and compared to experiment, with the best agreement identifying the structure. Different methods of calculating theoretical I-V curves have been described in several books on LEED. [4-6] The fit between experiment and theory is quantified by a reliability factor (R-factor). Various R-factors may be employed to measure the goodness of fit between peak position, intensity, or average deviation. A recent advance to this analysis is automated tensor LEED (ATLEED). This is a perturbative process which couples the R-factor to an automated search routine. With this method a "structural space" within 0.3-0.4Å of a calculated reference structure may be rapidly searched to find the best fit structure for the given experimental data. The process for the structure determination is outlined in Chapter 2. Several recent papers describe this approach in detail.[7-9]

While most LEED structure work is done on surface structures with well defined periodicities, LEED structure analyses may also be applied to disordered overlayers on surfaces. In the LEED scattering process there is no fundamental requirement for long range order. The diffracted intensities for any given position in momentum space (**k**-space) are dependent solely on the local surface geometry. Thus for a system in which there is *one* type of adsorption site geometry, it is possible to solve the surface structure by a model geometry just as in conventional LEED. [10] This process has been applied to a variety of systems such as K on Ni(100) [11], C_6H_6 on Pt(111) [12], and CO on Pt(111). [13]

Due to this local site dependence of the diffraction process, the adsorption site may be inferred for surface structures that have the same local environment but different chemical nature or different long range ordering. For example the I-V curves for O adsorbed in a 3-fold hollow site on a metal surface will look similar to C adsorbed on the same surface in the same site. This has been applied to several systems as a

"fingerprinting" technique to obtain qualitative structural information without a detailed calculation. [14-16].

10.2.2 Photon scattering and diffraction

X-rays have been used in several ways to determine surface structures. Although X-rays are more sensitive to the bulk structure of the material due to their penetration depth, when employed at extreme glancing angles from the surface, X-ray diffraction shows greatly enhanced surface sensitivity. The X-rays are scattered along the surfaces <1° from the surface normal and the diffraction measured to determine the surface structure. X-ray adsorption fine structure techniques and photoelectron diffraction analyze the interference and diffraction of ejected core level electrons. This approach produces very localized structural information and is useful for a determination of the local bonding of adsorbates. This structural information is extracted from a model and typically involves detailed calculations similar to those in LEED. The major restraint to this approach is the need for synchrotron sources to generate the required energy resolution and high photon flux used in the experiments. [17]

10.2.3 Scattering and diffraction of atoms and ions.

Atoms and ions may be used as probes of surface structure. In ion scattering noble gas ions such as He^+ or Ne^+ at high energies (~1 MeV) can be directed along particular crystallographic axes of a crystal. The passage of these beams through the crystal is dependent upon the nature of the surface structure which can be deduced from the "blocking" and "channeling" patterns observed. This method is particularly useful for studying relaxations and reconstructions of crystal surfaces. Large differences from bulk crystal structure however make the data interpretation very complicated. [17]

More direct images of metal surface structures may be obtained from field ion microscopy (FIM). In this technique a sharp metal tip with a radius of ~ 1000Å is placed at a potential of ~ 10 keV in a low pressure of He (~ 10^{-4} Torr). The gas is polarized by the high field and attracted to the tip where it is then ionized and subsequently projected onto a phosphor screen. This produces an image of the high field regions of the surface and shows all of the crystallographic planes present at the end of the tip. Surface reconstructions of clean or adsorbate covered surfaces may be studied by FIM, however, only the substrate atomic positions are observed. [17]

Atomic diffraction from a surface can also provide surface structural information. In this method a thermal beam of atoms is scattered from a surface and the angular dependence of the scattering is measured to determine the surface structure. An important advantage to this technique is that it is sensitive to only the outermost layer of the surface. This technique differs from other diffraction techniques in that scattering is from the electron charge distribution rather than the atomic core levels. This method has also been used to study surface structures under phase transitions. [18]

10.2.4 Scanning probe microscopies

In recent years direct measurements of surface structure have rapidly advanced under scanning probe microscopy. This area includes both scanning tunneling microscopy (STM) and atomic force microscopy (AFM). In STM a probe consisting of a sharp metal tip, (~ 1000 Å curvature) is scanned across a sample within a few Å of the surface. At these distances electron tunneling between the tip and the surface is possible. Tunneling currents on the order of 1 nA are produced. This current is supplied to a feed-back loop to precisely control the tip-surface separation. A current vs. position map can be generated as the tip is rastered across the surface. This map shows the charge density topography of the surface and enables the determination of atomic positions to within 0.1 Å. STM can

provide complimentary information to diffraction techniques, with the added advantage of being sensitive to local defects to which diffraction is insensitive. This technique however is limited to conducting or semiconducting materials. [19]

Through the development of AFM, similar topographic information can be obtained for insulating systems as well. In AFM surface structure is measured through monitoring the deflections of a sharp tip of a cantilever as the tip is rastered over the surface. The deflections of the tip caused by the corrugation of the surface are detected optically by the reflection of a laser beam off the back of the cantilever. This approach produces a real space map of the surface from which surface structure may be deduced. [20, 21]

10.3 Clean surfaces, relaxations and reconstructions.

In the last 25 years the model of the clean surface has changed from that of a rigid lattice with atoms in their bulk-like equilibrium positions to a relatively flexible interface where surface atoms may readily rearrange. In the four or five outermost layers of the surface region the atoms have been found to alter their atomic positions in order to minimize the surface free energy and increase the local degree of bonding at the surface. These observed changes in the atomic positions of surface atoms have been separated into two general classes, relaxations and reconstructions. Surfaces are described as *relaxed* when expansions or contractions of the interlayer spacings of the surface layers, with respect to the bulk interlayer spacings, are observed. Surfaces are described as *reconstructed* when the atoms of the clean surface unit cell no longer resemble the projection of the ideally bulk terminated lattice at the surface layer. Low-Miller-index surfaces make up the majority of the surface structures studied since these are the simplest and most closed-packed surfaces, and less likely to show complicated changes in surface structure. Here we will discuss clean metal, semiconductor, and oxide surfaces.

On clean metal surfaces relaxations are related to the roughness of the surface. The rougher the surface the greater the degree of relaxation. This correlation is shown in figure 10.2 for clean Al surfaces. Spacing relaxations on metals have been found typically to be oscillatory: often the first layer is contracted, the second expanded, the third contracted, etc., with the sizes of contraction and expansion decreasing into the material, until the bulk spacing is reached. Clean metals also have been shown to reconstruct. One example is the (1x2) "missing-row" reconstruction of fcc(110) metals such as Ir, Au, Pt, and Rh as shown in figure 10.3. When compared to the bulk terminated fcc(110)-(1x1) surface every other metal row is now missing. [22] Another unique metal surface reconstruction is the hexagonal reconstruction of Ir(100).[23] In this structure (figure 10.4) the more open square surface lattice now adopts the close-packed hexagonal arrangement.

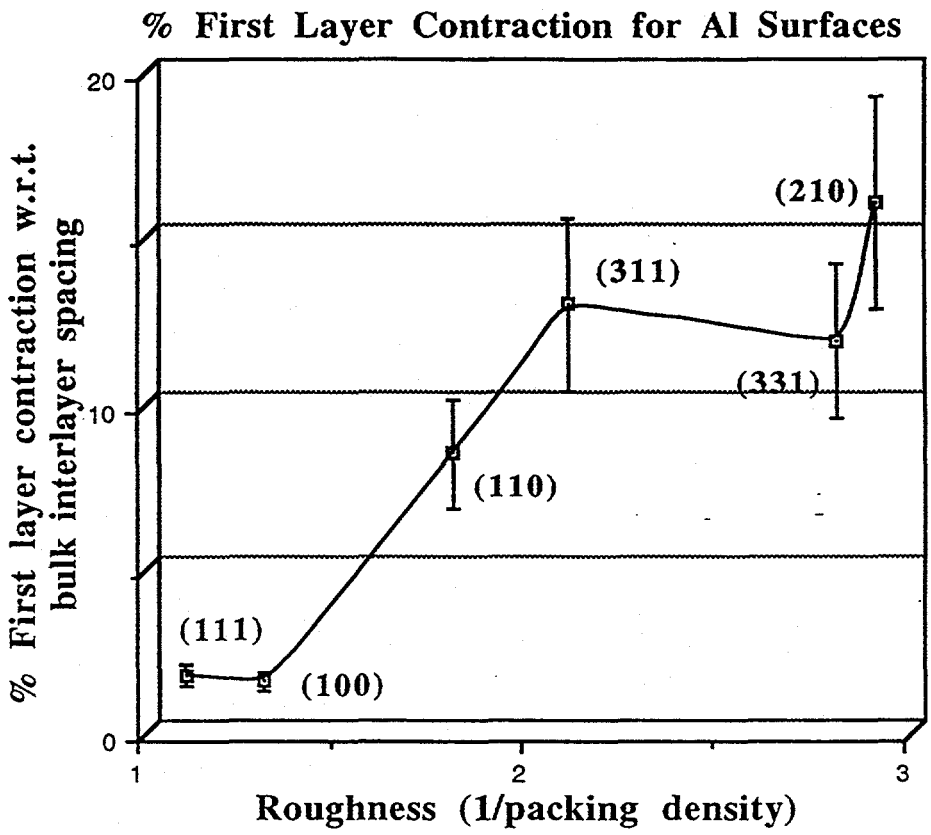

Figure 10.2: The percent contraction of the first interlayer spacing, with respect to the bulk interlayer spacing, versus surface roughness for various Al surfaces. The error bars are estimated as 20% of the displacement.

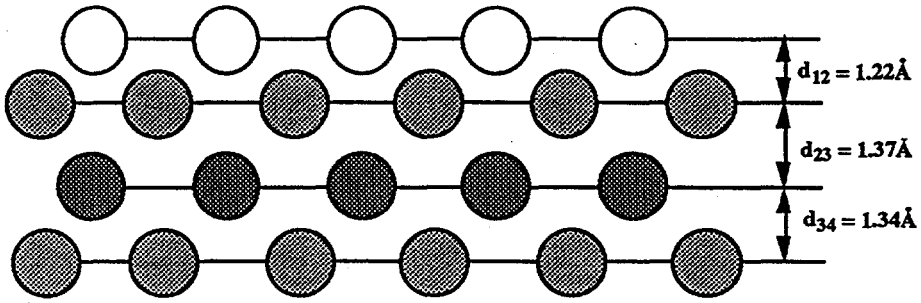

Side view: Rh(110)-(1x1) Surface

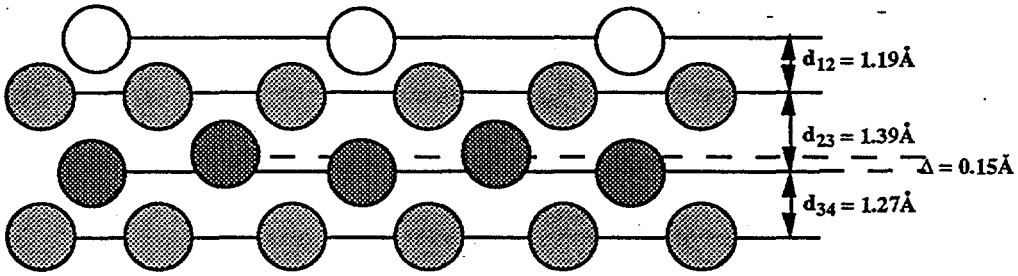

Side view: Rh(110)-(1x2) Missing-Row Surface d_{bulk} = 1.34Å

Figure 10.3: Side views of the (1x1) and (1x2) surfaces showing the missing-row reconstruction observed for clean Rh(110). This reconstruction occurs for Au, Pt, and Ir also. The relaxations in the surface are oscillatory, and increase on the more open (1x2) surface. A buckling of the (1x2) surface also occurs where the atom directly below the missing row moves upwards.

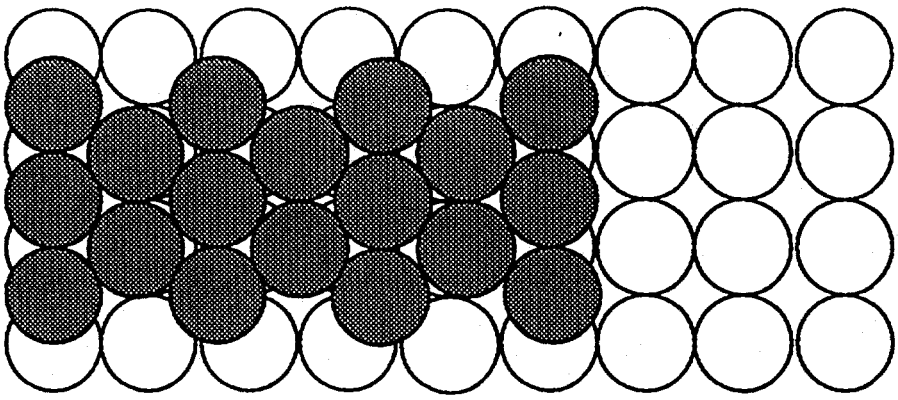

Ir(100)-(1x5) reconstruction **Ir(100)-(1x1)**

Top View

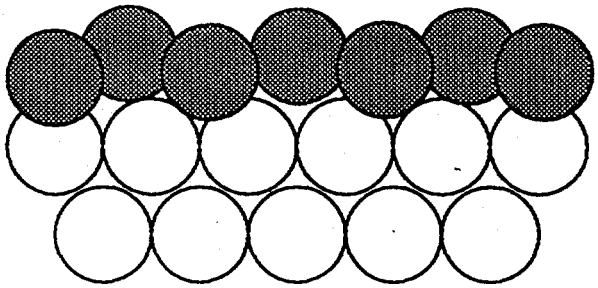

Side View

Figure 10.4: Top and side views of the Ir(100)-(1x5) surface reconstruction. The more open square (100) lattice is reconstructed into a close-packed hexagonal overlayer, with a slight buckling as shown from the side.

More recently, the structures of high-Miller-index metal surfaces have been examined. While these surfaces are more complex, they contain defect sites such as steps and kinks which are important in surface catalysis, melting, and surface growth phenomena. Of the few systems that have been studied, the trend of larger surface relaxations occurring with more open surfaces is clearly observed. The structures of atomic kinks and steps at the surface appear to rearrange in such a fashion as to smooth out the defect. This is seen on the Pt(210) surface (figure 10.5) whose top layer kink atoms are contracted by 23% of the bulk spacing, decreasing the surface roughness. [24]

Clean semiconductor surfaces have been shown to exhibit dramatic reconstructions. The driving force for surface reconstructions on semiconductor surfaces is the elimination of unstable high energy surface dangling bonds. The surface is forced to compensate for the loss of bonding partners at the surface. Since these bonds are directional, rather than delocalized as in metals, drastic atomic rearrangements almost always occur for clean semiconductor surfaces. Two important examples are the reconstructions of Si(111) and Si(100). The Si(111)-(1x1) surface is stable when terminated by hydrogen. Upon the removal of this hydrogen, the surface reconstructs to the more stable (7x7) [25] structure shown in figure 10.6 to minimize the surface free energy and reduce the number of surface dangling bonds from 49 to 19. On Si(100) the (1x1) surface reconstructs into a (2x1) structure [26] where half of the dangling bonds present in the (1x1) surfaces are now paired together. (figure 10.7) Surface vacancies (polarity) can also induce reconstructions. For example in compound semiconductors such as GaAs(100) a variety of surface structures are formed depending on the Ga to As ratio at the surface.

The understanding of oxide surfaces is less complete than for metals and semiconductors due to the incompatibility of the classical surface science electron spectroscopic techniques with insulating samples. These problems can be avoided by the growth of thin oxide films on metal single crystal surfaces or by doping the oxide with an appropriate donor. Oxide surfaces have been shown to be highly strained due to the large

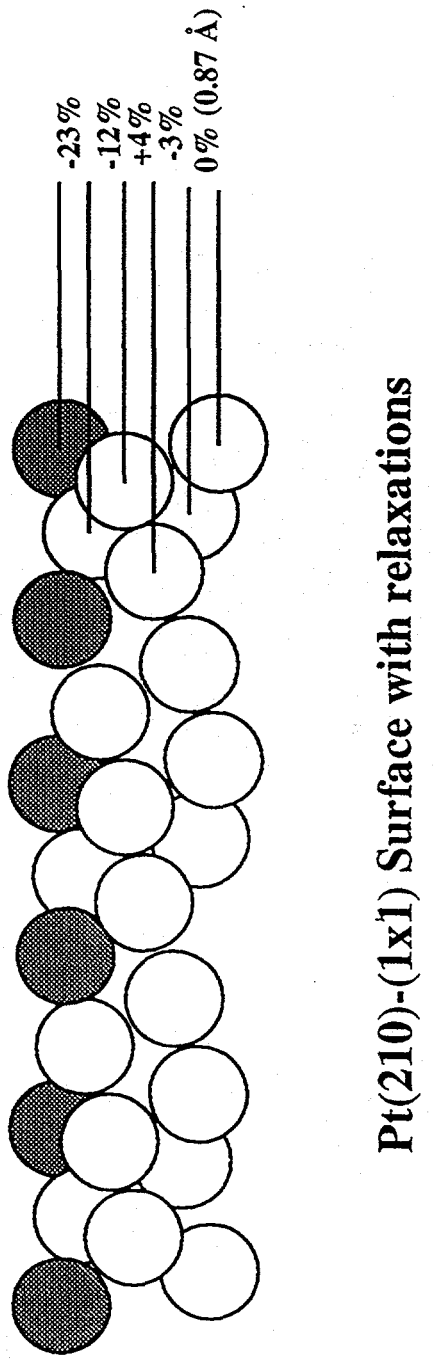

Figure 10.5: Spacing relaxations observed in the clean Pt(210) surface. The shaded atoms represent kink atoms on the surface whose contraction of 23% shows how the surface smoothes out the kinks to minimize the surface free energy.

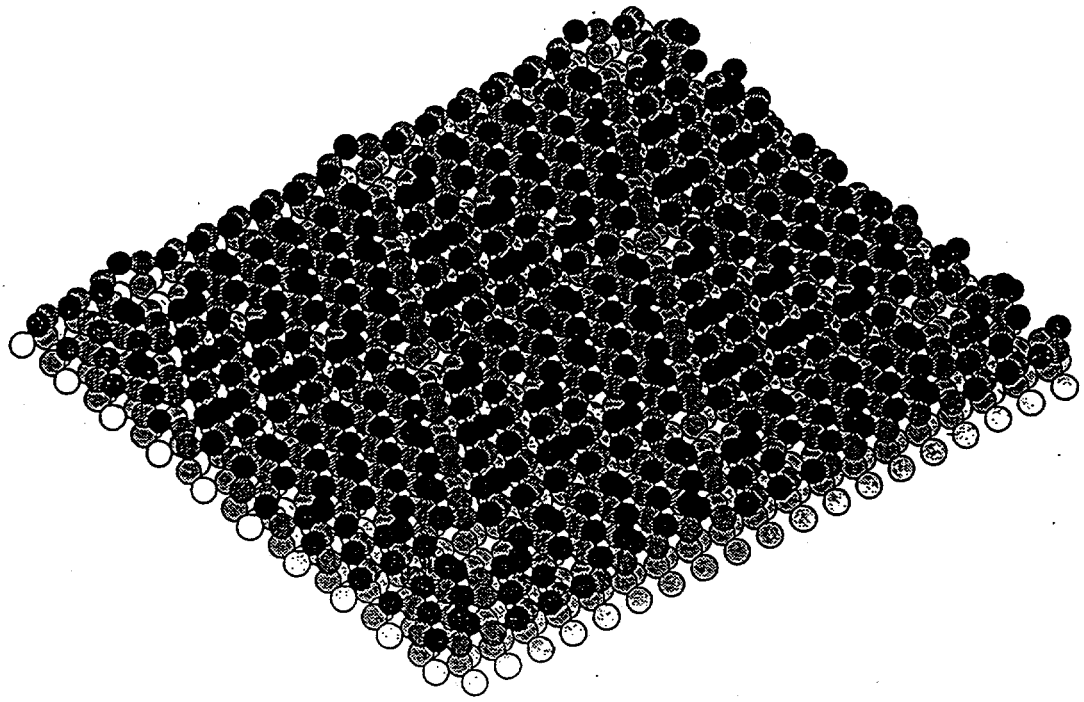

Figure 10.6: The Si(111)-(7x7) reconstruction that occurs after the desorption of H which caps the Si(111)-(1x1) surface. The black atoms are the remaining surface atoms with dangling bonds.

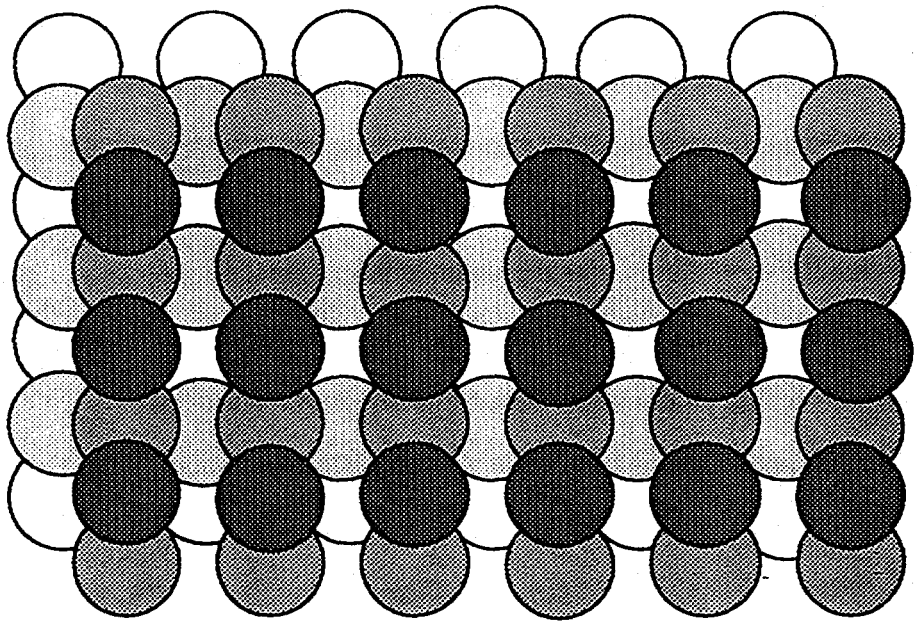

Top View: Si(100)-(1x1)

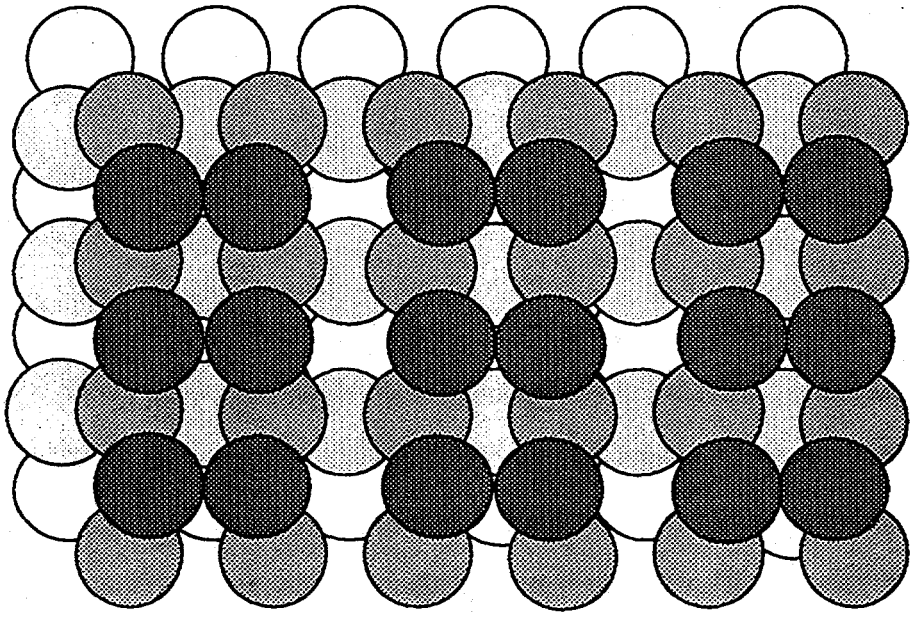

Top View: Si(100)-(2x1) reconstruction

Figure 10.7: The top views of the Si(100)-(1x1) and (2x1) reconstruction, showing the dimer pairing of the top layer Si surface atoms, which results in the removal of half of the clean surface dangling bonds.

local ionic charges at the surface. The polarity of the oxide surface is the driving force for the degree of reconstruction or relaxation. This can result in very large (> 0.2Å) relaxations in the surface layers. One example is the $Fe_3O_4(111)$ structure [27] grown on Pt(111). The top two oxygen layers are expanded by ~ 0.46 Å as shown in figure 10.8. This expansion of the clean oxide surface is the opposite of the contractions normally observed in clean metal surfaces. Also, just as in the compound semiconductor surfaces, vacancies at the surface can introduce reconstructions. For example the (100) surface of barium titanate reconstructs due to oxygen vacancies induced when annealed to high temperatures.

As described above clean surface atoms show changes in their bulk equilibrium positions in order to maximize their local bonding and minimize the surface free energy. Such relaxations and reconstructions can also be induced through the adsorption of atoms or molecules. The majority of surface structural studies that include adsorbates have been made on metal surfaces. We shall begin first with atomic adsorbates on metals.

10.4 Atomic adsorption on metals.

The adsorption of atoms or molecules on well ordered single crystal surfaces often results in ordered surface overlayers. The degree of ordering is determined by the balance between the adsorbate-substrate and adsorbate-adsorbate interactions. In chemisorbed systems at low coverages (< 0.5 monolayer), adsorbate-adsorbate interactions play little role in the adsorbate bonding. The majority of known overlayer surface structures involve atomic adsorbates such as H, C, N, O, and S on metals. These atoms often bond in the highest coordination sites to create the maximum possible number of adsorbate-substrate bonds at the surface. For example, on Rh(111) [28] and Rh(100) [29] , O bonds to the 3-fold (figure 10.9) and 4-fold hollow sites respectively, above the surface plane by ~ 1.0 Å. In some cases, the small size of an adsorbate allows for subsurface penetration.

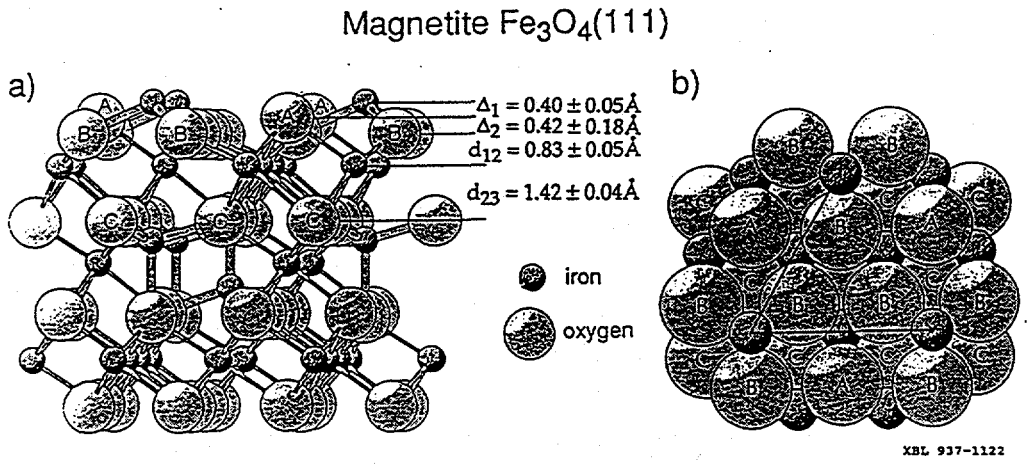

Figure 10.8: Side and top views of the Fe_3O_4(111) surface structure with the spacing relaxations shown. The corresponding bulk values are Δ_1=0.63 Å, Δ_2=-0.04 Å, and $d_{12}=d_{23}$=1.19 Å. The A and B layers are strongly expanded by ~ 0.46 Å.

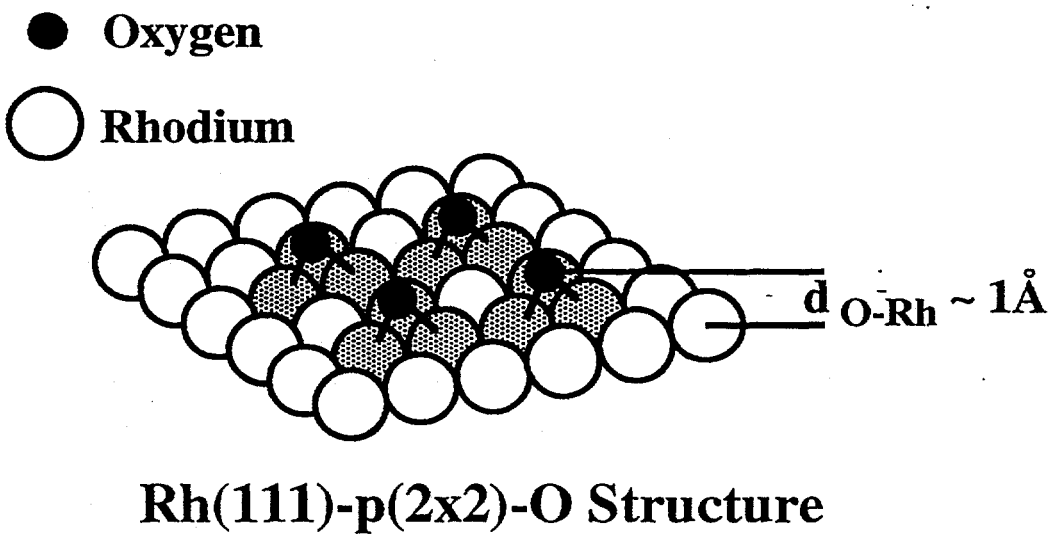

Figure 10.9: The adsorption of 0.25 monolayers of oxygen on Rh(111) results in an ordered (2x2) superstructure. The oxygen atoms are bonded in the fcc 3-fold hollow site ~ 1 Å above the surface plane.

Nitrogen on Ti(0001) [30] occupies interstitial sites between the first and second layers, (figure 10.10) which in essence represents the formation of a thin TiN film.

The high bonding coordination of atomic adsorbates reflects the strong bonds they make to the surface. Recall that clean surfaces often show relaxations at the surface layers due to the absence of bonding partners at the surface. When atomic adsorbates are present these relaxations are relieved and the metal surface atoms often return to near bulk-like equilibrium positions. For example, Rh(110) has a large relaxation of ~ 0.10 Å in the top interlayer spacing. Structure analyses of the adsorption of H, O, or S, on Rh(110) reveal that this relaxation is removed, and the metal atoms of the surface return to an essentially bulk-like structure. [31-33] (figure 10.11)

Detailed analyses of atomic adsorbate bonding show that the local bonding is actually *cluster-like* in nature. The nearest-neighbor atoms can suffer large distortions in position, while the next-nearest-neighbors show little to no change in position. The adsorbate can alter the positions of the clean metal atoms to which it is bonded not only via the removal of relaxations perpendicular to the surface, but laterally in the metal plane. When C is adsorbed on the (100) crystal plane of Ni, [34] the C induces large (~ 0.5 Å) lateral distortions in the top metal layer with respect to the normal bulk Ni(100) orientation. (figure 10.12) Adsorbates can also induce buckling of the metal layers near the surface.

Depending on the strength of the adsorbate-adsorbate, adsorbate-substrate, and substrate-substrate bonding *adsorbate induced reconstruction* may occur. For O on Rh(110), at some O coverages, a missing-row adsorbate induced reconstruction occurs. This has been investigated by both LEED [35] and STM [36]. At 0.5 monolayers of O, the surface is roughened and the O induces the missing-row reconstruction. (figure 10.13) As the O coverage is increased the number of missing rows decreases uniformly. A different type of reconstruction is observed for O on Cu(110) [37]. In this case the clean (1x1) Cu surface reconstructs to form Cu-O-Cu chains along the surface, figure 10.14. In other cases, surfaces reconstructions may be lifted by the bonding of adsorbates.

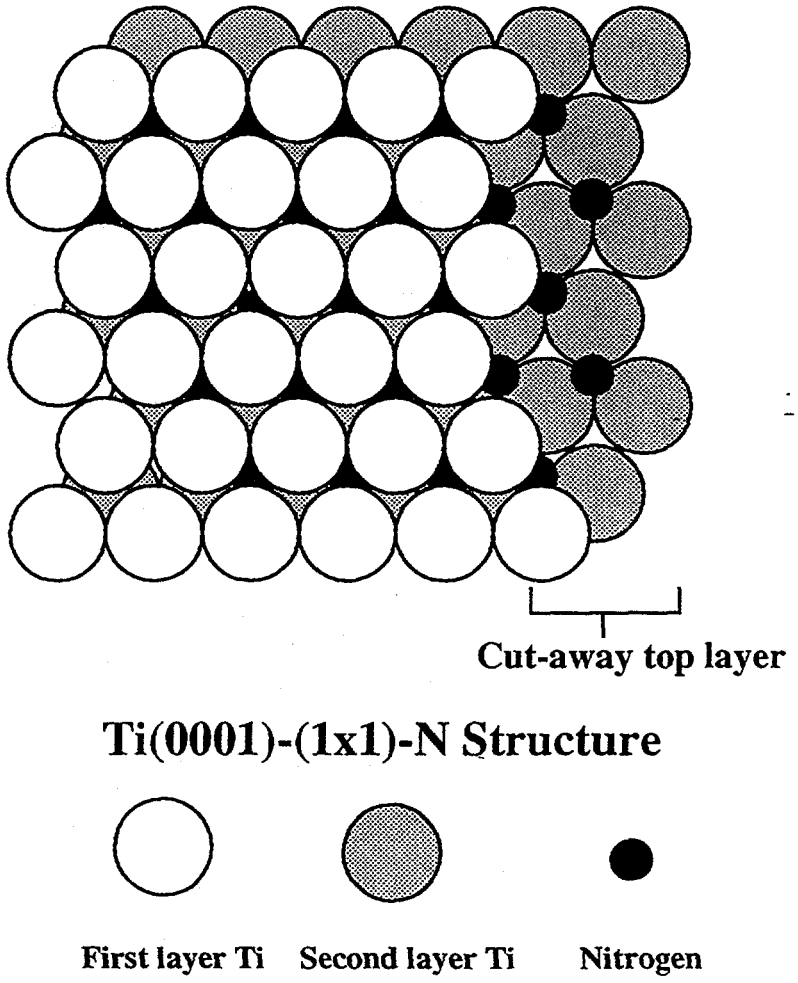

Figure 10.10: When the Ti(0001) surface is saturated with nitrogen a (1x1) structure is formed with the nitrogen occupying the interstitial sites between the first and second layers of the Ti surface, forming a TiN film.

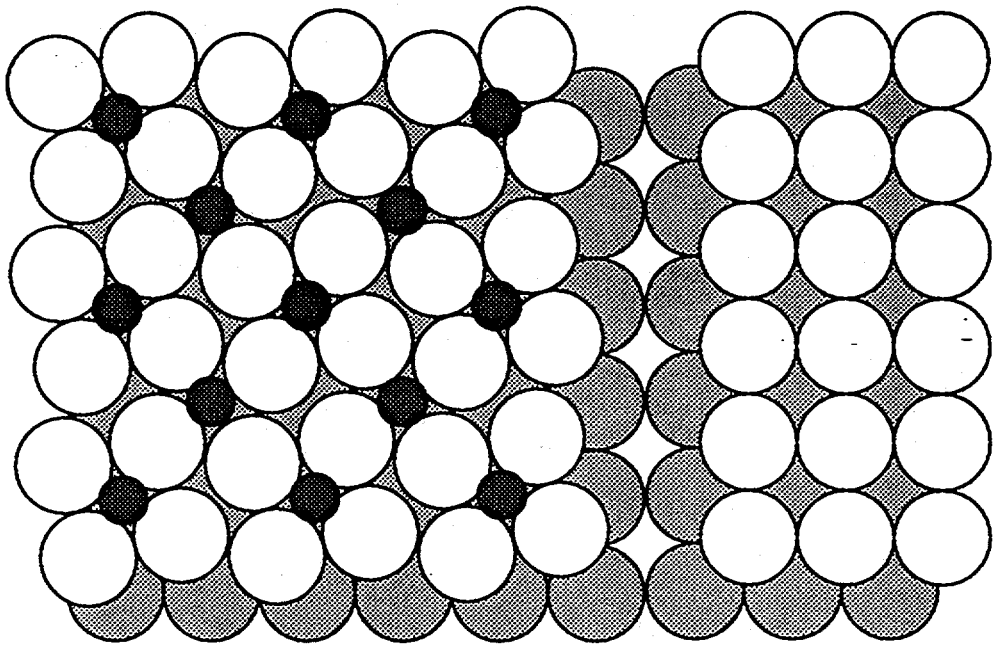

Ni(100)-p4g(2x2)-2C **Ni(100)-(1x1)**

Figure 10.11: The carbiding of the Ni(100)-(1x1) surfaces results in carbon atoms bonded in the four-fold hollow sites, with large lateral displacements of the top layer Ni atoms, producing the Ni(100)-p4g(2x2)-2C structure.

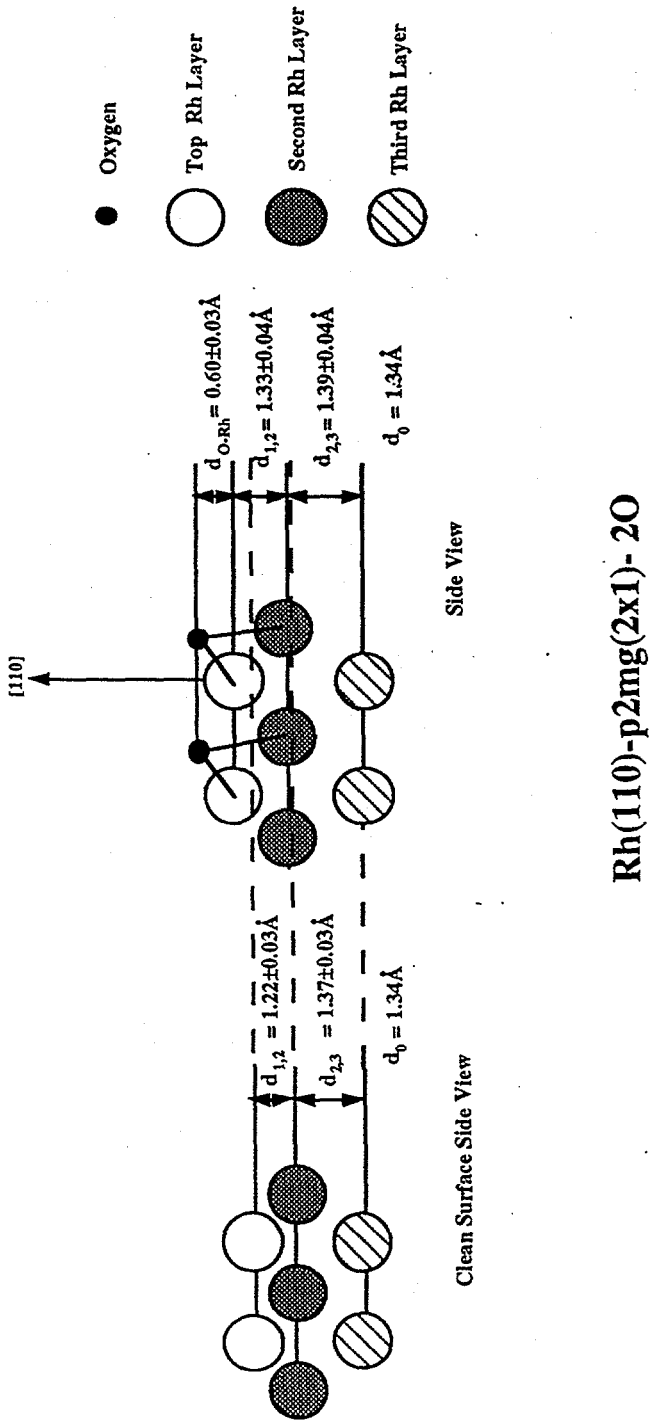

Figure 10.12: When 1 monolayer of oxygen is adsorbed on the clean Rh(110)-(1x1) surface, the clean surface relaxations are removed and the top interlayer spacing is expanded.

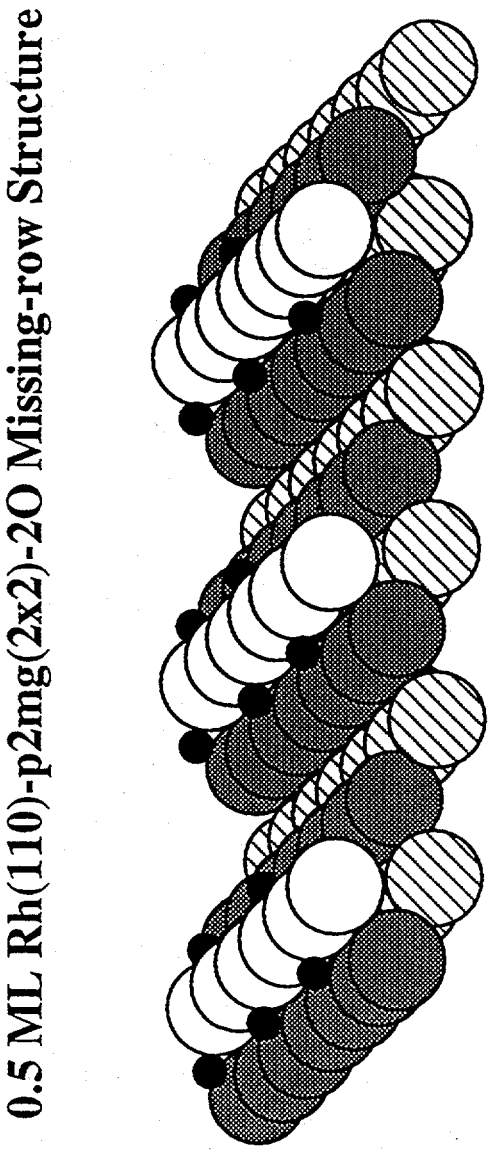

Figure 10.13: At 0.5 monolayers of O on Rh(110), the surface is reconstructed into a missing row structure, with the O atoms bonded in the 3-fold hollow sites at the top of the atomic ridges.

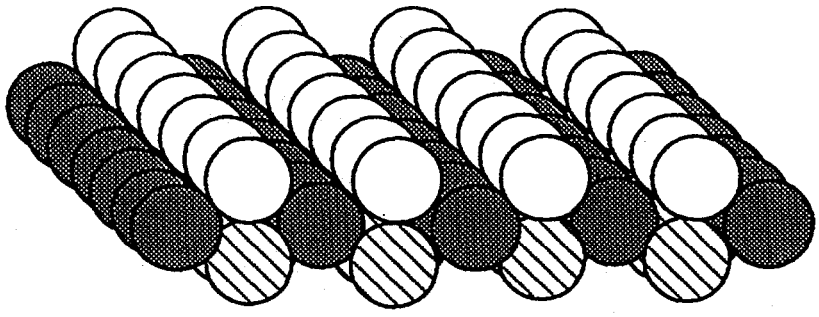

Cu(110)-(1x1)

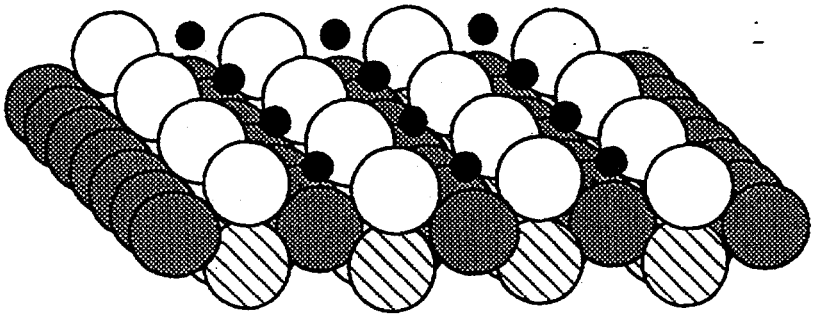

Cu(110)-(2x1)-2O

Figure 10.14: The Cu(110)-(2x1)-2O structure is a reconstructed surface with missing Cu atoms replaced by O atoms to form Cu-O-Cu chains along the surface. The O atoms are bonded to 4 nearest neighbor Cu atoms. The Cu(110)-(1x1) surface is shown for comparison.

Metallic adsorbate structure has also been examined on surfaces. In the absence of alloying, the overlayer structure of metallic adsorbates can initially adopt the periodicity of the substrate and grow on the surface with this periodicity. The substrate acts as a template for the growth of the deposited metal layers. This is usually referred to as epitaxial growth. Thicker adsorbate layers adopt their own periodicity but usually maintain an orientation prescribed by the substrate. One example is Pd deposited on Ag(100). [38] With these two fcc metals the Pd initially grows with the periodicity of the Ag substrate, with a 5.1% expansion of its bulk structure. Once the film becomes too thick to sustain the strain induced by this expansion (~ 3 monolayers) the Pd reverts to its normal bulk structure.

10.5 Molecular overlayers on metals.

Due to the increased complexity both theoretically and experimentally of determining molecular overlayer structures, there are significantly fewer structural studies of molecular adsorbates than of atomic adsorbates. The most common molecule used in the study of surface-molecular bonding has been carbon monoxide. CO can be readily adsorbed and desorbed intact from most metal surfaces. The vibrational spectroscopy for metal carbonyls is also well established and has been used to develop a rough correlation between the M_X-CO and C-O stretching frequencies to model the surface adsorption site coordination. An electronic model that describes the CO bonding interaction with the surface has been developed. In this model the 5σ orbital of the CO donates electron density to unoccupied d states in the surface and the occupied d states of the surface back-donate electron density to the anti-bonding $2\pi^*$ orbital of the CO. [39]

Even with this electronic model and vibrational spectroscopic characterization, the understanding of CO bonding to surfaces is complicated and incomplete. At low coverages CO usually bonds to a single surface atom, however the bonding site of CO is very sensitive to surface conditions. The site can change for different crystal planes of the same

metal and for different coverages on the same crystal plane. For example in the 0.33 monolayer ($\sqrt{3}x\sqrt{3}$)R30° structure of CO on the (111) surface of Rh the CO is bonded to the top site, while it is adsorbed in the 3-fold fcc hollow site on Pd. In both instances the CO molecular axis is perpendicular to the (111) plane and similar metal-C and C-O bond lengths are observed. [40] It has been proposed that a larger contribution of 4d electrons from Pd relative to Rh results in the high coordination adsorption site on Pd(111). [41] If we now examine the CO bonding on the (110) surfaces of these metals we find the opposite case, with CO bonded to the top site on Pd(110) and to the bridge site on Rh(110). This is due to the fact that in these compressed overlayers such as on the fcc (110) surfaces, strong CO-CO dipole repulsions are influencing the bonding. In fact, the CO-CO repulsions are so strong that the CO molecules bond in a tilted arrangement on the surface to avoid each other as much as possible. [42] (figure 10.15)

Such strong interactions can change the bonding of CO on the same surface as the coverage is increased. This is clearly illustrated for CO bonding on the Rh(111) surface. CO forms two ordered structures, a 0.33 monolayer ($\sqrt{3}x\sqrt{3}$)R30° structure and a 0.75 monolayer (2x2) structure. The ($\sqrt{3}x\sqrt{3}$)R30° structure consists of CO molecules bonded to top sites. As the CO coverage is increased the adsorption sites and geometries shift until in the (2x2) structure the molecules are arranged with one bridge bonded CO and two CO molecules bonded just off of top sites. (figure 10.16) The shift in adsorption sites minimizes the unfavorable intermolecular interactions. [40a,43]

The structural details of hydrocarbon adsorption have been investigated to develop an understanding of C-C and C-H bond cleavage on surfaces. Saturated hydrocarbons such as ethane often only physisorb to metal surfaces at low temperatures. Hydrocarbons such as acetylene, ethylene, and benzene however can have strong bonding interactions with the metal surface through their π–orbital system. The structural changes of these molecules during thermal decomposition have been thoroughly investigated to obtain details of structural changes that occur when bonds are broken on the surface. For example,

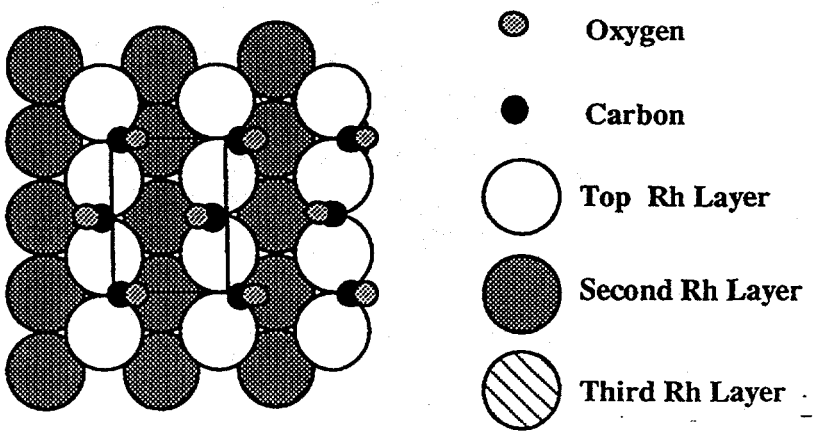

Top View

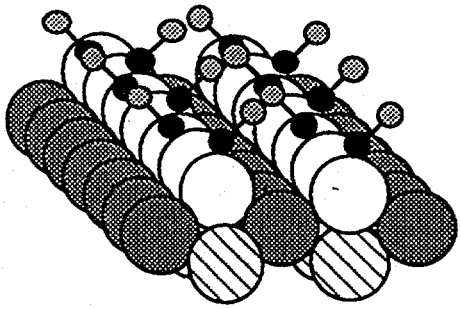

Side View

Figure 10.15: The Rh(110)-p2mg(2x1)-2CO structure. The CO-CO repulsions force the CO molecules to tilt from the surface normal by ~ 24°.

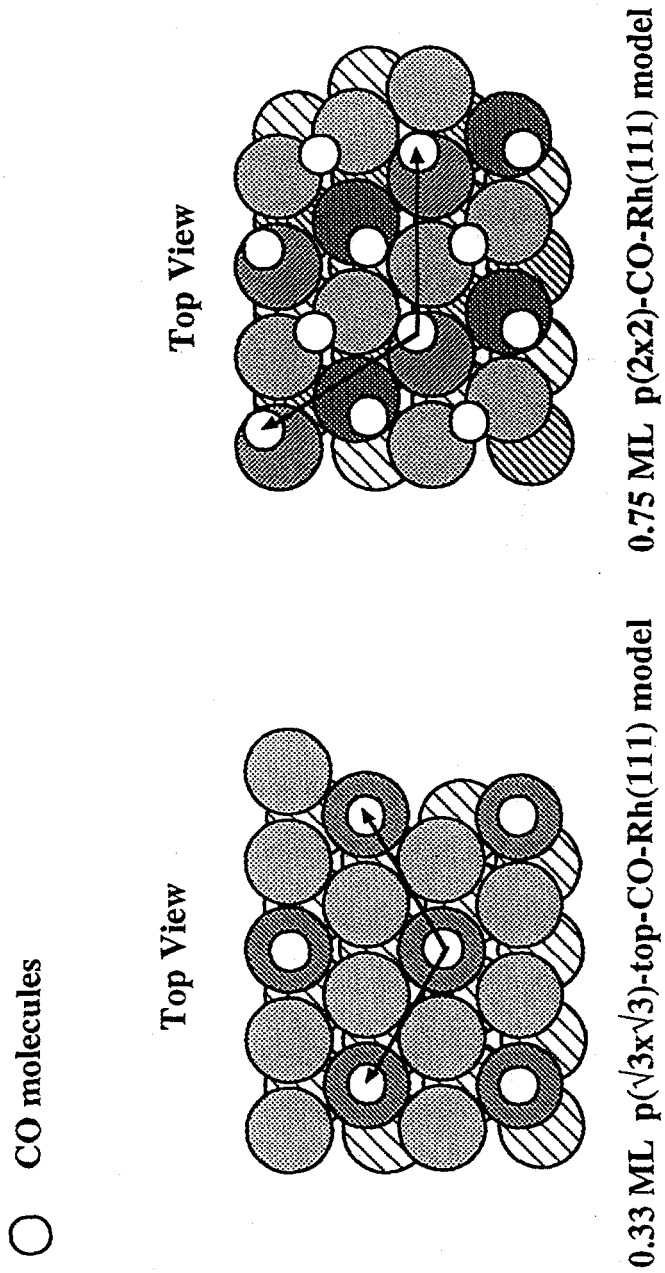

Figure 10.16: The change in CO bonding on Rh(111) as the coverage is increased from 0.33 monolayers to 0.75 monolayers of CO. The CO is initially top site bonded and when additional CO is added, the bridge sites begin to be populated.

vibrational spectroscopy has shown that at 77 K ethylene adsorbs intact on Rh(111). Upon heating the substrate to ~ 300 K the molecular ethylene undergoes C-H and C-C bond cleavage resulting in a structural transformation (rehybridization from sp^2 to sp^3 carbons) to an ethylidyne (CCH_3) species. The ethylidyne is bonded to the surface in the hcp 3-fold hollow site with 3 carbon bonds to the metal and the C-C axis oriented perpendicular to the surface. [44-46] (figure 10.17) The ethylidyne species is highly stable and has been found on several other metal surfaces. On Pt(111) the ethylidyne is similarly bonded in the slightly different fcc 3-fold hollow site. [47,48] In each of these cases, the local metal geometry around the adsorption sites is distorted with the metal surface plane buckled by ~ 0.10 Å. Some lateral displacements of ~ 0.10 Å are also observed in the CCH_3/Pt(111) case, drawing the bonded metal atoms closer to the adsorbate. (figure 10.18) The difference in site preference on these metals however is not well understood. Further thermal decomposition of ethylidyne produces CH_x and CCH_x (x=1,2) fragments on the surface, which eventually near 700 K form a graphitic overlayer.

Some other molecular adsorbates whose surface structures have been studied in detail include formate (HCO_2) on Cu(100) and Cu(110) [49,50], methoxy (CH_3O) on Cu(100) [51], acetonitrile (CH_3CN) on Ni(111) [52], and NO on Ni(111) and Pt(111). [53] In many of these systems similar types of molecular rehybridization as discussed above occur upon adsorption. A nice example is the rehybridization of acetonitrile upon adsorption on Ni(111). In the gas phase acetonitrile is a liner molecule with a C-N triple bond. On the surface this C-N bond is reduced to a double bond and the molecule becomes bent as shown in figure 10.19.

10.6 The co-adsorption phenomena.

In the previous sections only a single atomic or molecular species adsorbed on the surface was described. In catalytic systems however, the surface typically has more than

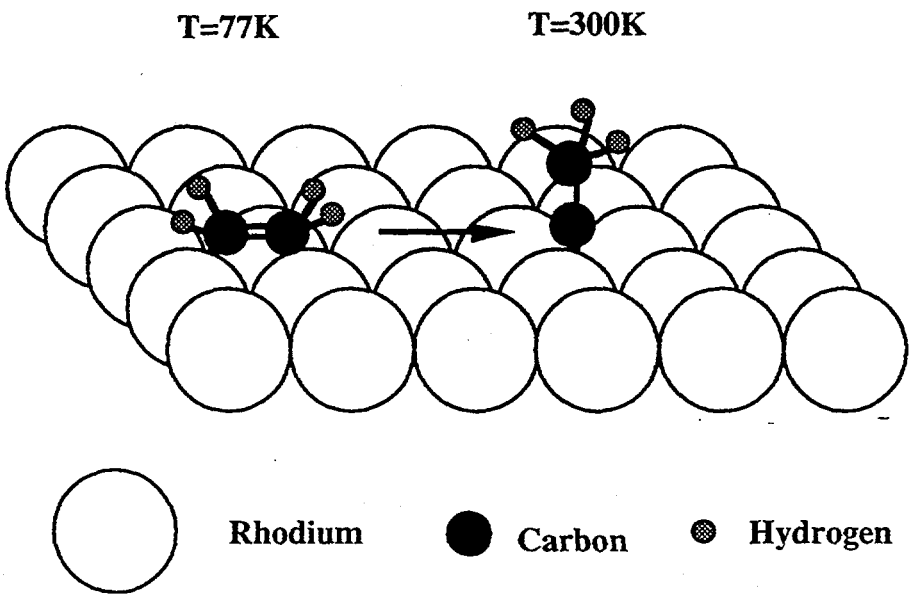

Conversion of ethylene to ethylidyne on Rh(111)

Figure 10.17: Molecular rehybridization occurs for ethylene on Rh(111), where at 77 K the molecule is π-bonded to the surface. Subsequent heating to 300 K results in sp^2 to sp^3 rehybridization of the C atoms to form the ethylidyne species.

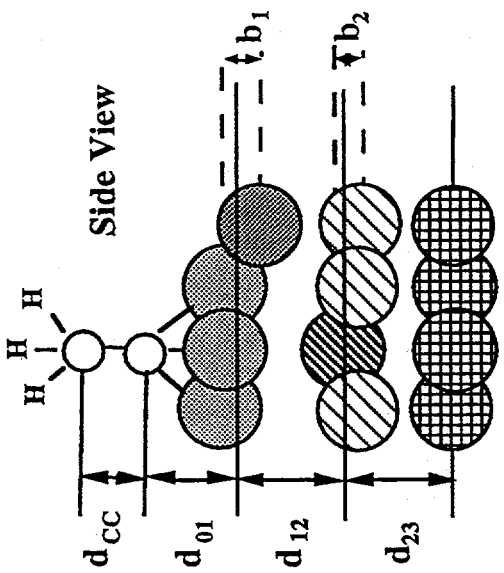

$d_{CC} = 1.45 \pm 0.04$Å
$d_{01} = 1.23 \pm 0.04$Å
$d_{12} = 2.26 \pm 0.06$Å
$d_{23} = 2.21 \pm 0.11$Å
$b_1 = 0.08 \pm 0.07$Å
$b_2 = 0.03 \pm 0.11$Å

Ethylidyne on Rh(111)

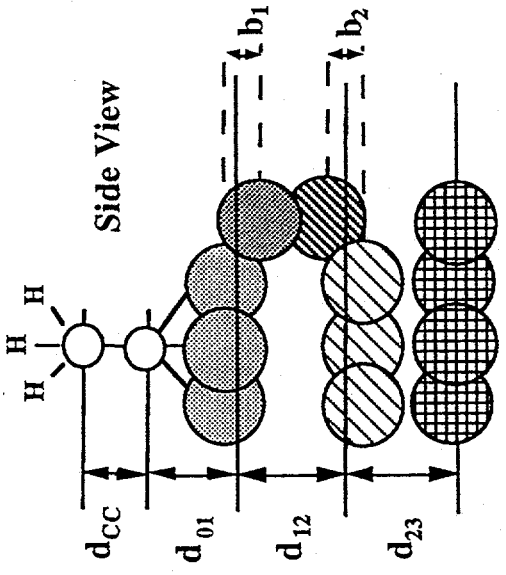

$d_{CC} = 1.49 \pm 0.05$Å
$d_{01} = 1.21 \pm 0.03$Å
$d_{12} = 2.30 \pm 0.03$Å
$d_{23} = 2.26 \pm 0.04$Å
$b_1 = 0.11 \pm 0.05$Å
$b_2 = 0.08 \pm 0.09$Å

Ethylidyne on Pt(111)

Figure 10.18: The structure of ethylidyne on Pt(111) and Rh(111). On the Pt surface the ethylidyne is bonded in the fcc 3-fold hollow, while on Rh(111), the hcp 3-fold hollow site is preferred. In each case, the molecular adsorption induced distortions in the top metal layers, pulling the nearest neighbor metal atoms up out of the surface plane, with the metal atoms not bonded to the molecule almost unaffected.

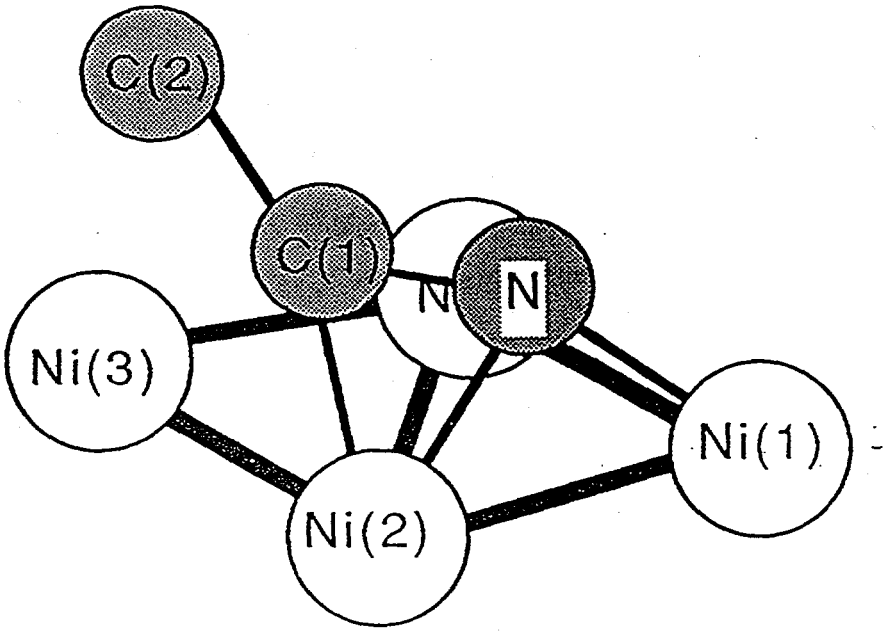

Ni(111)-p(2x2)-CH_3CN

Figure 10.19: Acetonitrile forms a (2x2) structure on the Ni(111) surface at 300 K. The dynamical LEED analysis shows that the molecule is rehybridized on the surface to a bent species, from its linear gas phase arrangement.

one type of adsorbed species on the surface at any given time. These mixed adsorbates can have interactions either through the surface via charge transfer, or through direct adsorbate-adsorbate interactions. The co-adsorption phenomenon acts in two ways; alteration of the electronic states of the surface through the acceptance or donation of electron density, and by sterically hindering further adsorption of other species. For example when K is pre-adsorbed on a Pt surface, the heat of desorption of CO from Pt increases as compared to that of CO in the absence of K. [54] The K perturbs the normal surface electron density by charge donation to the metal, strengthening the surface-CO bond which is accepting charge from the surface.

When the acceptor/donor pairing is an attractive interaction, it can stabilize molecular overlayer structures on surfaces and lead to uniformly mixed overlayers. Two example are the co-adsorption of ethylidyne with CO and NO, and the co-adsorption of benzene with CO. On the clean Rh(111) surface, ethylidyne is bonded in the hcp 3-fold hollow site, forming a (2x2) overlayer at of 0.25 monolayer coverage. If a surface first saturated with ethylidyne is then exposed to 0.25 monolayer of CO, a new c(4x2) structure is formed. In this structure the adsorption site of the ethylidyne is shifted from the hcp 3-fold hollow site to the fcc 3-fold hollow site. The CO, normally bonded at the top site on the clean surface, is now in the hcp 3-fold hollow site. When NO is the co-adsorbate, again a c(4x2) structure is formed; however in this case the ethylidyne is now bonded in the hcp site and the NO in the fcc site, the opposite of that with CO. [55]

In the case of benzene co-adsorbed with CO, the benzene structure is observed to change when CO is added to the pure benzene overlayer. The adsorption of pure benzene on Pt(111) is disordered. A structure analysis of this system shows a distortion of the aromatic ring with the benzene adsorbed with its center over the bridge site. The plane of the benzene ring also distorts with the 4 carbons that make up the 2 long bonds being out of the normal molecular plane by ~ 7° forming a boat shape. [56] In the presence of CO an ordered ($2\sqrt{3}$x4)-rect structure is formed with 2 benzene molecules and 4 CO molecules in

the unit cell. The adsorption site for the benzene is still the bridge site; however, it is rotated by 30° with respect to the pure benzene case and the ring is now planer. [57] The ability of mixed CO and benzene overlayers to form ordered structures has allowed for the bonding of benzene to be examined on several surfaces. [58-60] A direct comparison of these structures is found in Table 10.2. On each of the surfaces except Pd(111), a Kekulé distortion is found in which there are three short C-C bonds and three long C-C bonds. (figure 10.20) The magnitude of these distortions correlates with the strength of the benzene/metal bond, as expected.

With some co-adsorbed overlayers, islanding and compression rather than uniform mixing of the co-adsorbates occurs as a result of repulsive interactions between the adsorbates. For example, when CO is co-adsorbed with the 0.25 monolayer (2x2) oxygen structure on Pd(111), islands of CO and O form and the oxygen overlayer is compressed to the 0.33 monolayer ($\sqrt{3}x\sqrt{3}$)R30° structure. [61] This is observed in time in the LEED pattern. If one begins with the (2x2) oxygen pattern and then exposes the surfaces to a background pressure of the CO, the LEED pattern changes in time to the ($\sqrt{3}x\sqrt{3}$)R30° pattern.

This phenomena has been observed directly on the atomic scale with STM. When S is adsorbed at low coverages on Re(0001), CO can find bonding sites on the surface and co-adsdorbs. As CO is added to the well ordered (2x2)-S overlayer, the layer becomes disrupted as islands of CO begin to grow. A compressed area of S trimers forms around the CO islands. [62] The competing effects that drive the islanding and compression are S-S, CO-CO, and S-CO repulsions vs. the bonding energy gained from CO adsorption. At high S coverages CO adsorption is blocked due to the lack of suitable bonding sites and a sufficient energy gain from CO adsorption to overcome adsorbate-adsorbate repulsions.

Benzene adsorption geometries on transition metal surfaces.

System	C-C distances (Å)	metal-C distance (Å)	Benzene site	CO Site
Pd(111)-(3x3)-C_6H_6 + 2CO	1.41±0.10	2.30±0.05	fcc hollow	fcc hollow
Pt(111)-(2√3x4)-rect -2C_6H_6 + 4CO	1.76±0.15 1.65±0.15	2.25±0.05	bridge	bridge
Rh(111)-(3x3)-C_6H_6 + 2CO	1.50±0.15 1.37±0.15	2.19±0.05	hcp hollow	hcp hollow
Rh(111)-(2√3x4)-rect -2C_6H_6 + 4CO	1.76±0.15 1.65±0.15	2.25±0.05	hcp hollow	hcp hollow
Disordered C_6H_6 /Pt(111)	1.63±0.05 1.45±0.10	2.60±0.02 2.02±0.02	bridge	———
Gas Phase	1.397	———	———	———

Table 10.2: Structures of benzene, with and without CO co-adsorption, on transition metal surfaces.

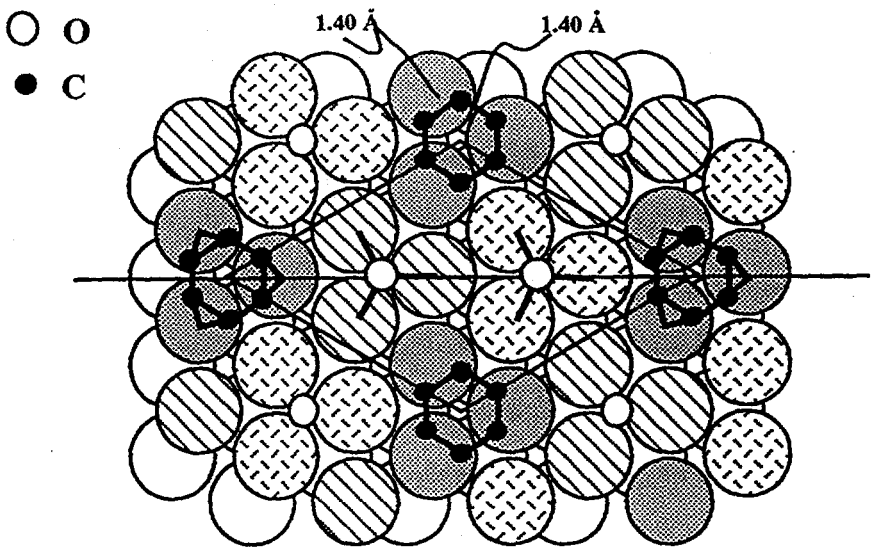

Pd(111)-(3x3) C_6H_6 - 2CO

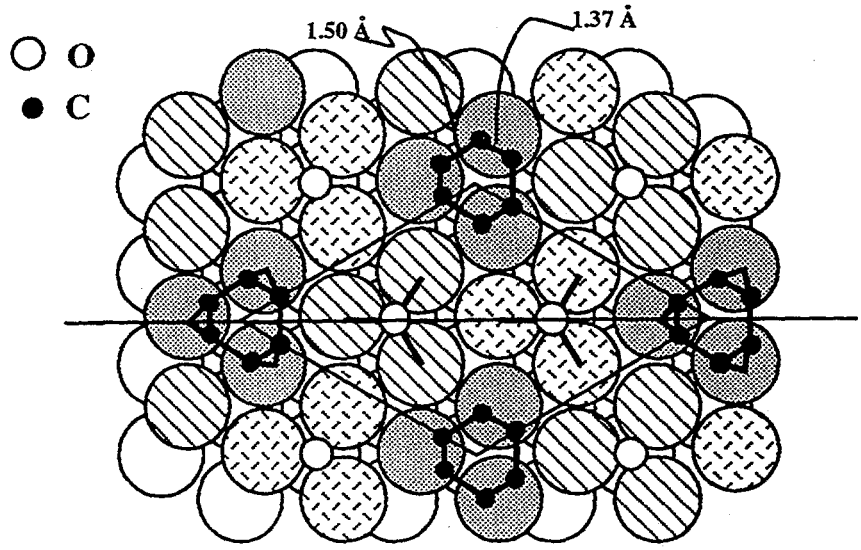

Rh(111)-(3x3) C_6H_6 - 2CO

Figure 10.20: The co-adsorption of benzene with CO on Pd(111) a) and Rh(111) b). On Pd the benzene molecule only interacts weakly with the surface and little change in the C-C bonds occur. On Rh(111) the interaction is stronger and a Kekulé distortion is observed.

10.7 The nature of surface chemical bonding.

Based on surface structural studies like those described here a model of surface chemical bonding has been developed. The rearrangement of surface atoms into atomic positions sometimes quite different from their normal bulk terminated positions is driven by the minimization of the surface free energy. These rearrangements appear as relaxations and/or reconstructions of the surface layers. The more open or atomically rough the surface is, the more mobile these surface atoms become. Defects at the surface such as kinks appear to be "smoothed over" to minimize surface free energy.

When atomic adsorbates are present, they typically adsorb to the highest coordination sites to maximize their bonding with the substrate. This can lead to adsorbate induced restructuring of the surface, where the surface atoms reorganize about the adsorbate. The rearrangement is a "cluster-like" bonding with the nearest-neighbor surface atoms, in which both the adsorbate-substrate and substrate-substrate bonds are optimized. This optimized chemical bond increases the heat of chemisorption to compensate for the weakening of the metal-metal bonds in the surface. When films are grown on surfaces, such optimization is responsible for the epitaxial growth of the overlayer, where the initial film structure is governed by the substrate structure.

The influence of adsorbed species on the surface structure often extends down into the second and even third metal layers and is expressed as expansions, contractions, buckling, or even reconstruction of the surface layers upon chemisorption. With molecular overlayers, the optimization of the surface molecular bond is even more evident, as molecules often undergo rehybridization upon adsorption. Such rehybridization of adsorbed molecules bonded on surfaces has been seen in several ways. The C-O bond is weakened upon chemisorption. The sp^2 π- bonded ethylene is rehybridized to the sp^3 ethylidyne species. Acetonitrile changes from a linear molecule in the gas phase to a bent

molecule on the surface. Such changes in molecular structure are very sensitive to surface conditions and often show sharp temperature dependence.

The bonded molecular and atomic species can have attractive or repulsive interactions. These interactions produce a coverage dependence on the bonding of adsorbed species. Repulsive interactions between the same adsorbates cause them to alter their bonding configurations and move apart in order to reduce the unfavorable interaction. With co-adsorbed systems, repulsive interactions often lead to islanding of the co-adsorbates, while attractive interactions lead to clustering and uniformly mixed overlayers. Much remains to be learned about these complex rearrangements of atoms at surfaces.

This chapter reviewed the techniques employed in the determination of surface structures and how these results have enhanced our knowledge of surface bonding. Many books have been written on this subject and the reader is referred to these for a more detailed overview [63-65]. The chapter concludes with an outlook for the future of surface structural studies.

10.8 An outlook . . .

The structures of many chemically and tribologically important systems still remain to be examined by surface science. Work in the area of molecular adsorption still remains mostly untapped. The adsorption properties of molecules at defect sites such as steps and kinks are largely unexplored structurally. Studies of the structures of oxide and alloy overlayers will also provide new challenges for the future.

The development of new techniques will play a key role in future studies. The ideal technique to study surfaces would be a direct structural technique with time resolution on the order of whatever surface reaction is being investigated, which operates under real conditions. This goal has been approached in several ways. Recently time-resolved reflection high-energy electron diffraction has been achieved with a pulsed electron beam

with a time resolution of ~ 1 ns. With this technique changes in surface structure under laser heating has been examined. [66] Time resolved STM has also been developed, allowing for atomic resolution images to be produced with ps time resolution. [67-69] Real time movies of surface processes will be able to be produced not too far in the future.

The level of theory being applied to the LEED structure calculations is also continually being advanced. [70] With today's technology, a detailed analysis may now be done on a personal computer rather than on a supercomputer. This makes surface crystallography more readily available to the surface scientist, just as X-ray crystallography has been available to the chemist and solid-state physicist. A database has already been established by the National Institute of Science and Technology that contains some 600 of the currently well known surface structures, [71] with more structures rapidly being added.

10.9 References

[1] P. Zeppenfeld, C.D. Lutz, and D.M. Eigler, Ultramicro. 42 (1992) 128.

[2] J. Frommer, Angew. Chem. Ed. Engl. 31 (1992) 1298.

[3] B.J. McIntyre, M.B. Salmeron, and G.A. Somorjai, J. Vac. Sci. Tech. A 11 (1993) 1964.

[4] M.A. Van Hove and S.Y. Tong, *Surface Crystallagrophy by LEED:Theory, Computation, and Structural Results,* Springer-Verlag, Berlin, Heidelberg, 1979.

[5] M.A. Van Hove, W.H. Weinberg, and C.-M.Chan, *Low-Energy Electron Diffraction: Experiment, Theory, and Surface Structure Determination,* Springer-Verlag, Berlin, Heidelberg, 1986.

[6] J.B. Pendry, *Low-Energy Electron Diffraction,* Academic Press, New York, 1974.

[7] M.A. Van Hove, W. Moritz, H. Over, P.J. Rous, A. Wander, A. Barbieri, N. Materer, U. Starke, and G.A. Somorjai, Surf. Sci. Rep. 19 (1993) 191.

[8] P.J. Rous, Prog. in Surf. Sci. 39 (1992) 3.

[9] P.J. Rous, M.A. Van Hove, and G.A. Somorjai, Surf. Sci. 226 (1990) 15.

[10] a) D.K. Saldin, J.B. Pendry, M.A. Van Hove, and G.A. Somorjai, Phys. Rev. B 31 (1985) 1216.

b) K. Heinz, U. Starke, M.A. Van Hove, and G.A. Somorjai, Surf. Sci. 261 (1992) 57.

[11] H. Wedler, M.A. Mendez, P. Bayer, U. Löffler, K. Heinz, V. Fritzsche, and J.B. Pendry, Surf. Sci. 293 (1993) 47.

[12] A. Wander, G. Held, R.Q. Hwang, G.S. Blackman, M.-L. Xu, P. de Andres, M.A. Van Hove, and G.A. Somorjai, Surf. Sci. 249 (1991) 21.

[13] G.S. Blackman, M. -L. Xu, D.F. Ogletree, M.A. Van Hove, and G.A. Somorjai, Phys. Rev. Lett., 61 (1988) 2352.

[14] W.S. Yang, F. Jona, and P.M. Marcus, Phys. Rev. B, 27 (1983) 27.

[15] P. Hu, L. Morales de la Garza, R. Raval, and D.A. King, Surf. Sci. 249 (1991) 1.

[16] D.E. Gardin, J.D. Batteas, M.A. Van Hove, and G.A. Somorjai, Surf. Sci. 296 (1993) 25.

[17] *The Structures of Surfaces*, eds. M.A. Van Hove and S.Y. Tong, Springer Series on Surface Science 2, Springer-Verlag, Berlin, Heidelberg, 1985.

[18] T. Engel and K.H. Rieder in *Structural Studies of Surfaces*, v. 91 Springer Tract in Modern Physics, ed. G. Höhler, Springer, Berlin, 1982.

[19] *Scanning Tunneling Microscopy I*, eds. H.J. Güntherodt and R, WiesendangerSpringer Series on Surface Science 20,

Springer-Verlag, Berlin, Heidelberg, 1992.

[20] E. Meyer and H. Heinzelmann, *Scanning Tunneling Microscopy and Related Methods*, ed. R.J. Behm, Kluwer, Dordrecht, 1990.

[21] J. Frommer and E. Meyer, J. Phys. Cond. Matt. 3 (1991) S1.

[22] a) C.-M. Chan and M.A. Van Hove, Surf. Sci. 171 (1986) 226.
b) W. Moritz and D. Wolf, Surf. Sci. 163 (1985) L655.
c) E.C. Sowa, M.A. Van Hove, and D.L. Adams, Surf. Sci. 199 (1988) 174.

[23] M.A. Van Hove, R.J. Koestner, P.C. Stair, J.P. Biberian, I. Batos, and G.A. Somorjai, Surf. Sci. 103 (1981) 218.

[24] X.-G. Zhang, M.A. Van Hove, G.A. Somorjai, P.J. Rous, D. Tobin, A. Gonis, J.M. MacLaren, K. Heinz, M. Michl, H. Lindner, K. Müller, M. Ehsasi, and J.H. Block, Phys. Rev. Lett. 67 (1991) 1298.

[25] a) K. Takayanagi, Y. Tanishiro, M. Takahashi, and S. Takahashi, J. Vac. Sci. Technol. A 3 (1985) 1502.
b) S.Y. Tong, H. Huang, C.M. Wei, W.E. Packard, F.K. Men, G. Glander, and M.B. Webb, J. Vac. Sci. Technol. A 6 (1988) 615.

[26] W.S. Yang, F. Jona, and P.M. Marcus, Phys. Rev. B 28 (1983) 2049.

[27] a) W. Weiss, A. Barbieri, M.A. Van Hove, and G.A. Somorjai,

Phys. Rev. Lett. 71 (1993) 1848.

b) A. Barbieri, W. Weiss, M.A. Van Hove, and G.A. Somorjai, Surf. Sci. 302 (1994) 259.

[28] P.C. Wong, K.C. Hui, M.Y. Zhou, and K.A.R. Mitchell, Surf. Sci. 165 (1986) L21.

[29] W. Oed, B. Doetsch, L. Hammer, K. Heinz, and K. Müller, Surf. Sci. 207 (1988) 55.

[30] H.D. Shih, F. Jona, D.W. Jepson, and P.M. Marcus, Surf. Sci. 60 (1976) 445.

[31] W. Puchta, W. Nichtl, W. Oed, N. Bickel, K. Heinz, and K. Müller, Phys. Rev. B 39 (1989) 1020.

[32] M. Gierer, H. Over, G. Ertl, H. Wohlgemuth, E. Schwarz, and K. Christmann, Surf. Sci. Lett. 297 (1993) L73.

[33] K.C. Wong and K.A.R. Mitchell, Surf. Sci. 304 (1994) L481.

[34] a) Y. Gauthrer, R. Baudoing-Savois, K. Heniz, and H. Landskron, Surf. Sci. 251/252 (1991) 493.

b) A.L.D. Kilcoyne, D.P. Woodruff, A.W. Robinson, Th. Lindner, J.S. Somers, and A.W. Bradshaw, Surf. Sci. 253 (1991) 107.

[35] C. Comicioli, V.R. Dhanak, G. Comelli, C. Astaldi, K.C. Prince, R. Rosei, A. Atrei, and E. Zanazzi, Chem. Phys.Lett. 214 (1993) 438.

[36] P.W. Murray, F.M. Leibsle, Y. Li, Q. Guo, M. Bowker, G. Thornton, V.R. Dhanak, K.C. Prince, and R. Rosei, Phys. Rev. B 47 (1993) 12976.

[37] S.R. Parkin, H.C. Zeng, M.Y. Zhou, and K.A.R. Mitchell, Phys. Rev. B 41 (1990) 5432.

[38] a) M. Pessa and M. Vulli, J. Phys. C 16 (1983) L629.
b) R.L. Fink, C.A. Ballentine, J.L. Erskine, and J.A. Araya-Pochet, Phys. Rev. B 41 (1990) 10175.

[39] G. Blyholder, J. Phys. Chem. 68 (1964) 2772.

[40] a) R.J. Koestner, M.A. Van Hove, and G.A. Somorjai, Surf. Sci. 107 (1981) 439.
b) H. Ohtani, M.A. Van Hove, and G.A. Somorjai, Surf. Sci. 187 (1987) 372.

[41] A.B. Anderson and M.K. Awad, J. Am. Chem.Soc. 107 (1985) 7854.

[42] a) D.J. Hannaman and M.A. Passler, Surf. Sci. 203 (1988) 449.
b) A. Wander, P. Hu, and D.A. King, Chem. Phys. Lett. 201 (1993) 393.
c) J.D. Batteas, A. Barbieri, E.K. Starkey, M.A. Van Hove, and G.A. Somorjai, Surf. Sci. (in press).

[43] M.A. Van Hove, R.J. Koestner, J.C. Frost, and G.A. Somorjai, Surf. Sci. 129 (1983) 482.

[44] R. J. Koestner, M.A. Van Hove, and G.A. Somorjai, Surf. Sci. 121 (1982) 321.

[45] A. Wander, M.A. Van Hove, and G.A. Somorjai, Phys. Rev. Lett. 67 (1991) 626.

[46] A. Barbieri, M.A. Van Hove, and G.A. Somorjai, Proc. 4th Int. Conf. on the Structures of Surfaces.

[47] L.L. Kesmodel, L.H. Dubois, and G.A. Somorjai, J. Chem. Phys. 70 (1979) 2180.

[48] U. Starke, A. Barbieri, N. Materer, M.A. Van Hove, and G.A. Somorjai, Surf. Sci. 286 (1993) 1.

[49] D. P. Woodruff, C. F. McConville, A.L.D. Kilcoyne, Th. Lindner, J. Somer, M. Surman, G. Paolucci, and A.M. Bradshaw, Surf. Sci. 201 (1988) 228.

[50] A. Puschmann, J. Hasse, M.D. Crapper, C.E. Riley, and D.P. Woodruff, Phys. Rev. Lett. 54 (1985) 2250.

[51] Th. Lindner, J. Somer, A.M. Bradshaw, A.L.D. Kilcoyne, and D. P. Woodruff Surf. Sci. 203 (1988) 333.

[52] D.E. Gardin, A. Barbieri, J.D. Batteas, M.A. Van Hove, and G.A. Somorjai, Surf. Sci. 304 (1994) 316.

[53] a) N. Materer, A. Barbieri, D. Gardin, U. Starke, J.D. Batteas, M.A. Van Hove, and G.A. Somorjai, Surf. Sci. 303 (1994) 319.
b) L.D. Mapledoram, A. Wander, D.A. King, Chem. Phys. Lett. 209 (1993) 409.

[54] E.L. Garfunkel, J.E. Crowell, and G.A. Somorjai, J. Phys. Chem. 86 (1982) 310.

[55] G.S. Blackman, C.-T. Kao, B.E. Bent, C.M. Mate, M.A. Van Hove, and G.A. Somorjai Surf. Sci. 207, 66 (1988).

[56] A. Wander, G. Held, R.Q. Hwang, G.S. Blackman, M.L. Xu, P. de Andres, M.A. Van Hove, and G.A. Somorjai, Surf. Sci. 249 (1991) 21.

[57] D.F. Ogletree, M.A. Van Hove, and G.A. Somorjai, Surf. Sci. 183 (1987) 1.

[58] a) M.A. Van Hove, R.F. Lin, and G.A. Somorjai, J. Amer. Chem. Soc. 108 (1986) 2532.
b) R.F. Lin, G.S. Blackman, M.A. Van Hove, and G.A. Somorjai, Acta Cryst. B 43 (1987) 368.

[59] H. Ohtani, M.A. Van Hove, and G.A. Somorjai, J. Phys. Chem. 92 (1988) 3974.

[60] A. Barbieri, M.A. Van Hove, and G.A. Somorjai, Surf. Sci. 306 (1994) 261.

[61] H. Conrad, G. Ertl, and J. Küppers, Surf. Sci. 76 (1978) 323.

[62] J.C. Dunphy, B.J. McIntyre, J. Gomez, D.F. Ogletree, G.A. Somorjai, and M.B. Salmeron, J. Chem. Phys.(in press).

[63] *The Structures of Surfaces II,* eds. J.F. van der Veen and M.A. Van Hove, Springer Series on Surface Science 11, Springer-Verlag, Berlin, Heidelberg, 1988.

[64] *The Structures of Surfaces III,* eds. S.Y. Tong, M.A. Van Hove K. Takayanagi, and X.D. Xie, Springer Series on Surface Science 24, Springer-Verlag, Berlin, Heidelberg, 1991.

[65] a) *Introduction to Surface Chemistry and Catalysis,* G.A. Somorjai, Wiley, 1994.
b) *Chemsitry in Two Dimensions, Surfaces,* G.A. Somorjai, Cornell University Press, 1979.

[66] H.E. Elsayed-Ali and J.W. Herman, Rev. Sci. Instrum. 61 (1990) 1636.

[67] S. Weiss, D.F. Ogletree, D. Botkin, M. Salmeron, and D.S. Chemla Appl. Phys. Lett. 63 (1993) 2567.

[68] M.R. Freeman and G. Nunes, Appl. Phys. Lett. 63 (1993) 2633.

[69] M.R. Freeman and G. Nunes, Science, 262 (1993) 1029.

[70] J.B. Pendry, Surf. Sci. Rep. 19 (1993) 87.

[71] P.R. Watson, M.A. Van Hove, and K. Herman, NIST Surface Structure Database Version 1.0, NIST Standard Reference Data Program, Gaithersberg, MD (1993).

[72] C.F. McConville, D.A. Woodruff, K.C. Prince, G. Paolucci, U. Chab, M. Suvman, and A.M. Bradshaw, Surf. Sci. 166 (1986) 221.

[73] S. Anderson and J.B. Pendry, J. Phys. C 13 (1980) 3547.

[74] L. Becker, S. Aminpirooz, B. Hillert, M. Pedio, J. Haase, and D.L. Adams, Phys. Rev. B 47 (1993) 9710.

[75] S.D. Kevan, R.F. Davis, D.H. Rosenblatt, J.G. Tobin, M.G. Mason, D.A. Shirley, C.H. Li, and S.Y. Tong, Phys. Rev. Lett. 46 (1981) 1629.

[76] L.G. Petersson, S. Kono, N.F.T. Hall, C.S. Fadley, and J.B. Pendry, Phys. Rev. Lett. 42 (1979) 1545.

[77] a) S.Y. Tong, A. Maldonado, C.H. Li, and M.A. Van Hove, Surf. Sci. 94 (1980) 73.
b) M.A. Passler, A. Ignatiev, F. Jona, D.W. Jepsen, and P.M. Marcus, Phys. Rev. Lett. 43 (1979) 360.
c) K. Heinz, E. Lang, and K. Müller, Surf. Sci. 87 (1979) 595.

[78] D.J. Hannaman and M.A. Passler, Surf. Sci. 203 (1988) 449.

[79] O. Knauff, U. Grosche, H.P. Bonzel, and V. Fritzsche, Molec. Phys. 76 (1992) 787.

[80] Z. Huang, Z. Hussain, W.T. Huff, and E.J. Moler, and D.A. Shirley, Phys.Rev. B 48 (1993) 1696.

[81] H. Ohtani, M.A. Van Hove, and G.A. Somorjai, Surf. Sci. 187 (1987) 372.

[82] R.J. Behm, K. Christmann, G. Ertl, and M.A. Van Hove, J. Chem. Phys. 73 (1980) 2984.

[83] A. Wander, P. Hu, and D.A. King, Chem. Phys. Lett. 201 (1993) 393.

[84] D.F. Ogletree, M.A. Van Hove, and G.A. Somorjai, Surf. Sci. 173 (1986) 351.

[85] G.S. Blackman, M.-L. Xu, M.A. Van Hove, and G.A. Somorjai, Phys. Rev. Lett. 61 (1988) 2352.

[86] M.A. Van Hove, R.J. Koestner, J.C. Frost, and G.A. Somorjai, Surf. Sci. 129 (1983) 482.

[87] R.J. Koestner, M.A. Van Hove, and G.A. Somorjai, Surf. Sci. 107 (1981) 439.

[88] J.D. Batteas, A. Barbieri, E.K. Starkey, M.A. Van Hove, and G.A. Somorjai, Surf. Sci. (in press).

[89] G. Michalk, W. Moritz, H. Pfnür, and D. Menzel, Surf. Sci. 129 (1983) 92.

[90] P. Piercy, P.A. Heimann, G. Michalk, and D. Menzel, Surf. Sci. 219 (1989) 189.